EVALUATION OF Bi_2O_3 AND Sb_6O_{13} AS OXIDANTS FOR SILICON FUEL IN TIME DELAY DETONATORS

LONJI KALOMBO

Submitted in partial fulfilment of the requirements for the degree of
Master of Science: Applied Science: Chemical Technology
Faculty of Engineering, Built Environment and Information Technology
University of Pretoria

March 2005

Abstract

This study considered bismuth (III) oxide (Bi_2O_3) and antimony hexitatridecoxide (Sb_6O_{13}) as potential substitutes for the red lead (Pb_3O_4) and barium sulphate ($BaSO_4$) oxidants currently used in time delay compositions for detonator assemblies.

Fine silicon powders with a specific surface area of 2 - 10 m^2/g were used as fuels. Some experiments were also done with a coarse manganese powder as fuel. Bi_2O_3 was synthesised by the thermal decomposition of $(BiO)_2CO_3$ by heating at 460°C for 15 hours. The yield was near quantitative, i.e. close to the 91,4% expected based on the complete conversion of the carbonate to the oxide. Sb_6O_{13} was obtained by heating colloidal antimony pentoxide (Sb_2O_5) for 8 hours at 315°C. This resulted in a ca. 20 % mass loss and yielded a reactive black powder.

In the Si-Bi_2O_3 system, compositions in the range 5 - 40% by mass Si were ignitable with shock tubing. Burn rates measured in lead tubes varied between 15 and 155 mm/s. This highest burn rate was obtained with 20% silicon. Addition of additives such as $KMnO_4$ and boric oxide had little effect on the burn rate. The fast burning Si-Bi_2O_3 system is a potential replacement for the commercial Si - red lead system.

The burning rate decreased with increasing compaction of the samples. Burn rate also decreased when the aluminium instead of lead tubes were used. This is attributed to a greater heat loss with the former.

The combustion products were characterised using DTA, FT-IR, XRD and SEM. The results show that the combustion reactions led to reduction of the oxidant to the corresponding metal form.

The Sb_6O_{13}-Si system requires an initiating composition such as Bi_2O_3-50%Si (Type 4). It is slow burning and thus a possible replacement for the commercial $BaSO_4$-Si system. The lowest sustainable and reproducible burn rate, in the absence of additives, was 4,8 mm/s. It was achieved using 10% silicon Type 4. Adding small

amounts of fumed silica (<2%) increased the burn rate. This is attributed to better mixing and compaction. However, lower burn rates (~2 mm/s) are possible if more fumed silica is added as inert diluent.

Replacing the silicon fuel with manganese powder gave more exothermic and even slower burning compositions.

Keywords: Pyrotechnic time delay compositions, bismuth oxide, antimony hexitatridecoxide (Sb_6O_{13}), silicon.

Acknowledgements

I am deeply grateful to my supervisor, Professor Walter W. Focke for his relevant guidance and inspiration. His continuous enthusiasm and willingness to assist was greatly appreciated.

Mr C. Conradie (from AEL) is gratefully acknowledged for his assistance during the course of this study.

I gratefully acknowledge the financial and technical support of the following institutions:

- University of Pretoria
- Xyris Technology CC
- THRIP programme of the Department of Trade and Industry
- National Research Foundation (NRF) of South Africa
- African Explosives Limited (AEL) of South Africa.

I am indebted to Ollie Del fabro for his continuous seeking to get a deep insight of the subject and his technical assistance. Sincere thanks to Isabel Ricco and Serei Sefanyetso for initiating the pyrotechnic project. I cannot adequately express my gratitude to my colleagues at the Institute of Applied Materials for their support. Very special thanks are due to Pravina.

I am very proud for my fellow-countrymen. They were very helpful!

Finally, I would like to dedicate this work to my dear mother, my family and my family in law for their prayers and deep love. My deceased father would have been very proud of his son.

For my pretty wife Masele and our brilliant children (Divin, Eternel and Beniciel), it is the crown of my Love.

Contents

List of Figures

Pages

List of Tables

Pages

List of Symbols

C_p	heat capacity	J/mol.K
D	diffusion coefficient	-
E_a	Arrhenius activation energy	J/mol.K
g(n)	reaction order n and varies between 1 and 2	-
G	Gibbs free energy change	J/mol
H	enthalpy change	J/mol.
k	rate constant	1/s
k_o	pre-exponential factor	1/s
L	thickness of the oxide layer	mm
P	pressure	kPa
R	gas constant (R = 8,314 J/mol.K)	J/mol.K
q	reaction heat	J/mol.
$\dot{q}$	rate of heat release	J/mol.s
S	entropy change	J/mol.K
t	time	s
T_{ad}	adiabatic reaction temperature	K
T_c	the maximum temperature of the burning column	K
T_{ign}	critical ignition temperature	K
T_m	melting point	K
u	burn speed	mm/s
w	volume of oxygen	m^3
x	degree of conversion	
Z	distance in the column of reaction	mm
Greek symbols		
α	thermal diffusivity	m^2/s
λ	thermal conductivity	W/m.K
ρ	density	kg / m^3
θ	Bragg angle	°
ξ	factor of direction	
Subscripts		
Ar	Arrhenius	
l	liquid	
o	initial conditions	
R	reaction	
s	solid	

1. Introduction

1.1 Pyrotechnic time delay systems

Pyrotechnics applications include military and civilian devices such as flares, tracers, signals, smokes, incendiaries and fireworks. Pyrotechnic delay systems are used in detonator assemblies to delay the terminal reaction by a precisely adjustable time interval that is determined by the burning rate of the composition (Ellern, 1968).

A detonator consists of a casing (aluminium tube), an explosive element, an initiator, a delay element, antistatic cap, a shock tube and a grommet (See Figure 1). The explosive element usually contains pentaerithritol tetranitrate (PETN) as the base charge. The initiator typically consists of a lead azide/lead styphnate mixture and is placed on top of the base charge. The delay element consists of a column of deflagrating explosive encased in a lead/aluminium tube. The antistatic cap serves to prevent static ignition and the grommet serves as seal and clamp for the shock tube. The delay composition is ignited by an electric discharge from an electric shock box via a shock tube and the shock cap. The time taken by the combustion wave to travel the length of the deflagrating explosive is called the delay between the initiation impulse and the detonation of the base charge. Delay times ranging from microseconds to a few seconds are generally required.

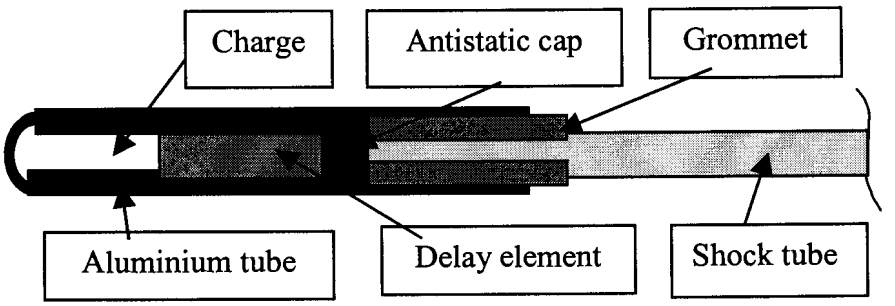

Figure 1.1 A typical detonator assembly.

The delay composition is constituted from a fuel and an oxidiser in the solid state. This redox reaction is readily initiated by a temperature impulse. The reaction commences as a self-propagating combustion wave that proceeds along the active

element at a constant velocity. The burning process in pyrotechnic time delays is analogous to the Self-propagating High Temperature Synthesis (SHS) method for ceramics. The latter is used to synthesize high refractory and abrasive compounds, e.g. borides, carbides, nitrides, silicides as monolithic components with desirable structural homogeneity (Munir, 1988).

1.2 Conventional delay composition

Delay elements in Shock Tube detonators are used to provide a delay between the time of ignition (from the spit of a Shock Tube) to the time of initiation of the explosive base charge. Typically delay times may vary from 20 ms to 10 s. This delay time is governed by the type of composition used in the element and the length of the element. Commercial shock tube detonators can have a 1, 2 or 3 element stack depending on their delay. All detonators have a sealing element with a narrow internal bore of pyrotechnic. This composition forms a hot slag once burnt that seals the element column and prevents venting of gases. This is critical in driving the burning front forward in a controlled manner. For the short period delays the sealing unit is the only element in the detonator and it thus acts as the timing element. For delays 150 – 1500 ms, the element stack comprises additional timing elements. For long time delays a starter element is required due to the insensitivity of the compositions used for the timing element. Process constraints restrict the length of the elements between 5 and 25 mm (to be extended to 40mm).

The pyrotechnic composition contains two or more reagents (fuel and oxidant) capable of a highly exothermic, propagating oxidation-reduction reaction. The most commonly used combinations are Si/Pb_3O_4 for short-period delays (SPD) ranging between 0.5 and 1000 ms and Sb/$KMnO_4$ for long period delays (LPD) between 0,5 and 13 seconds. Silicon is invariably used as the fuel although different grades of different particle size may be used. Burn rate is commonly controlled by the choice of oxidant. Typical oxidants include: red lead (Pb_3O_4), lead dioxide (PbO_2) and barium sulphate ($BaSO_4$).

1.3 Purpose of the present study

This project is part of a larger research effort with the ultimate objective of developing "green" pyrotechnic delay compositions that:

- Are easy and safe to process into delay elements,
- Burn in a lead or rigid tube within a specific burning speed range (from ±4ms/mm to ±250ms/mm),
- Feature highly consistent ignition and burn rate performance (batch variation <2%), and
- Consist of a single fuel in combination with a single oxidant system together with additives for modulating burn rate

This study considers bismuth oxide and antimony hexitatridecoxide as potential replacements for the current lead and barium-based compounds. Lead-based compounds are highly toxic and their use needs to be curtailed. The lead tubes that are currently used will ultimately also have to be replaced (De Vito, 1995).

Bismuth subcarbonate ($(BiO)_2CO_3$) and bismuth oxide (Bi_2O_3) are much less toxic than lead compounds (Kruger *et al.*, 1985). Bi_2O_3 is formed when $(BiO)_2CO_3$ is thermally decomposed. It was selected for study because of its potential to replace red lead in millisecond pyrotechnic delay compositions. Attempts were made to increase burn rates in the Si-Bi_2O_3 system by using additives such as boron, boric oxide and potassium permanganate.

Antimony hexitatridecoxide (Sb_6O_{13}) was investigated as a potential replacement of barium sulphate in long-period delays. It was prepared by an 8-hour thermal decomposition of colloidal antimony pentoxide (Sb_2O_5) at 315°C. In this case the influence of inert diluent (fumed silica) on the minimal burning rate was considered.

Lead tubes have found widespread use in delay elements owing to their considerable malleability. It allows facile compaction of the powder by a tube rolling process. Environmental concerns are restricting the use of lead-based materials. In future the lead tubes also need to be replaced. Consequently, the use of aluminium and

ceramic (alumina or pyrophillite) rigid delay were investigated. In these the effect of core diameter on the burn rate was determined.

2 Literature Review

2.1 Introduction

Delay elements in shock tube detonators are used to provide a delay between the times of ignition (e.g. from the spit of a shock tube) and initiation of the explosive base charge. The delay element system is an assembly comprising an ignition source, a small-diameter tube containing a compressed composition and an ignition transfer system (Wilson and Hancox, 2001). The type of composition, the dimensions of the element, i.e. its length and diameter, and the material of construction of the tube govern the delay time. A typical pyrotechnic delay composition consists of a fuel and an oxidant in combination with an optional binder. It is capable of an exothermic oxidation-reduction reaction. Following ignition, a combustion wave travels down along the tube at a constant velocity that ensures the transmission of initiation impulse to the detonator in a precisely adjustable time interval.

Preferred delay compositions will burn in an essentially gasless fashion (volume of gas evolved less than 10 cm^3/g of mixture (Charsley *et al.*, 1980)) and at a constant predetermined rate. The reaction must be exothermic, self-sustained and self-contained (Conkling, 1996).

2.1.1 Delay elements

A 'delay element' assembly consists of an ignition source, a tube filled with a pressed pyrotechnic composition and an ignition-transfer system (Wilson and Hancox, 2001). The combustion process of the pyrotechnic composition provides the required delay time interval between successive mechanical, electric or explosive events. Typically this ranges from a few tens of milliseconds to several minutes.

Any composition will take a finite time to burn over a given length. However, the requirements of safety, time reproducibility and ignition transfer reliability, particularly in modern military applications, have resulted in the development of specific

formulations known as pyrotechnic delays. Compositions of this type, when consolidated into a tube, burn at reproducible linear rates.

2.1.2 Pyrotechnic delay compositions

Until World War II, black powder was the basis of virtually all delay elements. It provides quite accurate time intervals. Black powder consists essentially of a 75:15:10 KNO_3–charcoal–sulphur composition. The drawback is the significant volume of permanent gas formed during combustion (about 300 ml/g of mixture) (Ellern, 1968). Modern weapons require higher performance levels with respect to reliability and reproducibility under a wide range of environmental conditions (pressure, temperature, moisture). This led to the replacement of the gassy delay systems with gasless delays. Actually, the latter are not exactly gasless as they do produce a small amount of permanent gas during combustion. However, they do provide an advantage with respect to greater burn stability: The burn rate is less affected by pressurisation of the burning front. These delay elements provide constant time intervals unaffected by external conditions. Time delays are the same whether the system operates at great depth underwater or in the vacuum of space. Moreover, hermetically sealed delay elements incorporating gasless delays can be stored for long periods without deterioration (Wilson and Hancox, 2001).

Table 2.1. Common oxidants and fuels used in time delay formulations (Krone *et al.*, 1992)

Oxidants	Fuels (non metals)	Fuels (metals)
Chlorates	Boron	Aluminium
Chromates	Carbon	Chromium
Dichromates	Phosphorus	Iron
Iodates	Selenium	Magnesium
Nitrates	Silicon	Manganese
Oxides	Sulphur	Molybdenum
Perchlorates		Titanium
Peroxides		Tungsten
Permanganates		Zirconium
Sulphides		

Table 2.1 lists some of the materials currently used in pyrotechnic delay formulations. Preferably the formulation should be non-hygroscopic; stable during handling and compaction; not affected by temperature; be readily ignitable and react without releasing gases to minimise the effects of pressure on the burn rate. In addition, a relatively low melting point or a polymorphic transition is also beneficial (McLain, 1980).

2.2 Solid State Reactions

2.2.1 The solid state

Most solids are crystalline in nature, i.e. they have a homogeneous structure in which the constituent atoms are arranged in a regularly repeated pattern. These repeated units are linked together in different ways: covalent bonds, ionic, metallic, or sometimes hydrogen and Van der Waal's bonds. The physical properties of a solid depend largely on the bonding forces and the specific crystal structure. With pyrotechnics the crystal habit, i.e. morphology also plays an important role (Kosanke *et al.*, 2000). However, the reactivity of a solid is highly dependent on the presence of imperfections such as lattice defects in the bulk solid (McLain, 1980).

2.2.2 Lattice defects

Some of defects that play a major role in the reactivity of solids are:

a) *Inherent defects*: These are essentially the Frenkel and Schottky defects, related to interstices and vacant sites in the lattice respectively.

b) *Non-stoichiometric defects*: It is well known that many chemical compounds deviate from stoichiometry; this is the case with some iron oxides, e.g. $Fe_{1-x}O$, due to the presence of some cation vacancies.

c) *Dislocations*: These may form as the growing crystal acquires more molecules that do not fit properly into the normal pattern. They are generally located between particle boundaries.

It has also been observed that most reactions of a liquid with a crystal begin at defect locations where bonds have been weakened (McLain, 1980).

2.2.3 Solid-state reactions

Reaction between a metal and a non-metal proceeds by two possible mechanisms: either the non-metal migrates through the product layer to the metal interface, or the metal migrates in the reverse direction. Since the reactant can migrate through the ionic product layer only as ions, electrons must also accompany the ionic migration. It appears obvious that reaction will not take place if the product layer is not capable of conducting electrons (McLain, 1980)

In the course of a solid-solid reaction, different reaction steps such as nucleation, growth, and transfer of matter across phase boundaries (by diffusion) occur. Besides defect thermodynamics, the diffusion theory forms the basis for the explanation of solid-solid reactions (Schmaltzried, 1976).

The role of defects in semi-conductors may be illustrated using the following reaction (McLain, 1980):

$$Ge + 2\ MoO_3 \rightarrow GeO_2 + 2\ MoO_2$$

Ge doped with n-type dopant (As and Sb) reacted with MoO_3 much faster than Ge doped with p-type dopants (Ga and In). The reactivity of Ge also depended on the concentration of the dopants. Increasing the concentration of the n-type dopants increased the rate of reaction, whereas increasing the concentration of p-type dopants decreased it. This observation is in agreement with the postulate stated below.

An oxidation-reduction reaction necessitates the transfer of electrons and can usefully be compared with semi-conductor activity. The reducing agent is the electron donor and the oxidising agent is the electron acceptor. This is analogous to the activity at an n-p semi-conductor junction where the n-type crystal creates the space charge potential by donating electrons to the p-type crystal. Therefore, an n-type reducing agent (Si doped with As) should be more reactive than a p-type (Si doped with Al) (McLain, 1980).

2.2.4 Solid-liquid reactions

Howlett *et al.* (1974) have shown that for the B-$K_2Cr_2O_7$ system, the ignition process is dependent on the transport of matter through a liquid phase. The combustion zone then propagates as a molten front.

Some eutectic oxide compositions have been used to increase the velocity of the wave front. They probably improve the reaction kinetics by increasing the interface between reactants. In these systems the surface tension of the liquid phase is relevant, because it determines the wettability of the granular reactants. Tribelhorn *et al.* (1995b) noted that the surface tension of Zn at its melting point is high compared to other low melting point metals, i.e. about twice that of Sb and Pb. Therefore, the movement of liquid Zn through pores and channels does not occur readily because the oxidant surfaces are not easily wetted.

2.2.5 Solid-solid and solid-gas reactions

Figure 2.1 illustrates the differences in the burning behaviours of loose and consolidated (compressed or compacted) powders. (Wilson and Hancox, 2001).

(a) Loose composition

Figure 2.1(a) shows a container filled with a loose pyrotechnic composition. An uncontrolled reaction ensues on initiation of the reaction because of the low bulk density of the filling, the travel of combustion products (gases, liquid and thermal radiation) and the added hot air through the voids. This may eventually lead to an explosion because of the confinement imposed by the container.

(b) Consolidated composition

By contrast, as shown in Figure 2.1(b), the compressed sample does not allow much motion for the combustion products through the consolidated column. Combustion is confined to a relatively thin propagation zone known as the 'burning front'.

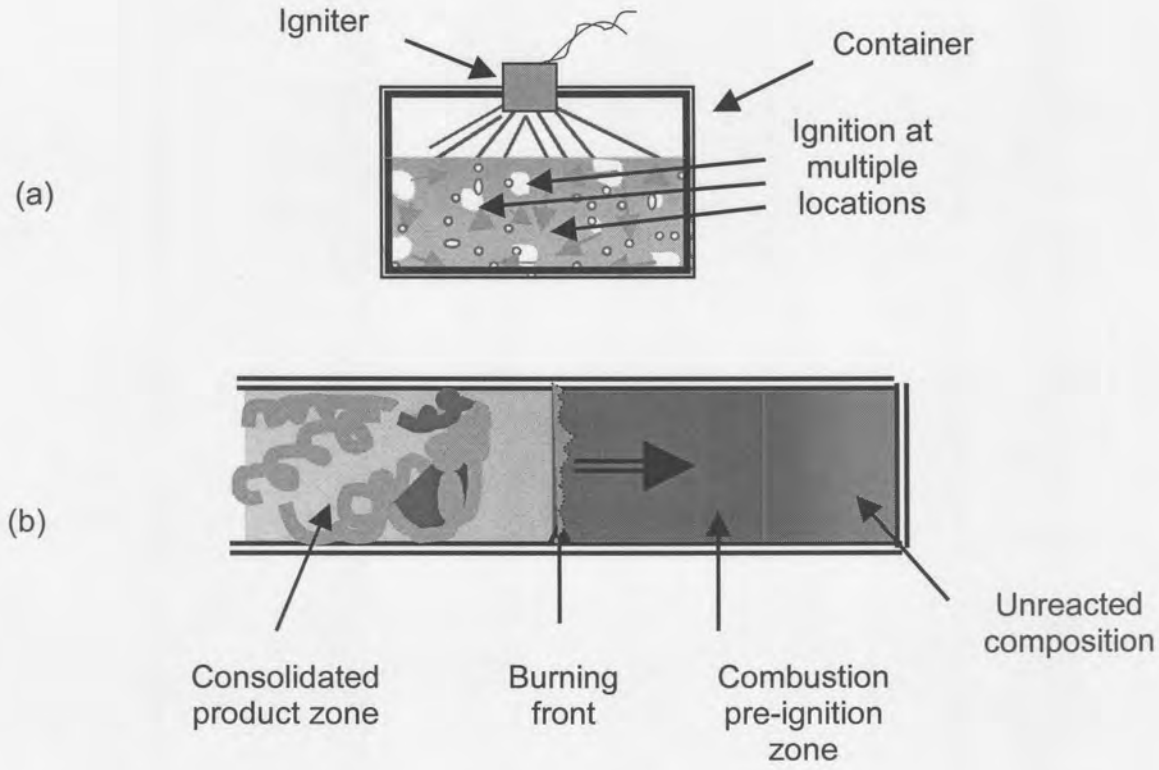

Figure 2.1 Combustion in the loose and consolidated states

Tribelhorn *et al.* (1995a) showed that pyrotechnic systems differ with respect to their sensitivity to compaction. The burn rate in the Fe/BaO_2 system initially increases with increase in compaction pressure. Increase in compaction pressure increases interparticle contact and this aids solid-solid reactions. At higher compaction pressures the rate decreases again. This suggests that gas transport ahead of the burning front is important. In fact it was concluded that the combustion wave in this iron system is preceded by a flow of oxygen generated by the decomposition of the oxidant.

However, in other systems, e.g. $Zn/KMnO_4$, the burning rate is decreased by compaction (Tribelhorn *et al.,* 1995b). This behaviour suggests that in this case the reaction rate is determined by solid-gas reactions: Oxidants such as SrO_2 and $KMnO_4$ decompose without melting to produce oxygen gas and a solid residue. Increased compaction may decrease the surface accessible to the oxygen gas or

may trap the gas in closed pores. In loose powders the oxygen gas flows is not impeded and burning is fast.

Burning in the Sb/$KMnO_4$ system also occurs via gaseous intermediates. In this case the O_2 (g) arised from the decomposition of the oxidant and possibly even the Sb_2O_3 reaction product (Beck and Brown, 1986). The Zn /Pb_3O_4 system is even more complex. Here the gas phase contain Zn and Pb vapour as well as O_2 (g) generated by the decomposition of the oxidant.

2.2.6 Reactivity

Chemical reactivity of solids is affected by the degree of lattice vibrations. As temperature rises, crystal atoms or ions vibrate with increasing amplitude about their average positions in the lattice. This can be thought of as the loosening of the bonds holding the solid together. Diffusion is enhanced and the atoms may exchange positions. At a sufficiently high temperature this leads to melting. In addition, at a lower temperature this may induce a transition from one solid state to another, i.e. a phase change.

Tamman used the ratio of the temperature of the solid to its melting point as a rough measure of lattice loosening (Kosanke and Kosanke, 1997). Ionic surface mobility becomes effective at $T/T_m \approx 0{,}3$ and lattice diffusion at $T/T_m \approx 0{,}5$ (McLain, 1980).

Enhanced reactivity is observed near the phase transition temperature, due essentially, to a similar occurrence of lattice disturbances. This is called the 'Hedvall effect' (McLain, 1980).

McLain (1980) lists the following important factors that influence reactivity:

- Deviations from the normal crystallographic or amorphous structure of a substance
- Lattice defects in the form of hereditary structures
- Formation of imperfect structures, e.g. transition from one modification to another on thermal decomposition
- Presence of guest particles in the lattice

- Differences in the crystallographic formation of different surfaces
- Corrosion
- Adsorption and catalysis
- Irradiation by absorbable wavelength
- Changes in the magnetic state
- Changes in the electric state

Hereditary structures

The history of the sample and the way in which the mix was crystallised, its impurities and defect content, all influence its further behaviour. For example, sulphate-derived oxide (Fe_2O_3) is more reactive than Fe_2O_3 derived from iron oxalate despite the fact that the former had a larger average particle size (McLain, 1980). X-ray powder diffraction patterns revealed that the sulphate-derived Fe_2O_3 was less crystalline.

Crystal shape

The reactivity of $KClO_3$ in match-head formulation decreases as the crystal changes from needles to thin lamellae to near-spherical nodules (McLain, 1980). Kosanke and co-workers (2000) noted the same phenomenon with respect to the effect of particle shape on reactivity. They found that, for the same nominal mesh size, flakes have the greatest reactivity and that they can be raised more quickly to their ignition temperature.

Mechanically enhanced reactivity

Milling, pulverising, atomising and grinding are considered to be interesting techniques for breaking down as many atomic bonds as possible before the materials are used in combination with another reactant.

Fracturing a macrocrystal creates new surfaces, edges and corners where the atoms are not bonded as strongly as internal atoms. This enhances the reactivity. Similarly milling enhances reactivity more by introducing lattice deformation and distortions rather than by reducing particle size (McLain, 1980).

Addition of particles – doping

Supersensitive $KClO_3$: Doping $KClO_3$ with $Cu(ClO_3)_2$ made it supersensitive to the extent that its mixtures with sulphur were capable of a spontaneous high-order detonation (McLain, 1980).

Highly reactive Fe_2O_3: Doping by co-crystallisation also makes Fe_2O_3 more reactive (McLain, 1980). The doping was accomplished by growing crystals of $CuSO_4.FeSO_4.xH_2O$ or $NiSO_4.FeSO_4.xH_2O$ in an acidic solution of the salts. The crystals were subsequently decomposed in O_2 at 200 – 250°C to produce Fe_2O_3. This improved the calorific value of a 50:50 Fe_2O_3-Ti mixture.

Reactive NiO: Doping of NiO with LiO_2 and Cr_2O_3 had a positive effect on the reactivity of NiO.

Fluxes

Fluxes are materials that reduce the effective melting temperature of a mixture. They introduce an amount of liquid phase that accelerates the solid-solid reactions.

Presence of water

The role of water vapour as catalyst and accelerator in pyrotechnic reactions is well known. The burning rate and colour of firework star compositions depend markedly on very small changes in the moisture content. A very small amount of 0.1% H_2O (moisture content) seems to be most effective. Above this proportion, it was observed to have an inhibiting effect (McLain, 1980). Moreover, it is well known that the presence of water vapour has a noticeable effect on sintering, structural rearrangement and crystal coarsening of oxides.

These phenomena are ascribed to the chemisorption of water vapour on oxide surfaces and interfaces. This leads, among other things, to an increase in the surface and particle boundary mobility of ions (Ubaldini *et al.*, 2003).

Corrosion inhibition

Chemical treatment to protect powder against corrosion is also a form of inhibition. This process does, therefore, lengthen the life of more reactive materials, including Al, Zn and Mg (McLain, 1980).

2.3 Pyrotechnic ignition and propagation

Kosanke and Kosanke (1997) provide an excellent review of the ignition and propagation processes in pyrotechnics. They describe pyrotechnics as mixtures of fuels, oxidisers and additives that are designed to produce energy on demand in the form of heat, light, sound, etc. Kosanke and Kosanke (1997) define ignition as the initiation of the self-sustained burning of the pyrotechnic material.

2.3.1 Thermodynamics of solid-solid reactions

Gasless pyrotechnic time delays are based on solid-solid oxidation-reduction reactions between an oxide and a metallic or non-metallic element. A unique characteristic of such reactions is the virtually total dependence on a favourable enthalpy change (ΔH_R). The second law of thermodynamics demands, as condition for the spontaneity of a reaction conducted at constant temperature and pressure, that the Gibbs free energy change, ΔG_R, must be negative:

$$\Delta G_R = \Delta H_R - T\,\Delta S_R \qquad (1)$$

The entropy change, ΔS_R, for reactions yielding solid products is usually very small (Spear, 1976). In addition, Kopp's rule states that the sum of the ionic specific heats remains unchanged. Thus, the only way in which ΔG_R can be large and negative is for ΔH_R to be negative. Therefore, the reaction must be exothermic.

Ellingham diagrams (Ellingham, 1944) show the variation with temperature of the standard Gibbs free energy of formation (ΔG^o) of the oxides or sulphides of metals and non-metals. They indicate the relative tendencies of the elements to combine

with oxygen or sulphur. This permits rapid evaluation of the reducibility for a specific oxide or sulphide by a given elemental reducing agent. Figure 2.2 shows the Ellingham diagram for selected oxides with oxygen taken a gas at a partial pressure of 1 atm. In this figure the formation of an oxide from its element is written in the following standard form:

$$\frac{2x}{yz} M_z + O_2 = \frac{2}{y} M_x O_y$$

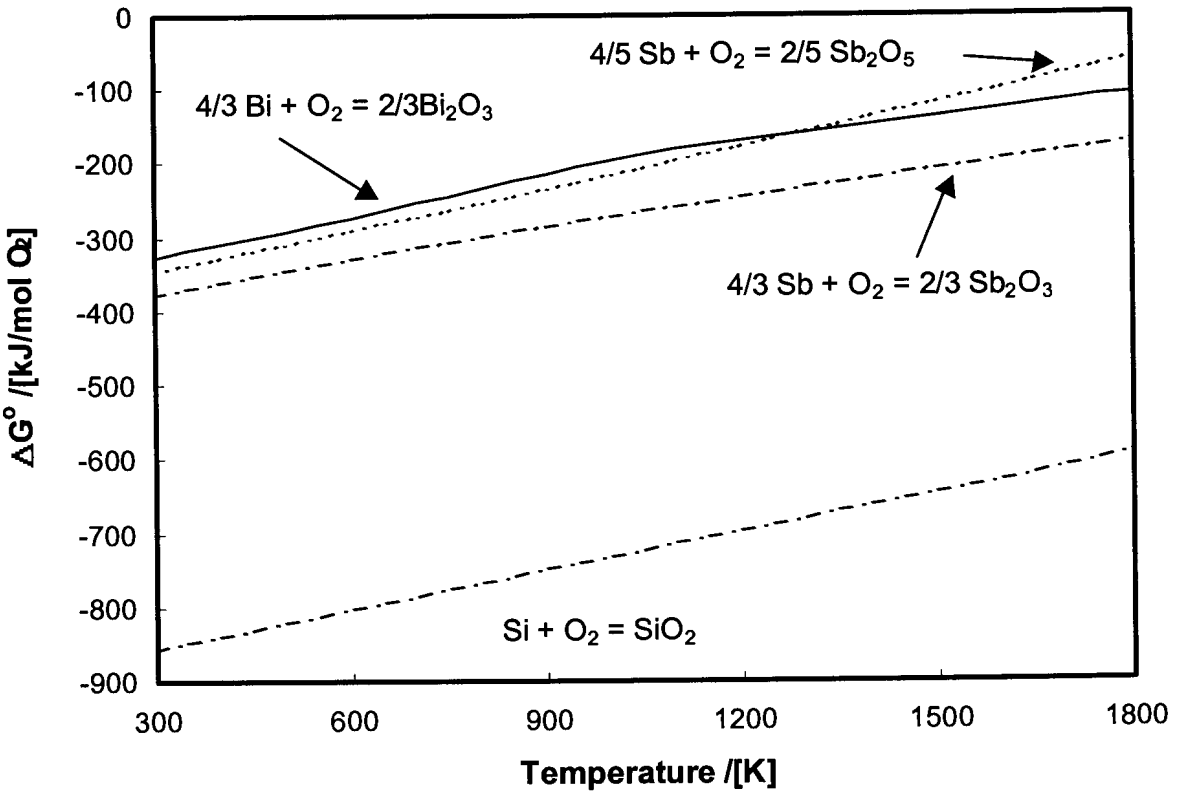

Figure 2.2 Ellingham diagram for oxides of interest in the present study.

For example for bismuth and silicon the oxidation reactions are:

$$Si + O_2 = SiO_2 \quad (I)$$

$$4/3\ Bi + O_2 = 2/3\ Bi_2O_3 \quad (II)$$

The reduction of bismuth oxide by silicon is expressed by:

$$2/3\ Bi_2O_3 + Si = 4/3\ Bi + SiO_2$$

Note that the net reaction is obtained by adding the "reverse" of the second reaction (II), i.e. in the form of a reduction reaction, to the first reaction (I). Note that O_2 then

appears on both sides and thus cancels out! Thus the difference at a given temperature between the values of ΔG^{o} on the diagram for these two reactions represents the Gibbs free energy or driving force of the reaction.

The lower down on the diagram the curve for a particular oxide lies, the greater is its stability and the lower is its reducibility (Ellingham, 1944). In Figure 2.2, for example, the curve for the formation of the oxide of silicon lies lower than that of bismuth oxide. This implies a positive tendency for elemental silicon to displace bismuth from its oxide.

2.3.2 Adiabatic reaction temperature

Consider the following irreversible reaction:

$$A(s) + B(s) \rightarrow C(s)$$

The adiabatic reaction temperature T_{ad} is the maximum temperature to which the product C, with melting point T_m, can be raised as a result of the exothermic heat of reaction. The adiabatic reaction temperature, for the reaction starting at 298°C, is calculated as follows (Zuhair, 1988):

a) If $\Delta H_{R,298} < \int_{298}^{T_m} Cp_s dT$, then $T_{ad} < T_m$ and it can be calculated from:

$$\Delta H_{R,298} = \int_{298}^{T_{ad}} Cp_s dT \qquad (2)$$

b) If $\Delta H_{R,298} > \int_{298}^{T_m} Cp_s dT$ then T_{ad} is evaluated from:

$$\Delta H_{R,298} = \int_{298}^{T_m} Cp_s dT + \Delta H_m + \int_{T_m}^{T_{ad}} Cp_l dT \qquad (3)$$

Preheating of the reactant mixture will result in a higher T_{ad}.

When no phase transition occurs and physical properties can be assumed constant the adiabatic reaction temperature is given by:

$$T_{ad} = T_o + \frac{\Delta H_R}{c_p} \tag{4}$$

2.3.3 *Ignition*

The combustion of the delay composition starts with the initial process of ignition. Ignition may be defined as the visible appearance of a steady combustion. External factors influencing ignition include the heating rate, the ambient temperature and the size, geometry and nature of the surface of the sample. Thus Pickard (2002) defines the critical ignition temperature, T_{ign}, as the minimum temperature to which a pyrotechnic charge of specified size, shape and boundary constraints must be heated in order to induce thermal runaway.

Figure 2.2 shows a schematic plot of the heat generated versus heat loss as a function of temperature (Kosanke and Kosanke, 1997). The generation of heat initially increases exponentially with temperature. This accords with the Arrhenius temperature dependence of the rate constants for oxidation. However, at higher temperatures the reaction rate becomes diffusion limited and the rate of heat generation tapers off. The rate of heat loss is roughly proportional to the difference in temperature between the flame and the surroundings.

The heat generation and heat loss curves intersect at three locations in the Frank-Kamenetzky plot shown in Figure 2.2. At these temperatures the rate of heat generation balances the rate of heat loss. Point A corresponds to a low temperature oxidation of the fuel. Point C corresponds to the equilibrium combustion temperature. Point B is unstable - at temperatures slightly lower than T_B the rate of heat loss exceeds the rate of heat generation and the material will cool down to T_A. At temperatures slightly above T_B the exothermic heat generated will exceed the heat loss and the sample will spontaneously increase in temperature to the steady state flame temperature T_C. Hence T_B corresponds to the ignition temperature under the test conditions. It is defined as the lowest temperature at which the sample

spontaneously ignites as witnessed by a sustained glow, the appearance of a flame or even an explosion.

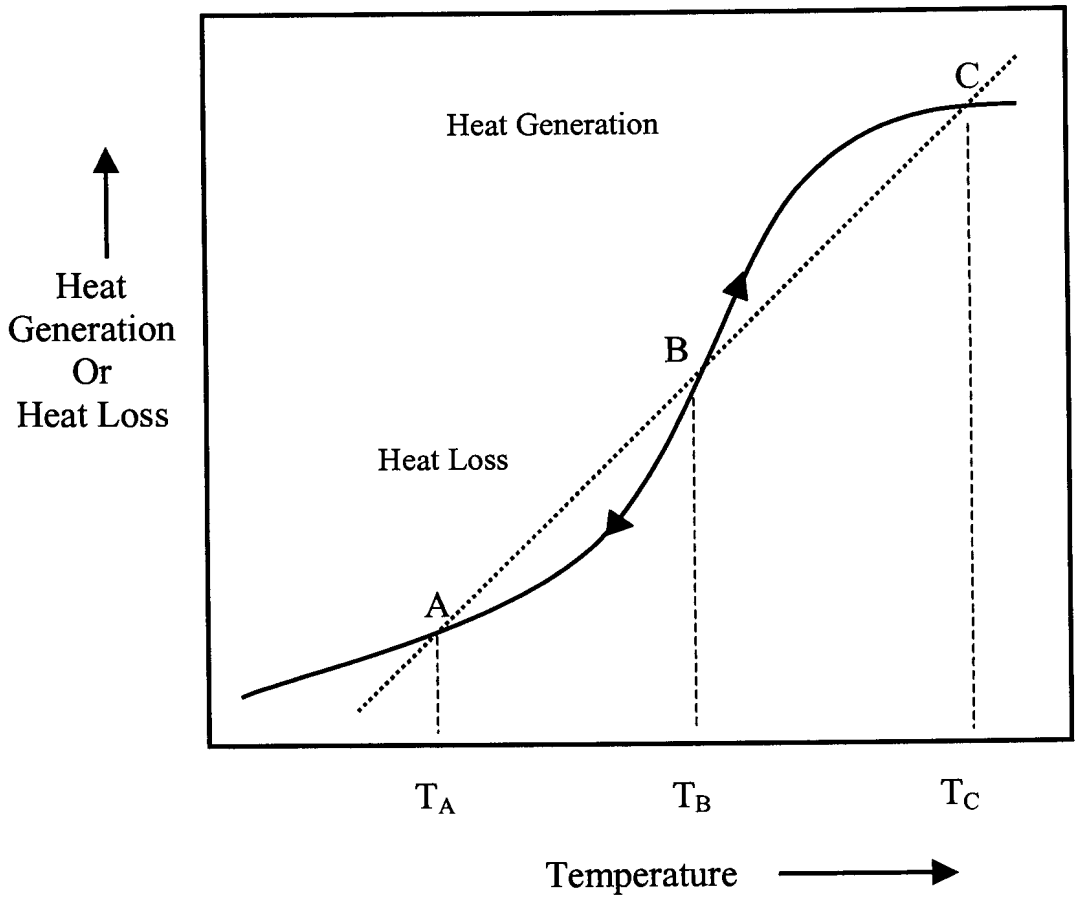

Figure 2.3 Frank-Kamenetzky plot of heat generation and heat loss versus temperature (Kosanke and Kosanke, 1997)

2.3.4 Solid state reactions: the importance of diffusion

Tribelhorn *et al.* (1995c) studied the burning behaviour of Zn/$KMnO_4$ mixtures in the composition range 30–75% Zn formed at compaction pressure up to 150 MPa. Based on thermal analysis results, they suggested that the Zn diffuses into the solid residue formed during the first stage of $KMnO_4$ decomposition. An exothermic reaction starting at 520°C was observed and attributed to the reaction of Zn with this 'K_2MnO_4' residue (Wilson and Hancox, 2001).

Drennan *et al.* (1992) reported on studies of the combustion of various systems, namely the Mn/BaO_2, Mo/BaO_2, Mn/SrO_2 and Mo/SrO_2 systems, and Tribelhorn *et al.*

(1995a) on the Fe/BaO_2 and Fe/SrO_2 systems. If we referred to the corresponding radii of the different metals and ionic species involved in the combustion, the diffusion via cation vacancies in the oxidant structure should be favoured in the BaO_2 lattice rather than in the SrO_2 lattice. However, for comparable oxidation states, the differences between the behaviour of Mn and Mo based on geometry should be small.

It was also observed after examination of the products from the combustion of Zn/peroxide systems that oxidation of the metals was generally incomplete, probably because of the presence of protective oxide layers (Tribelhorn *et al.*, 1995b).

The above observations lead one to the conclusion that diffusion effects will almost always affect the reaction rate in solids. Diffusion aspect must therefore be taken into account when modelling the solid-state reactions of pyrotechnic compositions.

2.3.5 Kinetics of isothermal solid-state reactions

Beretka (1984) provides a critical review of the kinetic equations proposed for isothermal solid-state reactions. He found that Jander's model for three-dimensional diffusion best describes experimental data:

$$(1-(1-x)^{1/3})^2 = k\,t \tag{5}$$

Here x is the degree of conversion and k is an apparent rate constant. In practice, the conversion values of the individual particles vary because of gradients in the temperature and variations in the partial pressure of evolved gas within the sample matrix caused by mass and the heat-transfer phenomena (Koga and Criado, 1998).

2.3.6 Apparent kinetic constant

It is conventional to assume that the rate constant k follows simple Arrhenius kinetics (Laye, 1997):

$$k = k_o \exp(-E_a / RT) \tag{6}$$

Boddington *et al.* (1986) advocate evaluation of the activation energy E_a for pyrotechnics from time-to-ignition data obtained under isothermal conditions. The usual route to determine the activation energy is from the gradient of $ln\ t_{ign}$ plotted against $1/T$, i.e. assuming relationships of the form

$$t_{ign} = \exp(E_a/RT) + C \tag{7}$$

Apparent activation energies determined using this method or by using temperature profile analyses yield values about an order of magnitude less than results obtained by thermal analysis (Laye, 1997). Such low activation energies for the pyrotechnic reaction imply that they are controlled by a diffusion mechanism (Boddington *et al.*, 1990). To correct for diffusion effects, Laye (1997) proposed the apparent rate constant should be viewed as a combination of a "true" Arrhenius reaction rate constant and an activated diffusion:

$$\frac{1}{k} = \frac{1}{k_{Ar}} + \frac{1}{BT^n} \tag{8}$$

The factor B in equation (7) represents a diffusion coefficient. Equation (7) combines the Arrhenius behaviour at low temperature, which predicts a rapid raise in temperature, with diffusion-controlled behaviour at high temperature, where the rate becomes less dependent on temperature.

2.3.7 Propagation Index

Once the exothermic reaction has been initiated, the temperature will rise rapidly, at least in the neighbourhood of the reaction sites. Such temperature rises can produce phase changes and/or oxidant decompositions, which can significantly alter the mechanisms and the overall course of the reaction. It is now important to establish the degree to which the reaction will be self-sustaining.

Excessive heat loss to the environment is the main reason for failure to propagate through the entire length of the column. This is more likely to occur in small diameter

metal tubes and at low ambient temperatures. The propagation index (PI) provides an indicator for the ability of a gasless delay composition to sustain combustion McLain (1980):

$$PI = \Delta H / T_c \tag{9}$$

The most effective delay composition is the one with the highest index.

2.3.8 *Combustion wave velocity for gasless combustion*

Booth (1953) studied the burning of compressed powders in the form of cylindrical rods. He observed that, when ignited at one end, the rate of progression of the reaction zone along the axis is fairly uniform and reproducible for a given powder. This type of behaviour, generally referred to as 'layer- to-layer' burning, is observed only when the reaction is strongly exothermic, i.e. when a considerable amount of heat is evolved in the chemical change (Booth, 1953).

The combustion event in the time delay element is governed by a number of parameters. The thermal diffusivity of the mixture is important as wave propagation depends on repeated re-ignition of adjacent layers along the burning path. Good mixing and adequate inter-particle contact between reactants is required for stable and reproducible burning owing to the low values of the diffusion coefficients (Tribelhorn *et al.*, 1995a).

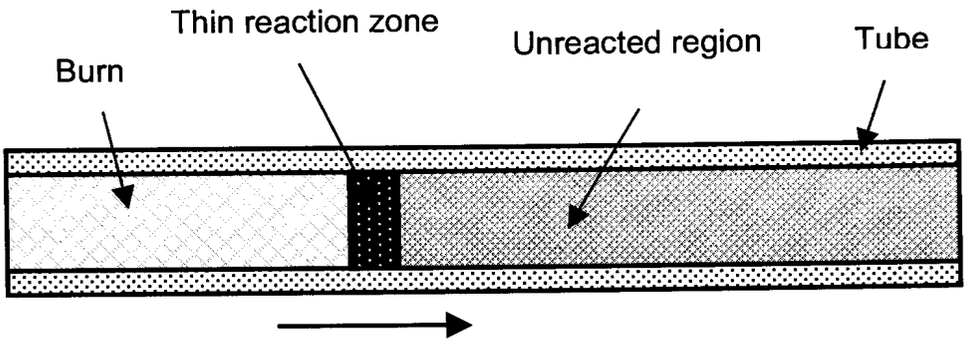

Figure 2.4 Schematic of the burning event in a time delay element

Figure 2.4 shows a schematic of the burning event inside a tubular time delay element. The reaction zone is confined to narrow region. Ideally the burning front

propagates along the tube at a constant pace. The objective here is to relate the rate of burning to the physical properties of the pyrotechnic system. Only the simplest theory (Zuhair, 1988; Khaikin and Merzhanov, 1966), that relates the burning speed to the physical properties of the mixture, is considered here. The following simplifications make the problem mathematically tractable (Booth, 1953; Zuhair, 1988):

- Mass diffusion is neglected at the macroscopic level as in solids heat conduction occurs much faster (Tribelhorn *et al.*, 1995a).
- No heat transfer due to radiation.
- The lateral loss heat is negligible.
- The thermal properties and the density are independent of the temperature and the composition.
- Propagation is one-dimensional.
- Constant physical properties (i.e. independent and temperature)
- Phase transformations and heat loss to the environment are ignored.
- Reaction kinetics can be modelled in terms of an exothermic, n^{th} order, solid-state chemical reaction with an Arrhenius-type temperature dependence for the rate constant:

$$\frac{dx}{dt} = k(1-x)^n \tag{10}$$

with

$$k = k_o e^{-E_a/RT} \tag{6}$$

With the above assumptions the propagation of a combustion wave is described by the one-dimensional energy equation for unsteady heat conduction with a heat source:

$$\rho c_p \frac{\partial T}{\partial t} = \lambda \frac{\partial^2 T}{\partial z^2} + \dot{q} \tag{11}$$

The rate of heat release is proportional to the rate of reaction and the reaction enthalpy, ΔH_R:

$$\dot{q}_R = \rho \Delta H_R \frac{dx}{dt} \tag{12}$$

If the burn rate is constant, it is characterised by a combustion wave that travels through the element at a constant pace as shown in Figure 2.5. Under steady state conditions the temperature profile is invariant and it can be expressed in terms of a single variable: $\eta = z - ut$, i.e.

$$T(z,t) = T(\eta) = T(z - ut) \tag{13}$$

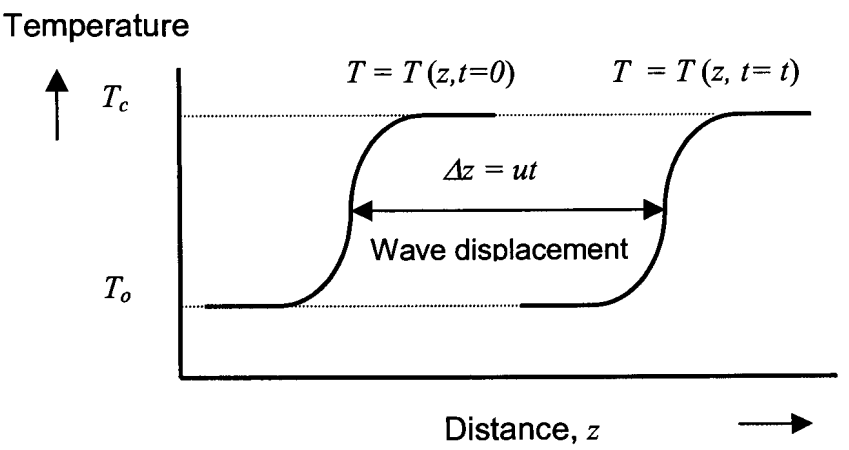

Figure 2.5 The combustion wave travels at a velocity u along the solid filling

This allows equations (1) and (2) to be transformed into ordinary differential equations:

$$\frac{dx}{d\eta} = -\frac{k}{u}(1 - x)^n \tag{14}$$

$$\rho u c_p \frac{dT}{d\eta} + \lambda \frac{d^2T}{d\eta^2} = u \rho \Delta H_R \frac{dx}{d\eta} \tag{15}$$

The boundary conditions are:

$$\eta \to -\infty \qquad T = T_c \qquad \frac{dT}{d\eta} = 0 \qquad \eta = 1 \tag{16a}$$

$$\eta \to \infty \qquad T = T_o \qquad \frac{dT}{d\eta} = 0 \qquad \eta = 0 \tag{16b}$$

Equation (15) can be integrated from $-\infty$ to η:

$$\rho u c_p (T - T_c) + \lambda \frac{dT}{d\eta} = -u \rho \Delta H_R (1 - x) \tag{17}$$

Dividing equation (10) by (12) yields:

$$u^2 \frac{dx}{dT} = \frac{\lambda k (1 - x)^n}{\rho c_p (T_c - T) - \rho \Delta H_R (1 - x)} \tag{18}$$

At this stage the "narrow reaction zone" hypothesis is invoked. It states that the reaction rate is negligible except at $T = T_c$ (Frank-Kamenetski, 1938; Khaikin and Merzhanov, 1966):

$$u^2 \frac{dx}{dT} = -\frac{\lambda k (1 - x)^{n-1}}{\rho \Delta H_R} \tag{19}$$

In principle this equation can be integrated using separation of variables. Unfortunately an analytic solution to the temperature integral is not possible. However, the temperature term can be approximated as follows:

$$k(T) = k_o e^{-E/RT} \approx k_o e^{-2E/RT_c} e^{ET/RT_c^2} \tag{20}$$

Note that this approximation matches both the value and the slope of the rate constant $k(T)$ at $T = T_c$. With this substitution the integration can be performed with the result (Frank-Kamenetski, 1938):

$$u = \sqrt{g(n) \frac{\lambda k_o R T_c^2}{\rho E_a \Delta H_R} \exp\left(-\frac{E_a}{R T_c}\right)} \tag{21}$$

with $$g(n) = 2 - n \tag{22a}$$

Equation (22a) is only correct for a zero order reaction where the reaction temperature approaches the adiabatic reaction temperature. For higher order

reactions the reaction rate is also significant at other temperatures. Khaikin and Merzhanov (1966) derived a revised expression for $g(n)$ using the "thin-zone" approximation:

$$g(n) = 2\left[\Gamma\left(\frac{n}{2}+1\right)\right]^{\frac{2-n}{2}}\left[\frac{n}{2e}\right]^{\frac{n^2}{4}} \tag{22b}$$

The plot shown in Figure 2.5 shows that $g(n)$ is close to unity but that it is a decreasing function of the reaction order n. The maximum value of $g(n)$ = 2 for a zero order reaction.

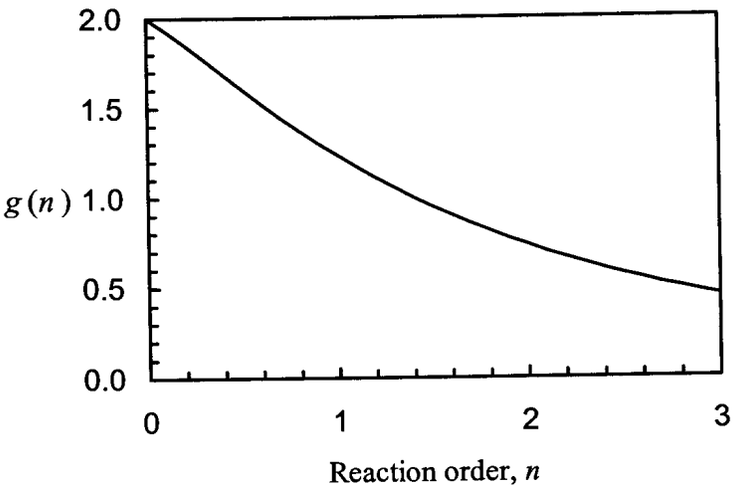

Figure 2.6 Variation of the function $g(n)$ with the reaction order n.

According to equation (21), the combustion wave temperature, T_c, is the most significant variable affecting the burn rate. The reaction temperature can be controlled by adjusting the reagent stoichiometry and by adding inert substances. Equation (21) also suggests that a slow burn speed requires a composition that reacts slowly while releasing a large amount of heat to sustain the thermal wave of reaction.

2.4 Factors affecting the burning rate

Ultimately the intrinsic burning rate of a delay composition is determined by the chemical nature of the ingredients, their relative proportions and the thermo-physical properties of the system. However, apart from those intrinsic to the compositions themselves, a wide range of other factors can influence the burning rate. This includes aspects related to the device into which they are filled and combustion environment itself (Wilson and Hancox, 2001).

2.4.1 Effect of thermal conductivity and density on wave propagation rate

The burning front in a compressed delay composition propagates in a layer-by-layer fashion along the burning path. This requires repeated re-ignition of adjacent layers. According to equation (21) the thermal conductivity and density are the primary physical properties that determine the rate of burning. With all other parameters and properties fixed, it predicts:

$$u \propto \sqrt{\frac{\lambda}{\rho}} \tag{23}$$

From this formula it can be deduced that:

- Increasing the thermal conductivity enhances the burning rates, and
- The more loosely the powder is packed, the more rapid is the burning velocity (Booth, 1953).

The last deduction is counter-intuitive! It should be remembered that the model used is based on apparent rate laws and physical constants that are interrelated. It would in general be difficult to separate individual effects.

Adding inert material changes the thermal conductivity of the mixture. Adding low thermal conductivity fillers, e.g. kaolin, reduces the rate of heat transfer through the mix. Conversely, adding thermally conductive fine Cu and Ag powders to gasless delay compositions can significantly increase the rate of burning (McLain, 1980).

2.4.2 *Thermochemistry and stoichiometry: The heat of reaction*

According to equation (21):

$$u \propto \sqrt{\frac{T_c^2}{\Delta H_R}\exp\left(-\frac{E_a}{RT_c}\right)} \tag{24}$$

In the absence of phase changes and assuming constant physical properties, equation (4) predicts that

$$T_c \propto T_o + \frac{\Delta H_R}{c_p} \tag{25}$$

Equations (25) and (24) indicate that a fuel that produces more heat on oxidation, e.g. boron (ΔH_R = 58,96 kJ/g), will react faster than a less exothermic fuel such as silicon (ΔH_R = 32,40 kJ/g).

Stoichiometry can also influence the product spectrum as shown in Table 2.2 for the reaction of silicon with PbO_2 (McLain, 1980). Such changes can also influence the heat released. This is illustrated in Table 2.3 for the oxidation of manganese metal.

Table 2.2. Reactions of PbO_2 – Si systems (McLain, 1980)

% Si	Reactions	Products
2,3	$Si + 4PbO_2$	$Pb_4SiO_6 + O_2$
3,1	$Si + 3PbO_2$	$SiO_2 + 3PbO + ½ O_2$
4,8	$Si + 2PbO_2$	Pb_2SiO_4
6,0	$2Si + 3 PbO_2$	$2PbSiO_3 + Pb$
8,7	$Si + PbO_2$	$SiO_2 + Pb$
12,6	$3Si + 2PbO_2$	$SiO_2 + 2SiO + 2Pb$
16,1	$2Si + PbO_2$	$SiO_2 + Pb + Si$
22,3	$3Si + PbO_2$	$Pb + Si + 2SiO$

Heat is also removed from the system when a component undergoes a phase change at higher temperature during the combustion process. This has the effect of slowing down the progression of the burning front. Heat loss through the tube walls has a similar effect but is discussed in more detail in Section 2.8.3.

Table 2.3. Effect of reagent stoichiometry on the heat of oxidation of manganese (Wilson and Hancox, 2001)

Stoichiometry	ΔH_R, kJ/g
$Mn_{(s)} + 0{,}5\ O_{2(g)} \rightarrow MnO_{(s)}$	5,43
$Mn_{(s)} + O_{2(g)} \rightarrow MnO_{2(s)}$	5,98
$2\ Mn_{(s)} + 1{,}5\ O_{2(g)} \rightarrow Mn_2O_{3(s)}$	6,07

2.4.3 Effect of gassing

Aldushin *et al.* (1992) and Norgrove *et al.* (1991) investigated the case of a steady combustion wave in a porous reacting mass. They considered the effect of gas formation on the combustion wave. Depending on the confinement conditions, the produced gas moves either forward or backward relative to the flame front (Norgrove, 1991). For a sealed element, the ratio of gas flow forwards to gas flow backwards will depend on the confinement conditions and will change as the flame passes along the delay element.

When the gas moves with the combustion wave, it may assist the propagation of the front by means of convective mechanism (Aldushin, 1992). The travelling gas phase pre-heats the system, increases the adiabatic combustion temperature and increases the rate of burning. The overheating of the combustion zone depends on the proportion of gas present in the system, its thermo-chemical properties and its pressure (Bamford and Tipper, 1969). Aldushin *et al.* (1992) have derived an equation that relates the increase in the adiabatic temperature to the rate of gas convection (backward or forward motion):

$$T_{ad} = T_o + \frac{\Delta H_R}{c_p}\left(1 - \xi\frac{\nu c_{p,g}}{c_{p,s}}\right) \tag{26}$$

For a backward flow of gas through the condensed product, ξ=0 and for a flow accompanying the propagation wave, ξ=1.

Zuhair (1988) has shown that if the reacting powder interacts with the gas phase, i.e. oxygen, its partial pressure must be above the characteristic pressure of dissociation of the oxide formed at the ignition temperature.

2.4.4 Effect of pressure

The burning rate of most pyrotechnic compositions is expected to increase with pressure according to Vieille's law (Bamford and Tipper, 1969):

$$\frac{u}{u_o} = \left(\frac{P}{P_o}\right)^n \tag{27}$$

The constant *n* is system specific and typically varies between 0,1 and 0,6. Its value depends on the amount of gas produced during the combustion.

In practise it is found that burning rate initially increases but that it stabilises or even decreases above a certain threshold limit. Consider, for example, the slow burning B/Si/$K_2Cr_2O_7$ (4:5:91) gasless delay formulation used in accurate missile delay detonators. Its burning rate increases sharply with pressure between 0,1 and 0,4 MPa. Thereafter, the burning rate increase is slower. Above about 2 MPa the burning rate is unaffected by pressure (Howlett and May, 1974).

Other examples include the PbO-Si, Pb_3O_4-Si and $KMnO_4$-Si systems. In all of these the velocity of propagation increases with pressure until a maximum function of composition is reached (McLain, 1980). With the red lead–silicon compositions the burn rate decreases beyond pressures of approximately 6,90 MPa. This effect is attributed to pressure stabilisation of the PbO phase in the reaction mixture (McLain, 1980).

2.4.5 Environmental factors

The temperature of the delay column, both prior to and during combustion, also influences the burning rate. For military and aerospace applications, delay elements

must provide an accurate time interval, which is specified to within certain limits over a set environmental temperature range, often between –40 and +60°C (Wilson and Hancox, 2001).

Depending on the formulation, most gasless delay compositions burn about 25% slower at the lower temperature and 25% faster at the higher temperature than they would at room temperature. Gassy delay compositions are less affected by temperature variations (Wilson and Hancox, 2001).

2.5 Formulating pyrotechnic delay compositions

2.5.1 Fuel

Table 2.4. Heats of combustion for metal fuels at 298,15K (Barin, 1989)

Fuel	Product oxide	-ΔH (kJ /g fuel)
B	B_2O_3	58,9
C	CO_2	32,8
Si	SiO_2	32,4
Al	Al_2O_3	31,1
Mg	MgO	24,7
Zr	ZrO_2	12,0
Mn	Mn_3O_4	8,42
Fe	Fe_3O_4	7,54
W	WO_3	4,59
Sb	Sb_2O_3	2,96

Fuels include metals such as Al, Al/Mg, Cr, Fe, Mg, Zr, W and Zn. Table 2.4 lists the heats of reaction of some metal fuels. Note that fuels are not limited to pure metals and non-metals: alloys such as ferrosilicide ($FeSi_x$) and calcium silicide ($CaSi_2$) (Krone *et al.*, 1992) can also be used. Organic fuels (e.g. sorbitol, hexamethylene tetramine, potassium benzoate, etc.) and some inorganic fuels (C, S, P) generally produce much gas during combustion. This causes pressure build-up that affects the

reaction rate and thus the delay time. As a result, the main charge may be ignited prematurely (Ellern, 1968).

2.5.2 *Effect of metal reductant content on burning rate*

Usually it is found that the maximum burning rate occurs at a somewhat higher reductant content than does the maximum heat of reaction. This displacement is generally greater for metal reductants such as Fe, Sb and Mn and is smaller for non-metal reductants such as S and C or the metalloids B and Si (McLain, 1980). This phenomenon is associated with the effect of heat transfer on columnar burning.

The slope of the burning rate curve is usually steeper below the maximum than above (percentage reductant above stoichiometry). This is ascribed to the fact that the addition of a good heat conductor, such as a metal or a metalloid, causes departure from the stoichiometry, but may increase the thermal conductivity sufficiently to cause a net increase in the burning rate. In effect, an excess of either oxidant or fuel represents an inert diluent. Excess oxidiser acts like a heat insulator and this retards the burning. In contrast, the excess of a conductive reductant accelerates the burning rate (McLain, 1980).

2.5.3 *Silicon as a fuel for pyrotechnic delay composition*

Several workers have investigated the behaviour of silicon as fuel (Al-Kazraji and Rees, 1979; Goodfield and Rees, 1985; Yoganarasimhan, 1987). The oxidation of silicon by gaseous oxygen occurs in the temperature range of 990 to 1200°C. The rate of oxidation in wet oxygen atmospheres is faster than in dry oxygen atmospheres. The kinetic of oxidation in wet and dry atmospheres is a function of the partial pressures of H_2O and O_2 respectively (Rugunanan, 1991a)

The oxidation occurs at the Si/SiO_2 interface and O_2 has to diffuse through the oxide layer for the reaction to occur. The layer of SiO_2 that adheres to the silicon particle surface represents a diffusion barrier. If this coating layer is very compact, further oxidation could be inhibited. The rate of oxidation depends on the thickness of the oxide layer. In general a parabolic rate law describes the oxide growth:

$$AL^2 + BL = t + C \tag{28}$$

Where A, B and C are empirical constants. For thin films (~2nm), the rate of oxide growth is linear:

$$BL = t + C \tag{29}$$

The oxidation of transition-metal silicides was reported to occur at a faster rate than the oxidation of pure silicon and refractory-metal silicides, possibly owing to higher electron mobility (Rugunanan, 1991a).

2.5.4 Oxidisers

The following heavy metal oxides are suitable for used in delay compositions: Fe_2O_3, Sb_2O_3, Cu_2O, Bi_2O_3, Pb_3O_4, PbO_2, ZnO, MnO_2. A recent trend is to use complex oxides, e.g. $Cu_2O.Sb_2O_3$, $ZnO.Sb_2O_3$ or $BaO.MoO_3$ (Krone *et al.*, 1992). Nitrate, chromate, chlorate and perchlorate salts are used for other pyrotechnic effects (light emissions, signalling smokes, whistling sounds, etc.) (Ellern, 1968). Conkling (1996) discusses factors affecting oxidiser selection. The most important factor is the relative affinity towards oxygen between the metals of the oxidiser and the fuel.

2.5.5 Additives

Additives are mixed to the main composition to effect the following: ensure intimate contact between the particles, protect against the environment, premature reaction or to improve mechanical properties. Addition of a third component can alter the burning rate of a binary system. Such additives may be:

- Chemically inert substances
- An additional fuel
- An additional oxidant
- A source of some reactive intermediate.

Suitable agents include:

- *Binders.* Binders are used to maintain the homogeneity of the blended mixture. They also play a minor role as internal lubricants during the compacting phase (Krone *et al.*, 1992). Binders can be organic or inorganic in nature. *Organic binders* include synthetic polymers (polyethylene, polyurethane, polyvinyl chloride and some copolymers), biopolymers (dextrin and starch) and natural resins e.g. gum Arabic and gum acaroid. *Inorganic binders* include gypsum, water glass and bentonite.
- *Formulation aids* include anti-caking agents (pyrogenic SiO_2, Al_2O_3, $CaCO_3$, $MgCO_3$) and lubricants (graphite, talc, wax, Teflon, silicone).
- *Catalysts*: Fe_2O_3, $CuO.CrO_2$, V_2O_5 and MnO_2.
- *Burning rate modifiers*: kieselguhr, diatomaceous earth, fumed silica. Addition of such chemically inert additive may simply reduce fuel/oxidant contact. It may also alter the thermal properties of the system (e.g. additives of high heat capacity may lower the combustion temperature). Inert additives with a low melting point may act as fluxes. Table 2.5 illustrates the use of the inert additive SiO_2 for reducing the burning rate in the $Sb/KMnO_4$ system.

Table 2.5. Effect of SiO_2 on the burning rate of a 30:70 $Sb:KMnO_4$ composition (Beck and Brown, 1986).

SiO_2 content, %	0	7	19
Burn speed (mm/s)	1,9	1,6	1,3

2.5.6 Empirical rules for the design of new mixtures

McLain (1980) recommended that the following rules of thumb be observed when designing a new pyrotechnic mixture:

- Maximise the burning rate for a given mix by using more than the stochiometric proportion of the reducing agent.
- Decrease the heat of reaction to reduce the burning rate: use a metal that produces less heat or reacts in several different ways depending on its

proportion in the mix (e.g. Mn), or add an inert thermal insulator such as powdered glass, kieselguhr, fuller's earth or fumed silica.

- Use tubes with an inside diameter of 6 mm or larger for mixtures which burn slower than 25 mm/s,
- Do not use tubes made from good heat conductors like brass or copper.
- A mixture with the highest possible propagation index should be used to achieve the desired burn rate.
- The following factors should be kept in mind:

  The particle size and size distribution of the constituent powders; the size and chemical nature of guest particles; adsorbed gases on the particle surfaces; the loading method and pressure; the mix homogeneity; temperature and type of ignition; the mix type (low gas or gassy) and the humidity during mixing and loading.

2.6 Review of Selected Pyrotechnic Delay Compositions

2.6.1 Silicon / lead oxides

Silicon/lead oxide preparations have found widespread application as millisecond time delay systems. These gasless delay compositions were formulated to replace the older fuse materials, which were unreliable under low pressure at high altitudes, e.g. in space research (Al-Kazraji, 1979).

Si-PbO system

Al-Kazraji (1979) studied the DTA response of a 30:70 Si: PbO powder mixture in air. He observed three exotherm peaks at 590, 665 and 710°C respectively. The first reaction corresponds to the conversion of PbO to Pb_3O_4 (red lead) and commences at 350°C (Rugunanan, 1991a):

$$6\ PbO\ (s) + O_2\ (g) \quad 2\ Pb_3O_4\ (s)$$

The Pb_3O_4 reacts with silicon above 540°C and regenerates PbO:

$$2\ Pb_3O_4\ (s)\ +\ Si \rightarrow 6\ PbO(s) + SiO_2\ (s)$$

At 665°C more silicon is oxidised by the freshly formed PbO and O_2 (from the atmosphere):

$$PbO\ (s)\ +\ ½\ O_2\ (g) + Si \rightarrow Pb\ (l) + SiO_2\ (s)$$

Si-PbO_2 system

DTA analysis of PbO_2 reveals several endotherms corresponding to its step-wise decomposition:

$$PbO_2 \xrightarrow{435^o} PbO_{1.56} \xrightarrow{465^o} PbO_{1.43} \xrightarrow{495^o} Pb_3O_4 \xrightarrow{573^o} PbO$$

The fifth endotherm observed at ~875°C indicates the melting of PbO (Rugunanan, 1991a).

The observed and calculated heats of reaction ΔH_R show a maximum near 10,5% Si (McLain, 1980). This suggests that this is the stoichiometric quantity of Si that is required to consume all the oxidiser and it is consistent with the following reaction:

$$PbO_2\ (s)\ +\ Si \rightarrow Pb\ (l) + SiO_2\ (s)$$

The maximum burning rate of Si/PbO_2 mixtures occurs at 35% Si. This burning rate also decreased with increasing particle size (McLain, 1980).

Si- Pb_3O_4 *system*

Al-Kazraji and Rees (1978) investigated the fast pyrotechnic delay composition Si – red lead. Their thermal analysis results revealed three main exothermic peaks: 590, 670, and 760°C. Their observations can be explained in terms of the following sequence of events. The red lead (Pb_3O_4) decomposes above 540°C to yield a solid residue of PbO that reacts readily with silicon. This occurs at the onset of the first exothermic peak (590°C) obtained from DTA:

$$Pb_3O_4\ (s) \rightarrow 3\ PbO(s) + \tfrac{1}{2}\ O_2\ (g)$$

$$2\ Pb_3O_4\ (s) + Si(s) \rightarrow SiO_2\ (s) + 6\ PbO\ (s)$$

$$PbO\ (s) + Si\ (s) + \tfrac{1}{2}O_2\ (g)\ (\text{from air}) \rightarrow Pb\ (l) + SiO_2\ (s)$$

The reaction corresponding to the second exotherm (665°C) releases more heat and is associated with the oxidation of the molten lead from the previous reaction to lead oxide, which in turn reacts with excess silicon at the onset of 665°C. That produces sufficient heat to raise the temperature for a further reaction to take place in bulk after diffusion through the layer of reaction products formed around the reactants. When the flow was nitrogen, the second reaction was less violent because of the absence of atmospheric oxygen.

The third peak (760°C), smaller than the second and very pronounced for silicon-rich compositions, is possibly due to the reaction between PbO and $PbSiO_2$ (lead silicate) at the melting point of the silicate (Mellor, 1925).

Moghaddam (1981) also investigated the thermal response of Pb_3O_4/Si systems. He found that the DTA curve in air shows two exothermic peaks at the same temperature ranges found for the PbO/Si reaction.

However, the first exotherm of the Pb_3O_4 system, larger than the second, is also larger than the first peak of PbO/Si, indicating that the main reaction occurs in this temperature range. It was also observed that the oxygen resulting from the decomposition of Pb_3O_4 did not react with silicon. The high reactivity of Pb_3O_4/Si mixtures at lower temperatures is attributed to the presence of highly reactive PbO freshly formed with a larger specific surface area. The highly reactive PbO reacts more readily with silicon, producing burning rates almost three times faster than those of ordinary PbO/Si systems (Moghaddam, 1981).

The maximum burning rate was observed at approximately 30% Si for coarse silicon ($d_{avg} \approx 5$ µm) and 15% Si for fine silicon ($d_{avg} \approx 1{,}9$ µm) (Rugunanan, 1991a). In

addition, the composition at which the maximum burning rate occurred did not correspond to the composition of maximum enthalpy (~ 10%). The maximum burning rate increased (from 16 to 300 mm/s) when the specific surface area of the silicon was increased from 0,08 to 5,36 m^2/g (Hedger, 1983).

Moghaddam (1981) suggested that the mechanism for the reaction is essentially the formation of a eutectic of PbO and SiO_2 around 720°C. The PbO and SiO_2 melt at 886 and 1 610°C respectively. Thus, the delay time depends on the kinetics of the formation of the eutectic.

2.6.2 Silicon / zirconium / bismuth oxide

Boberg *et al.* (1997) patented the use of the Si-Bi_2O_3 system in pyrotechnic delay systems. It was found that addition of Zr as co-fuel results in enhanced ignitability and increased burn speed (See Table 2.6). Burn speeds up to 100 mm/s were obtained with Zr contents above 25% (expressed as part of fuel).

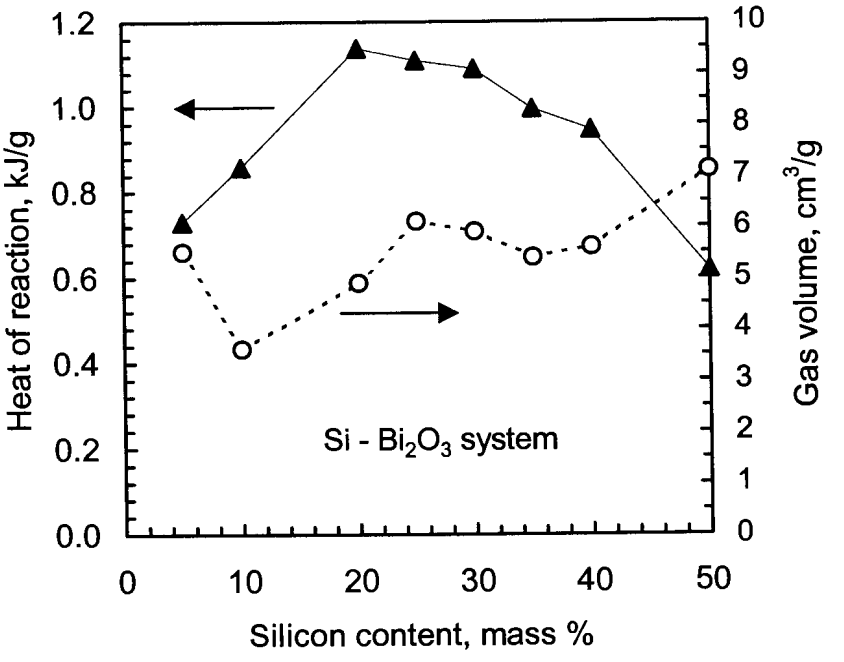

Figure 2.7 The effect of stoichiometry on gas evolution and reaction heat for the Si-Bi_2O_3 system (Brammer et al., 1996)

Figures 2.7 and 2.8 show data obtained by Brammer *et al.* (1996) for the Si-Bi_2O_3 system. Little gas is produced during combustion. Maximum heat release occurs at about 20% Si.

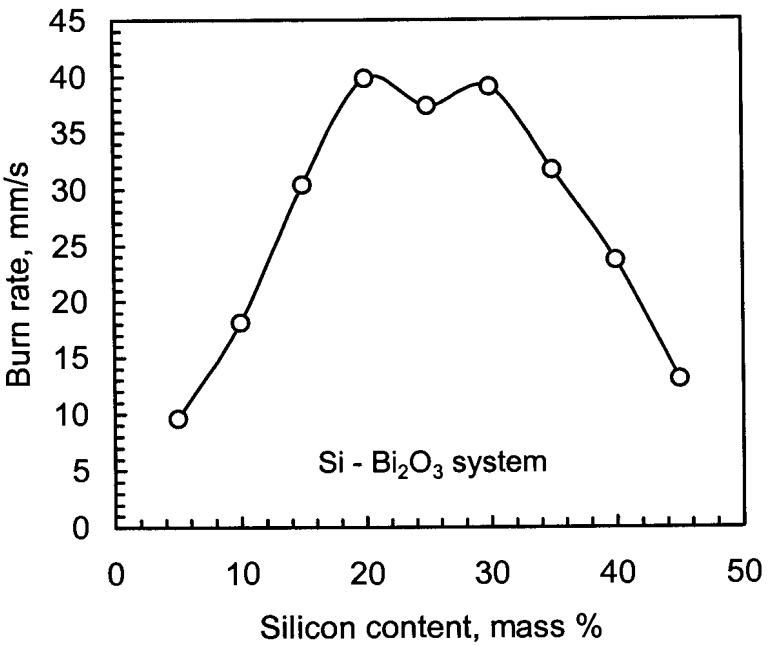

Figure 2.8 The effect of stoichiometry on the burn rate for the Si-Bi_2O_3 system (Brammer et al., 1996).

Table 2.6. Effect of zirconium on the burning rate of Si/Bi_2O_3

Composition*, %				Burning rate (mm/s)
Si	Zr	Bi_2O_3	TiO_2	
28	5	67		76
30	20	50		100
3	10	60	27	9

* Particle sizes: Silicon: 3 µm; Zirconium: 2 µm; Titanium oxide: < 1 µm; and Bi_2O_3: 5 µm.

2.6.3 Silicon / barium sulphate

This system has found much use in long-period delays. The 42% Si composition gives a burning rate of ca. 4.3 mm/s. It has been established that the system burns only when the Si-content of the composition is in the range 33,5–50%, with a specific surface area between 0,45 and 2,36 m^2/g for the $BaSO_4$.

Beck and Flanagan (1992) patented delay compositions consisting of a basic formulation of 45,5% Si/$BaSO_4$ in combination with 2-10% V_2O_5 as an ingredient acting as a flux. The consolidation was done to a density about 2 g/cm^3 in a 22 mm zinc delay element (inner diameter: 3,1 mm, outer diameter: 6,4 mm), containing a 6 mm-long, fast burning igniting sealing composition. Burn rate results are reported in Table 27.

Table 2.7. Effect of V_2O_5 on Si-$BaSO_4$ (45,5:54,5) delay compositions.

V_2O_5 content	%	0	1	2	10
Burn rate	mm/s	Failure	4,025	4,05	4,05

Particle surface areas: Silicon: 7 m^2/g; $BaSO_4$: 0,8 m^2/g; V_2O_5: very fine.

The melting flux assists the initiation of the Si/$BaSO_4$ without participating in the main combustion reaction. The content is efficient in the range 1–10% by mass. Above 10% the dilution effect of the inert flux tends to quench the reaction (Beck and Flanagan, 1992).

2.6.4 Silicon / boron / potassium dichromate

Charsley and co-workers (1980) showed that in the binary system B/$K_2Cr_2O_7$, the combustion reaction is self-propagating above a fuel content of 5%. For mixtures prepared from 4% B/$K_2Cr_2O_7$, the presence of a few percent of silicon is beneficial and indeed is responsible for propagating the combustion.

DTA curves recorded for mixtures of Si/$K_2Cr_2O_7$ showed an exotherm at approximately 950 K. Such mixtures are more difficult to ignite and self-propagating combustion requires a Si content of more than 15%. The combustion process is recorded as a single exotherm immediately following the onset of dichromate fusion.

The boron in the ternary mixture then burns in a matrix of molten oxidant, which progresses through the burning compositions as a molten front. However, the

determining step of the kinetic mechanism involves the formation of a liquid phase (Howlett and May, 1974).

In B/Si/$K_2Cr_2O_7$ systems, ignition also occurs immediately after fusion of the oxidant. The boron acts as a trigger by burning with the molten oxidant prior to the combustion of the silicon. The silicon then reacts, as a follow-up reaction.

The ignition temperature of the ternary mixtures is about 660 K. It was observed that the addition of silicon increased the maximum reaction temperature and the rising slope of the temperature profiles (Charsley *et al.*, 1980), and that the addition of 25% Si to 5% B-$K_2Cr_2O_7$ is critical because further addition decreased the exothermicity.

2.6.5 Zinc / lead oxides

Zinc has a low melting point (420°C) that is readily reached during combustion in Zn/oxidant pyrotechnic systems. Tribelhorn *et al.* (1995) found that Zn burned in combination with any of the lead oxides (PbO_2, Pb_3O_4 and PbO) over a range of compositions (10–70% Zn). The burning rates varied in the range 2,2–90 mm/s for compositions containing 20 to 50% Zn. However, as the compaction pressure was increased the range of compositions that burned decreased. For example, at a compaction pressure of 55 MPa, only Zn/PbO_2 sustained combustion and then only in the range 20–45% Zn. Mixtures of Zn/PbO only burned in loose powder form.

It was observed that compositions with higher percentages of Zn were more gassy and burned more rapidly and violently. The gas should be a mixture of O_2 and vapours of Zn and Pb respectively.

Only in the case of Zn/Pb_3O_4 the oxidant was fully reduced and converted to Pb. The maximum temperatures reached during the combustion of all the Zn/PbO_2 or Pb_3O_4 mixtures were above 1800°C. The Zn/PbO_2 combustion residues showed a spongy appearance that indicated gas evolution. These systems were not suitable for use as pyrotechnic delays because of the gassy combustion (Tribelhorn *et al.*, 1995b).

2.6.6 Iron / barium oxides

Tribelhorn *et al.* (1995) also investigated the formulation variables and the compaction pressure on the behaviour of iron-fuelled binary pyrotechnic systems. Burning rates for the iron/barium oxide system ranged from 2,3 to 39 mm/s reaching a maximum around 30% Fe. The burning rates for compositions compacted at 55 MPa were higher than those for loose compositions. Increasing the compaction pressure beyond 55 MPa led to a decrease in burning rates.

Compaction promotes interparticle contact and hence the rate of solid-solid reactions. When solid-gas reactions are also involved, increased compaction slows the rate of burning as the fuel surface area accessible to the gas is decreased.

The effect of additives and environmental factors was studied using 20% Fe/BaO_2 as the base formulation. Addition of 5% barium hydroxide [$Ba(OH)_2$] inhibited combustion. Although mixtures containing >15% $BaCO_3$ supported combustion, its formation on the surfaces of BaO_2 decreased the reactivity of the system.

The presence of even 1% water inhibits the ignition of the composition. This is attributed to the coating of BaO_2 particles with $Ba(OH)_2$. Such layers apparently inhibit combustion more than having a few separate particles of $Ba(OH)_2$ interdispersed throughout the mixture. It was also observed that the endothermic decomposition of the hydroxide regenerated water vapour during the combustion and this also affected the combustion rate. Water may have a deleterious effect on the burning rate by corroding the surfaces of the iron particles to form oxides and hydroxides.

The main reactions likely to be involved in combustion of the Fe/BaO_2 system are:

$$2\ Fe(s) + 3\ BaO_2(s) \quad Fe_2O_3\ (s) + 3\ BaO\ (s)$$

$$3\ Fe(s) + 4BaO_2(s) \quad Fe_3O_4\ (s) + 4\ BaO\ (s)$$

$$Fe(s) + BaO_2(s) \quad FeO\ (s) + BaO\ (s)$$

The reaction order varied with the Fe content of the mixture and ranged from 0,50 to 0,71. The corresponding activation energies observed varied erratically between 7 and 13 kJ/mol. with the Fe ratio. These low apparent activation energies are indicative of diffusion-controlled processes.

2.6.7 Zirconium / iron oxide

Cheng *et al.* (1984) investigated the use of the Zr/Fe_2O_3 system as a pyrotechnic delay element. DSC showed a strong exotherm at 395 to 430°C for mixtures containing from 10 to 80% Zr. Cheng *et al.* (1984) also observed a pre-ignition of reaction in the range of 310–330°C. The overall reaction is:

$$3\ Zr\ (s) + 2\ Fe_2O_3\ (s) \rightarrow 4Fe\ (s) + 3\ ZrO_2\ (s)$$

This is a composite of the following two reactions:

$$Zr\ (s) + 2\ Fe_2O_3\ (s) \rightarrow\ ZrO_2\ (s) + 4\ FeO\ (s) \qquad (\Delta H = -\ 1{,}29\ MJ/kg)$$

$$Zr\ (s) + 2\ FeO\ (s) \rightarrow\ ZrO_2\ (s) + 2\ Fe\ (s) \qquad (\Delta H = -\ 2{,}36\ MJ/kg)$$

The nature of the combustion products, identified by XRD analysis, depended on the fuel content of the mixture. See Table 2.8.

Table 2.8. The combustion products of the Zr/Fe_2O_3 system.

% Zr in reactants	Identified products
30	ZrO_2, Fe, FeO
50	ZrO_2, Fe
70	ZrO_2, $ZrFe_2$

Burning rate and the heat of reaction showed similar trends with respect to the composition dependence. The burning rate did not vary significantly in the Zr content range 48 to 56%. The maximum heat of reaction was obtained with 50% Zr. The compaction pressure had only a slight effect on the burning rate.

2.7 Pyrotechnics processing

It is important in pyrotechnic technology to ensure the homogeneity of the mix as this will result in the regularity, reproducibility and uniformity of the combustion wave motion for a particular composition. Processing also has an effect on the ease of manufacture and loading as well as safety.

Preparation of raw materials

Grinding

A micropulveriser is used to reduce the particle size and to ensure that each batch is prepared in the same way. The standard operating procedure for all inorganic oxidisers is to dry, micropulverise (no more than 2 days before use) and then dry again (McLain, 1980).

Ball milling

Ball mills also serve to reduce the particle size of relatively brittle substances, such as oxidiser salts. It was proved that milling increased the reactivity of the reactants. This change may be the result of the reduction in particle size (increase of specific surface area), the distortion of the structure, the breaking up of agglomerates or, more likely, of stripping the metal particles from inhibiting surface layers (Ellern, 1968). The success of this technique is a function of material properties, such as fragility and hardness. A ball mill or micropulveriser should not be used to mix a flammable pyrotechnic, nor should they be used interchangeably for oxidisers and reductants since small residues of the one can react with the other (McLain, 1980).

Coating

In order to avoid possible surface deterioration of the metal powders, protective coatings are applied. Coating materials such as paraffin, linseed oil, stearic acid and polyvinyl chloride (PVC) may be applied by dipping or spraying (McLain, 1980).

Heat treatment

Heat treatment enhances the uniformity of processed materials by desorption of moisture or other materials that have covered the surface of particulates. For example, $PbCrO_4$ and $BaCrO_4$ are preheated at 400°C before use (McLain, 1980).

The heat treatment of a mixture delay composition requires precautions to avoid ignition. The temperature is therefore kept far below runaway conditions. For example, the fast burning Pb_3O_4/Si mixture is dried below 70°C.

Mixing

Proper mixing eliminates non-uniformities and concentration gradients. This operation is essential to ensure homogeneity of the reaction mixture. Several techniques have been used to achieve the objectives:

Brush screening

This is accomplished on a set of brush screeners, similar to flour sifters that are assembled on top of each other. The rotating brushes are usually pulley-driven from a drive shaft connected to a motor (McLain, 1980). They are remotely operated to avoid exposing personnel to the hazards of fire and toxic dust.

Mechanical mixing – dry

Different techniques are used for this processing, such as rumbling (the most efficient technique), dough mixers and double-cone blenders. Bladed mixers and ribbon blenders can cause fires (McLain, 1980).

Mechanical mixing – wet

Wet mixing process equipment includes:

- Simpson Intensive Muller or Lancaster Mix Muller apparatus, consisting of a central rotating shaft and two wheels with ploughshares inside each wheel. They are used for high viscosity mixtures.
- Sigmoid blade mixer for high-viscosity mixtures.
- Hobart apparatus, usable for mixtures with consistencies ranging from a thin gruel to heavy dough.
- Vibrating screens (McLain, 1980).

Co-precipitation

This is mainly used to produce mixtures with close bonding between the reductant and the oxidant. Examples are:

- The co-precipitation of a B-$BaCrO_4$ mixture.
- The co-precipitation of Mn-$BaCrO_4$-$PbCrO_4$ mixtures as described by McLain (1980).

Co-acervation

In pyrotechnics, co-acervation is a type of co-precipitation that depends on the ability of ethyl alcohol to pre-empt the solvent capacity of water.

Soluble ionic compounds form stable solutions in water because of hydration: the formation of a stable water shell around the ions bonded by ion-dipole interactions. It is the enveloping water layers that prevent re-association and thus stabilise the solution. Ethyl alcohol molecules bond more strongly to the water molecules than do the cations. Consequently, the addition of the alcohol to a water solution of salt strips the ions of their protective coating and causes re-association or precipitation.

This technique has been used in the preparation of Mg-$NaNO_3$ illuminating flare mixtures and $K_2Cr_2O_7$-Si-B delay mixtures (McLain, 1980).

Methods of processing highly hazardous mixes

- Wet mixing
- Polymer precipitation:

This process involves dissolving the polymer in a solvent, adding the dry ingredients and stirring vigorously, then adding a non-solvent to the system to cause precipitation of the mix. The end product is a homogeneously dispersed mix of ingredients uniformly coated with the precipitated polymer. This product does not require screening, which is of special benefit with compositions that are hazardous to screen because of friction sensitivity (McLain, 1980).

Binders for pyrotechnic compositions

Polymeric binders play multiple roles in pyrotechnic compositions and, in general they contribute towards better mechanical strength and provide moisture-absorption resistance. This latter leads to improved shelf life.

Beck *et al.* (1986) found that binders also contribute significantly to the performance of composition by lowering the activation energy (ignition temperature) and increasing the combustion temperature and burning rate. Boiled linseed oil (~2%) was added to a 15% Sb (<53µm)/ $KMnO_4$ composition, which does not normally burn. The composition with the binder did burn.

Barton *et al.* (1982) found that the addition of 2 to 3% of acaroid resin to a mixture of Mg/BaO_2 lowered the ignition temperature by more than 200°C.

Generally, the silicon and red lead system is slurried by the addition of an aqueous solution of carboximethyl cellulose, which acts as a binder. The slurry is stirred thoroughly to ensure even distribution of the two species, and the water is evaporated by placing the slurried composition on a steam-heated copper tray. The binder prevents segregation of Si and Pb_3O_4 (Al-Kazraji and Rees, 1979). It was also observed that the addition of the binder makes the composition sensitive to impact and friction.

Novel powder-processing techniques

A major problem in the processing of powdered formulations is agglomeration. This problem can be encountered when one or more of the powdered constituents are:

- Hygroscopic, e.g. ammonium perchlorate or sodium nitrate
- Waxy or oily (TNT or nitroguanidine)
- Unusually shaped, such as needle-type or flake particles.

The agglomeration increases as the particle size decreases and the moisture content increases. The latter leads to caking of the powder. This means that most fine particle powders have to be specially handled in all processing techniques, i.e. drying the powder at elevated temperature, screening to break up or remove agglomerates, and desiccating to prevent moisture uptake (Tulis, 1980).

The milling of hygroscopic materials must be done under conditions of near-absolute dryness. As the particle size is reduced, the surface area increases and moisture absorption becomes extensive. When milled, the waxy materials 'freeze' and become sufficiently brittle to fragment (Tulis, 1980).

Powder conditioning

Flow-conditioner additives are intensively used to overcome agglomeration problems. These are usually very fine powders of sub-sieve particle size and include various types of silicates, stearates, phosphates, diatomaceous earth, starch, magnesium oxide, talc and fatty amines.

These conditioners proceed in various ways to improve flowability and inhibit agglomeration, e.g.:

- Form a solid barrier between the powder particles, reducing their attractive forces
- Lubricate the solid surfaces, reducing friction between the particles
- Neutralise electrostatic charges (Tulis, 1980).

Colloidal hydrophobic fumed silica, in powder form, is a powerful flow-conditioner additive. Normal silica aerogel is hydrophilic. It can be converted to the hydrophobic state by replacing the surface hydroxyl groups with siloxane groups (Tulis, 1980) by reaction with e.g. hexamethyldisilazane.

The advantages of this flow conditioner are:

- It has an exceedingly light bulk density, about 0,05 g/cc.
- The particle size is about 7 nanometer.
- The conditioner can be premixed before milling and will allow milling of waxy or oily materials.
- The treated powder becomes water repellent, even if initially hygroscopic.
- Low dosage required: Less than one percent, on a mass basis, is often adequate.
- The resultant powder generally has a higher bulk density.
- It is chemically inert, allowing it to be used with sensitive propellants, explosives and pyrotechnics.

The exceptionally high water repellence of powder conditioned with hydrophobic silica is attributed to air entrapment on the surface of the powder particles. One advantage of this technology is associated with the increased bulk density. Because of the better flowability, the particles flow and slip past each other readily so that they compact better (Tulis, 1980).

The addition of 1 to 2% of hydrophobic silica to pyrotechnic mixes proves to be efficient in the milling (Tulis, 1980).

Powder preparation

Molecular sieves are used to achieve near-absolute drying of powders. They are crystalline zeolites that have angstrom-sized pores that allow a selective adsorption of polar gases and liquids. Moisture is transferred from the powders to the molecular sieves. This is an equilibrium process. The efficiency of molecular sieves has been demonstrated in the milling of a water-ignitable pyrotechnic composition of B/AgF_2 (Tulis, 1980).

Direct contact of molecular sieves with sensitive materials, such as explosives, must be avoided: The heat of adsorption might be sufficient to cause ignition of sensitive materials (Tulis, 1980).

In certain milling operations, synergism was observed when using a combination of molecular sieves and hydrophobic silica. The former dried the particles and the latter coats their surfaces once fragmented (Tulis, 1980).

2.8 Design of pyrotechnic delay elements

2.8.1 Porosity and compaction pressure

The degree of preheating of the reactants in a given system is affected by the forward intrusion of hot combustion products. This, in turn, is partly determined by the porosity of the compacted material. Consolidated compositions exhibit microscopic

voids between the ingredients even when compressed at very high loads. Even at densities approaching the theoretical maximum (TMD), the voids may constitute upward of 2% of the total volume. The reason is that beyond a critical density further displacement of the particles is precluded. The loading pressure for a delay charge is usually around 200–275 MPa (Cheng *et al.*, 1984).

The void volume of a composition depends on the formulation, the physical characteristics of the ingredients such as the size and the shape of the particles; and the presence of substances such as waxes or resins that can deform or flow under pressure (Wilson and Hancox, 2001).

The effect of compaction pressure on the burning rate should be considered when designing a delay element. With the incremental method of filling the delay elements, there will be periodic variations in the degree of compaction. It is believed that the interfaces between the individual increments may cause a momentary slowing of the burning front (Wilson and Hancox, 2001).

2.8.2 Design and manufacturing factors

Design and manufacturing factors that can affect the delay interval produced by a delay element include (Wilson and Hancox, 2001):

- Design of the delay element, e.g. length and diameter of the column
- Density of the column packing
- Type of ignition source used
- Ignition transfer and mechanical strength of the column
- Thermal conductivity of the tube housing the column

Gasless compositions that burn at a rate lower than 3 mm/s tend to be unreliable. This limits the practical time delay to about 25 seconds for a 75 mm stubby.

Delay elements for longer time intervals have been made utilising long, straight lead tubes made by the extrusion technique and pressing them into a flat 'C' section or by preparing spirally wound units. In this way time delays of several minutes can be obtained (Wilson and Hancox 2001).

2.8.3 Thermal conductivity of the tube wall

Heat loss through the container walls is essentially dealt with by tubular geometry. The heat flow decreases as the thickness of the tube increases; whereas an increase in the diameter increases the heat loss for a constant wall thickness.

The heat loss will be greater from a tube with high thermal conductivity of the container. The internal tube diameter will have to be kept larger to sustain combustion in a tube of high thermal conductivity, e.g. an aluminium tube. One effect of high heat conductivity along the column wall may be a premature initiation of whatever terminal charge follows the delay column (Ellern, 1968).

Table 2.9 shows the effect of wall thermal conductivity on the burning rate of a specific composition of the Sb-$KMnO_4$ system. The dramatic decrease in the burning rate in Perspex (polymethylmethacrylate) tubes in an open system is attributed to severe melting and degradation. However, in a closed system the degradation products caused the development of high pressures. This increased the burning rate to approximately 8,2 mm/s and caused a high proportion of tubes to burst.

Table 2.9. Effect of container material on the burning rate of 30% Sb/$KMnO_4$ in open systems. (Beck *et al.*, 1986)

Container material	Burning rate (mm/s)
Column supported in air	1,9
Aluminium	2,2
Polyether imide	2,5
Perspex	1,3
Packed in SiO_2	2,4
Packed in $CaCO_3$	2,2

The use of heat-resistant polymers (e.g. polycarbonate, PTFE, Kevlar and high-temperature 40% glass-filled polyether imide) did not reduce the quantity of gaseous

degradation products sufficiently to prevent bursting of the detonator tubes. This suggests that polymers are not suitable tube materials for pyrotechnic delays.

Table 2.10 lists the physical properties of potential tube materials.

Table 2.10. Thermal properties of some materials (Perry *et al.*, 1973 and Brydson, 1975)

Material	Thermal conductivity (λ) $W.m^{-1}.K^{-1}$	Density (ρ) $10^3\ kg.m^{-3}$	Heat capacity (C_p) $J.kg^{-1}.K^{-1}$	Thermal diffusivity: (α) $10^{-6}\ m^2.s^{-1}$
Al	220	2.7	960	85
Pb	35,3	11,34	160	19,45
Stainless steel	15	8,0	500	3,8
$CaSi_2$	0,42	2,5	960	2,04
Si	0,35	2,33	720	3,42
Al_2O_3	0,22	3,97	780	1,54
Nylon 6	0,24	1,12	1590	0,13
Polycarbonate	0,20	1,2	1260	0,13
Teflon	0,30	2,20	1050	0,13
Perspex	0,2	1,2	1500	0,11

Some work has been done on the use of ceramic containers (Ellern, 1968). The selection of ceramic bodies rather than metallic ones could have a favourable influence on marginal situations, especially where multiple columns occur in close proximity (Ellern, 1968).

3 Experimental

3.1 Reagents and Apparatus

3.1.1 Reagents

Powdered silicon was supplied by Millrox and obtained via AEL. The three types of silicon used in the present study, are listed in Table 3.1. Manganese powder with a specific surface area of 0,6 m^2/g was supplied by Manganese Metal Company (Pty).

Table 3.1. Specific surface area for different types of silicon

Silicon type	2	3	4
Specific surface area [m^2/g]	2,51	6,30	10,1

Table 3.2. Properties characteristics of bismuth subcarbonate

Property	Unit	Value
BET Specific Surface Area	m^2/g	5-9
Bulk density	g/cm^3	0,4
Density (theoretical)	g/cm^3	6,9-8,3
Appearance		White
Particle size (from SEM images)	µm	6
Nitrate content	%	0,1
Alkalis and alkaline earth	%	0,3

Adcock Ingram supplied bismuth subcarbonate ($Bi_2O_2CO_3$) with the properties shown in Table 3.2. Bismuth oxide supplied by Aldrich Chemical Company, Inc., [*1304-76-3*]. Dry colloidal antimony pentoxide supplied by Nyacol® Nano Technologies, Inc.

Boron [*7440-42-8*] powder (Merck Cat. No.12070) was used as an energetic fuel additive. Di-boron trioxide [*1303-86-2*] (Merck Cat. No. 9024721) was used as flux additive. Potassium permanganate [*7722-64-7*] (Saarchem Cat. No. 504 68 20) used as additional oxidant. Fumed silica Aerosil 200 (supplied by Degussa) was used as inert diluent.

Synthesis of Bi_2O_3

Bismuth sesquioxide can be produced by several paths including the heating at high temperature (750-800°C) of either bismuth metal or bismuth monoxide in air. A similar result is obtained by thermal decomposition of bismuth compounds such as the basic carbonate, the carbonate, the nitrate or the oxalate (Long *et al., 1992*). The thermal decomposition of bismuth basic carbonate was chosen in this study as the process for the production of the trioxide.

In a typical procedure the heavy bismuth subcarbonate powder weighed into a ceramic crucible and then placed in a convection oven. The temperature was ramped up to 460°C at a rate of 145°C/h and maintained there for 15 hours. Thereafter the product was quenched to room temperature in air as suggested by Levin *et al.* (1962). To prevent re-carbonation the crucible was covered with a stainless steel lid immediately after removing from the oven.

Synthesis of Sb_6O_{13}

Heating antimony pentoxide ultimately yields antimony trioxide (Mellor, 1933). This transformation proceeds stepwise through a series of intermediates: Sb_6O_{13} (400°C); Sb_2O_4 (700°C) and Sb_2O_3 at 900°C (Mellor, 1933). The cubic Sb_6O_{13} (antimony hexitatridecoxide) was obtained as follows. The white colloidal Sb_2O_5 powder was placed in a crucible and covered with a steel lid with a small hole to allow gases to escape. It was then subjected to an 8-hour thermal treatment at 315°C in a convection oven. Thereafter the product was allowed to cool slowly back to room temperature in the oven. This resulted in a dark brown powder. It was characterised by XRD.

3.2 Sample preparation

3.2.1 Preparation of pyrotechnic compositions

The required quantities of the different ingredients (fuel, oxidant and additives) sufficient to yield 20 g batches were weighed into plastic containers (length = 120

mm and diameter = 80 mm) and blended thoroughly in a tumble mixer for 4 hours. Thereafter the mixture was passed gently through a 125 µm sieve using a soft brush. This process was repeated using the same sieve. In some instances a 53 µm sieve was used during the second brush-mixing. The sieve-brush-mixing operation was done to ensure break-up of agglomerates.

3.2.2 Preparation of delay elements

a. Lead delay elements

The powder mixture was poured into a 165 mm long lead tube with an average inner diameter of 6 mm. The tube wall thickness was between 2 and 3 mm. The tube ends were sealed by crimping with a pair of pliers. The composition in the tube was consolidated and compressed by a rolling operation that reduced the diameter in ten successive steps to 6 mm. A proprietary tube-rolling machine, supplied by AEL, was used for this purpose. During each rolling operation, the sealed tube was passed through a hole with a smaller diameter. This operation yielded a final tube approximately 420 mm long. The external diameter and wall thickness were 6 and 1,5 mm respectively. In this way, good compaction of the powdered delay composition was ensured. The rolled lead tube was then cut to a standard length of 45 mm to form the delay elements.

Where a starter composition was needed, a short increment of the required starter was filled into the top of the core after removing 3 mm of the main composition from the lead tube.

b. Aluminium delay elements

Aluminium delay elements were made by drilling holes through aluminium rods (6 mm ϕ) cut to a length of 45 mm. These tubes were filled incrementally. The mixture was compacted after adding each increment by inserting a punch and applying controlled compaction pressure that was measured by means of a load-cell device (HBM Komm). For most of the elements prepared in this way, the pressure was set at approximately 42 MPa. A dwell time of about one second was used before

relieving the stress. Thereafter the filled tube is sealed after introduction of different accessories including the anti-static cup, grommet and shock tubing.

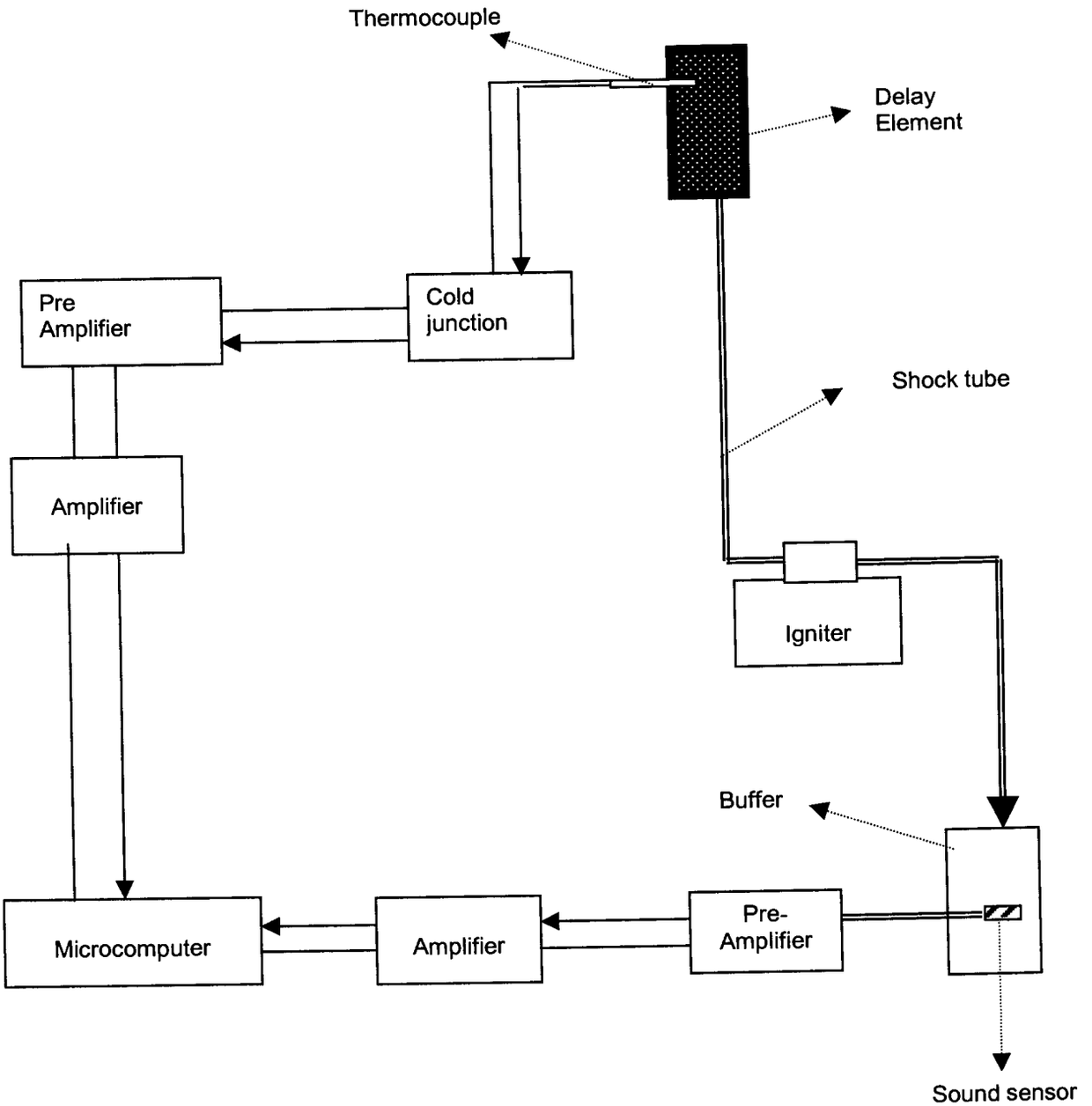

Figure 3.1 Apparatus for burning rate determination

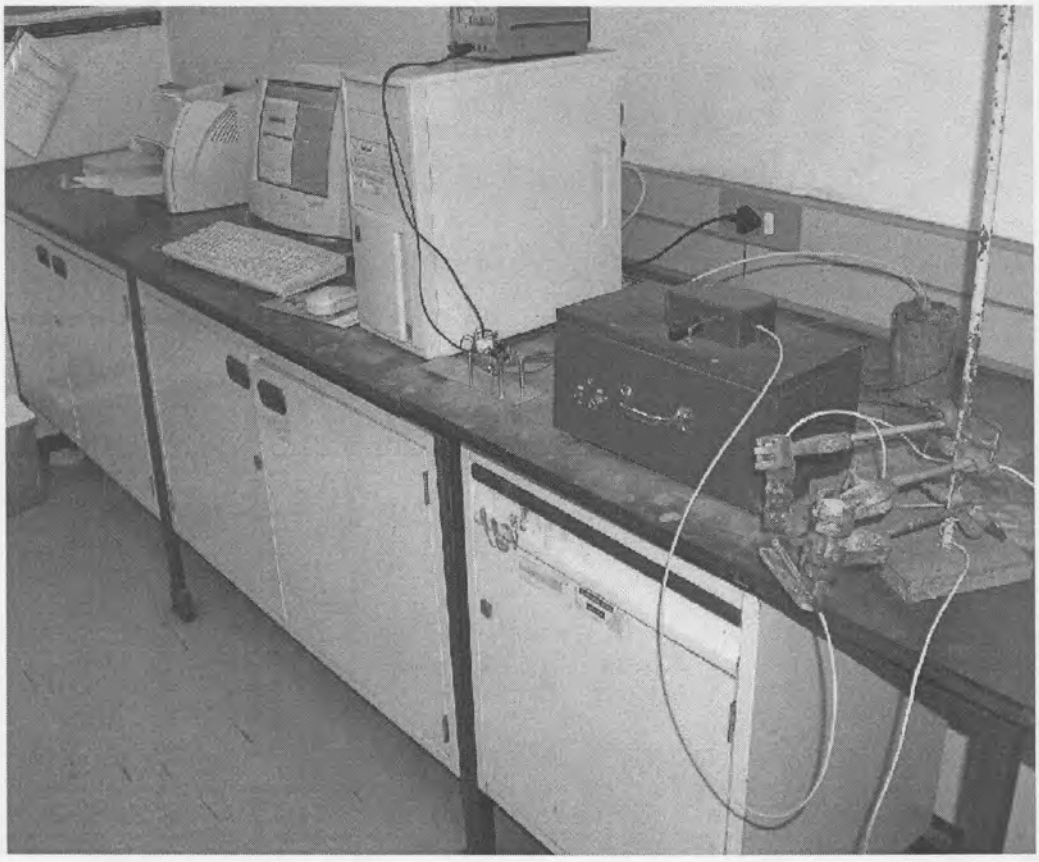

Figure 3.2 Equipment for determination of the burning rate.

3.2.3 Delay detonator assembly

The delay elements were incorporated into a standard non-electric delay detonator assembly for burn-rate testing. First the delay element was placed inside an aluminium tube that was sealed at the other end. A plastic anti-static cup was introduced and pushed against the end of the lead tube followed by a rubber sealing grommet into the aluminium tube. It provided the anchor for the shock tubing. The latter that was inserted until it touched the bottom of the anti-static cup. At this point the free end of the aluminium tube was crimped to complete the assembly and to prevent any relative axial motion of individual elements in the assembly.

A hole (3mm) was drilled at the end of the element body, where a type R (0,38mm in diameter) thermocouple was embedded for measurement of burning rate.

3.2.4 Experimental set-up for burn rate measurements

The burn rates were measured using the experimental set-up shown schematically in Figures 3.1 and 3.2.

3.3 Burning rate measurement

3.3.1 Testing method

The trigger box emits an explosive noise when ignition of shock tube occurs. A sound sensor placed in the box (buffer) records this signal as the starting point for the burn reaction. This signal is transmitted to an electronic system provided with pre-amplification and an amplification circuit which delivers the required signal voltage to the computer.

The end of the burn is detected by means of thermocouple measurements recorded via a computer interface. A Pt-Pt 13% Rh thermocouple (type R) with a diameter of wires equals to 0,38mm, joined by flame, was embedded in the composition through a 3 mm hole in the closed end. The reaction speed was then calculated as the ratio of the length of the element and the burn time-interval. The latter was taken as the time difference between the starting signal (sound signal) and the final thermal signal provided by the thermocouple.

3.3.2 Recording of results.

The thermocouple output was sent via an electronic cold junction compensator to data capture software on an EAGLE PC 30F personal computer. The gain of amplification was varied between 100 and 1000. The signal-to-noise ratio was improved by utilising the digital filter described by Ricco (2004). The sound sensor output, after amplification, was also sent to data capture to get the starting signal.

3.4 Experimental variables

In this investigation the effect of the following variables on the burning rate of the appropriate delay composition was studied:

- Reagent stoichiometry
- Specific surface area of the composition ingredients
- The presence of additional fuels or oxidants
- The effect of diluents
- The nature and design (core size) of the tube materials.

3.5 Characterisation of reagents and combustion products

3.5.1 X-Ray Powder Diffraction Analysis (XRD)

Phase identification was carried out by XRD analysis performed on a Siemens D-501 automated diffractometer Cu Kα (1.5406 Å) operated at 40 kV and 40 mA. This machine is equipped with a divergence slit of 1°, a receiving slit of 0,05°. The sample was scanned from between 3 to 70°, on a 2θ-scale with a counting time of 1,5 s at room temperature.

3.5.2 X-Ray Fluorescence analysis (XRF)

The purity of reagents was determined using a wavelength-dispersive XRF spectrometer (ARL 9400 XP + XRF). The powders were ground in a tungsten carbide milling vessel and roasted at 1000°C for determination of the loss on ignition (LOI). An organic binder (ethyl cellulose) was used during pelletization of samples.

3.5.3 Scanning Electron Microscope (SEM)

Colloidal particles were viewed with a JEOL JSM 6000F cold field emission gun scanning electron microscope at high magnification. Ordinary materials, after gold-

coated, were viewed with a low magnification scanning electron microscope, a JEOL 840 SEM. Images and identification of some phases on residue samples have been obtained thanks to a backscatter JEOL JSM-6300 scanning microscope combined to a NORAN EDS System.

3.5.4 Brunauer-Emmett-Teller analysis (BET)

The specific surface area of different powders was performed with BET (Nova 1000e) under a constant gas flow of nitrogen.

3.5.5 Thermal analysis (DTA/TGA)

A Mettler Toledo A851 simultaneous TGA/SDTA machine was used for the thermal and gravimetric analysis. The TGA and DTA curves were obtained with air or nitrogen as purge gas at a scanning rate of 10°C /min. Experiments were performed in a 70µl alumina crucible with or without lids.

3.5.6 Fourier-Transform Infra Red Spectroscopy (FT-IR)

Bruker IFS 113 spectrometer at low pressures, operated at 32 scans with powder samples in pressed KBr pellets, was used to obtain infrared spectra. The wavelengths were recorded from 3500 to 400 cm^{-1} in transmission mode of mid-infrared rays.

4 Results and Discussions

4.1 Results

4.1.1 Synthesis of Bi_2O_3

Bismuth sesquioxide was produced by thermal decomposition of the heavy-type subcarbonate ($Bi_2O_2CO_3$). The latter was kept in a convection oven at 460°C for 15 hours whereafter it was quenched in air. This temperature was chosen on the basis of the thermal behaviour of $Bi_2O_2CO_3$ observed in a TGA scan. See Appendix D: Figure 3. The decomposition reaction is:

$$Bi_2O_2CO_3\ (s) \rightarrow Bi_2O_3\ (s) + CO_2\ (g) \qquad (I)$$

Product yields were 91,10 ± 0,2%, i.e. very close to the theoretical expected yield of 91,4%. XRD scans confirmed that the yellow powder obtained as product was the monoclinic phase of α-Bi_2O_3 (See Figure1 in Appendix A). XRF analysis suggested a purity of 97,8% with CuO and Na_2O as the major impurities. The presence of Bi_2O_3 was also confirmed by FT-IR. The vibration bands at 546,06; 512,70; 443,43 cm^{-1} were in agreement with the pattern for a pure sample of Bi_2O_3 [*1304-76-3*] obtained from Aldrich Chemical Company [Figures 1 and 2 in Appendix B].

SEM revealed a spherical dendrite-like morphology where some nodules (1µm) are attached to the ends of a 3µm-long crystal (see Plate 1in Appendix C). A specific surface area of 0,9 m^2/g was obtained by BET analysis. TGA of a 5 mg sample of this Bi_2O_3 at a scan rate of 10°C/min in nitrogen revealed a large weight loss (95%) at 1100°C. Figure 1 and 2 of appendix D show the TGA curves of pure Bi_2O_3 and the Bi_2O_3 produced in this study, respectively.

4.1.2 Synthesis of Sb_6O_{13}

DTA/TG analysis (at a scan rate of 20°C/min and a constant nitrogen flow maintained at 50 ml/min) of white colloidal Sb_2O_5 showed an endothermic decomposition at

330°C associated with a weight loss of approximately 17%. The crucible was covered with a lid during the decomposition (see Appendix D: Figure 4).

Based on this observation an 8-hour thermal treatment in convection oven at 315°C was chosen for the preparation of Sb_6O_{13}. This resulted in a mass loss of 19 ± 0,5% and yielded a dark brown powder. XRD confirmed that it was cubic Sb_6O_{13} (antimony hexitatridecoxide) but also showed that Sb_2O_3 was present as an impurity (see Figure 5 in Appendix A).

When the thermal transformation of the antimony pentoxide was attempted in an uncovered alumina crucible, a brown and yellowish powder mixture corresponding to a poorly defined blend of Sb_6O_{13}, Sb_2O_3, and $NaSb_5O_8$ was obtained. See XRD data in Figure 4: Appendix A). BET analysis showed that the specific surface area increased from the 4,55 m^2/g for the colloidal hydrated pentoxide form to 32,1 m^2/g for the final product (Sb_6O_{13}).

The SEM micrographs shown in Appendix C (Plates 2.a and 2.b) reveal the presence of closely packed nanoparticles in a coarse spherical conglomerate (diameter: 15 μm). Figure 5 in Appendix D, shows the TGA measured mass loss of Sb_6O_{13} when heated in nitrogen.

4.1.3 Burning rate

Sb_6O_{13} – Si systems

The burn rate measurements for this system were performed using an initiating starter increment (3 mm) based on the Bi_2O_3 – 50% Si (Type 4) mixture. The following variables affected the burning rate.

Effect of stoichiometry

The reaction between silicon and antimony hexitatridecoxide is described by the following reaction:

$$Sb_6O_{13} + 13/2\ Si \rightarrow 6Sb + 13/2\ SiO_2 \qquad (II)$$

Figure 4.1 shows the effect of silicon content on the burn rate. Reaction (II) predicts a stoichiometric composition of 19,4% Si for this mixture. The observed maximum in the burning rate corresponds closely to this value. Note however that the data shows considerable scatter at this composition. A minimum burn rate of 4,8 mm/s was obtained with 10% Si (Type 4). Compositions containing less than 10% Si (Type 4) did not ignite. Above 20% Si (Type 3) the reaction released a considerable amount of heat and gas to the extent that the thermocouple was blown out.

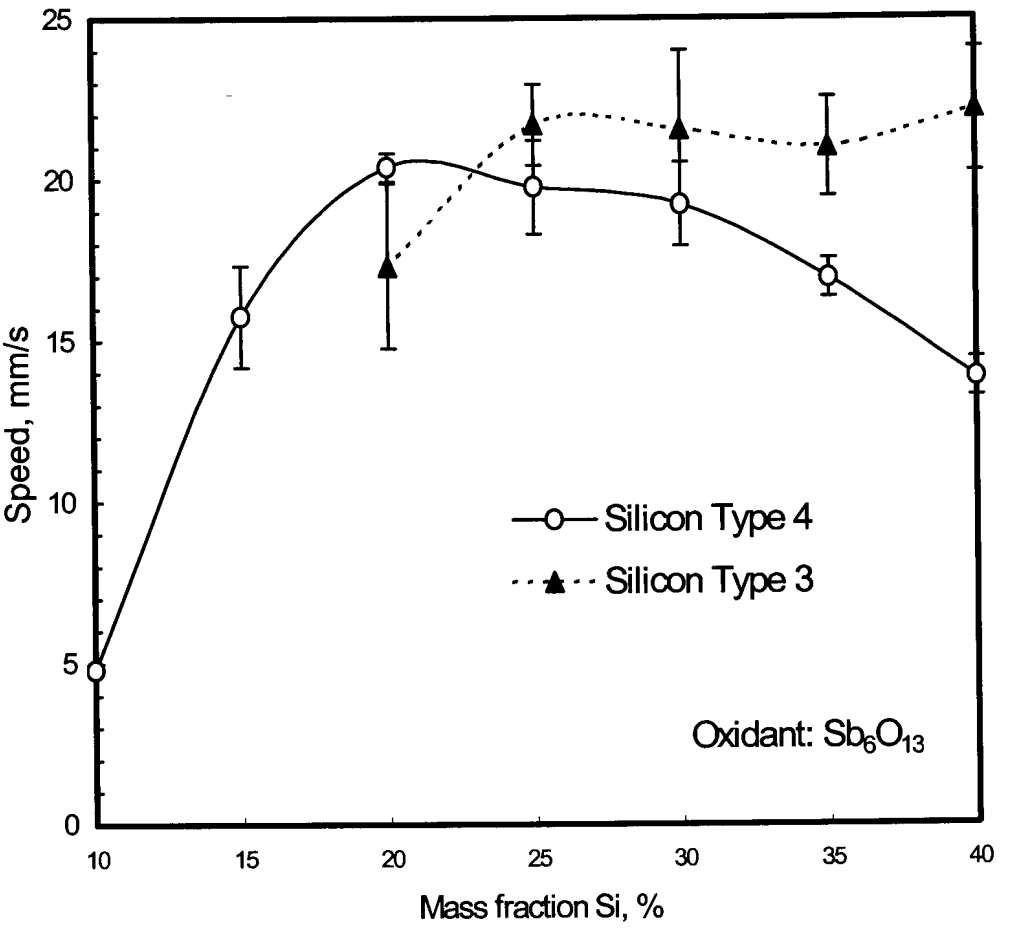

Figure 4.1 Effect of stoichiometry on the burning rate of Si-Sb_6O_{13} system.

Effect of the specific surface area of the fuel (Si)

Figure 4.1 shows that silicon Type 3, with a lower surface area than Type 4, actually burned faster. The reasons for this unexpected result are presently unknown. Note however that this fuel did not sustain the propagation in composition containing less than 20% Si whereas Type 4 did. Compositions containing an even coarser fuel (silicon Type 2) did not ignited at all.

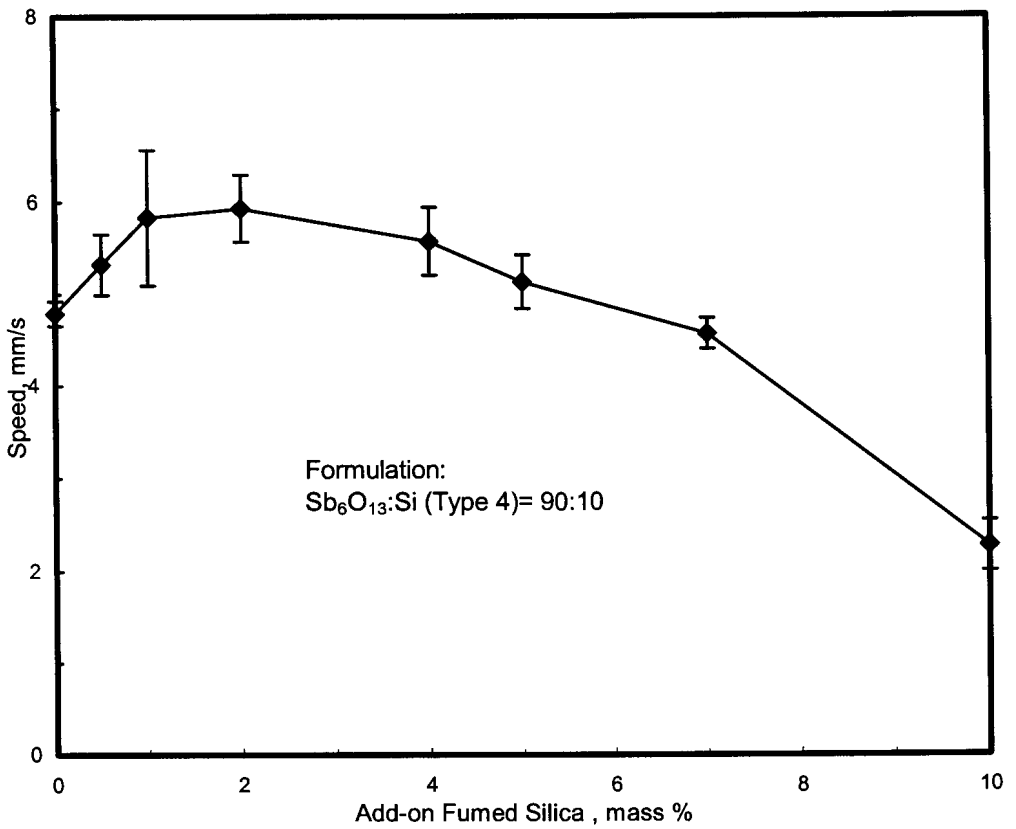

Figure 4.2 The effect of diluent fraction on the burning rate of Sb_6O_{13} –10% Si (Type 4).

Effect of diluents

Figure 4.2 shows the effect of adding the inert diluent, i.e. fumed silica to a composition composed of Sb_6O_{13} with 10% Si (Type 4). Adding small amounts (< 2%) actually improved the burn rate. This may be attributed to the silica acting as a

mixing promoter and a compaction aid. Tulis (1980) proposed this explanation on the basis of theoretical principles. Beyond a 2% addition the burn rate decreases. Surprisingly compositions containing 10% fumed silica (add-on basis) still burned reliably giving a burning rate of 2,3 mm/s.

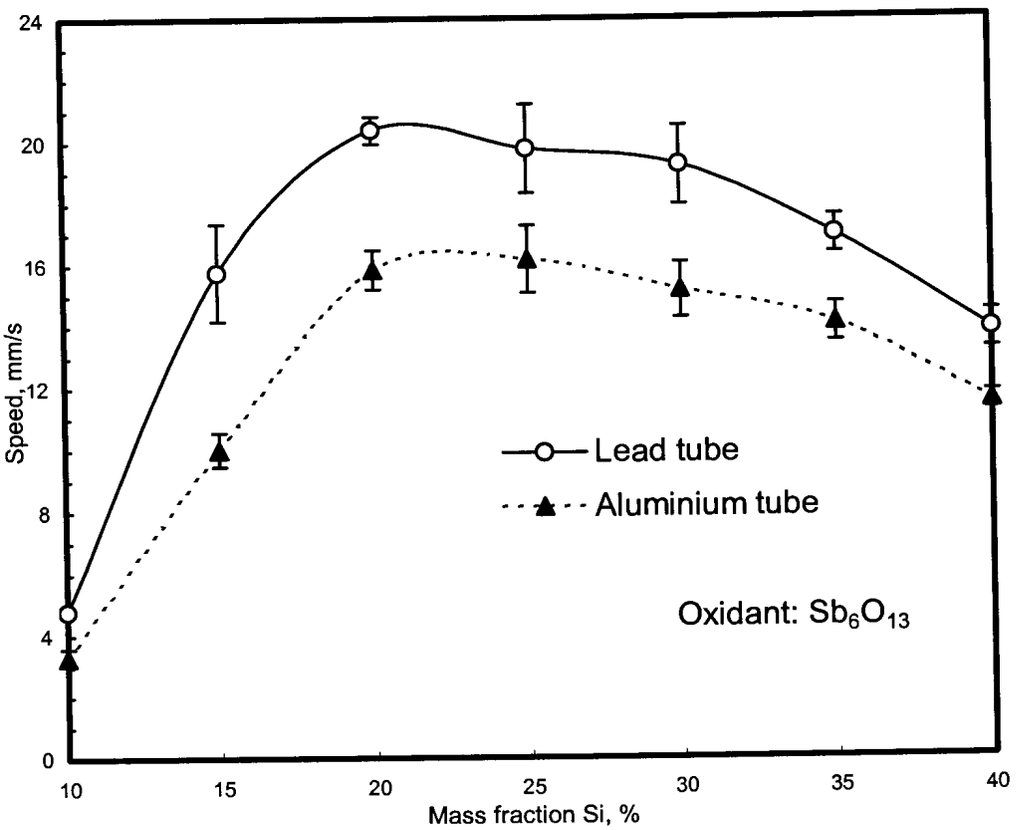

Figure 4.3 Effect of the container on the burning rate of Sb_6O_{13} – Si (Type 4) system.

Effect of tube material

Two different tube materials were tested: Lead tubes with standard dimensions (length = 45mm; ID = 2-3 mm; OD 6mm) were prepared by rolling. Aluminium tubes were filled incrementally using a press. The compaction pressure was about 42 MPa applied for about 1 second for each increment. The influence of the nature of the tube is shown in Figure 4.3. Measured burn rates in the lead tubes were about 20-50% faster than those measured with the aluminium tubes.

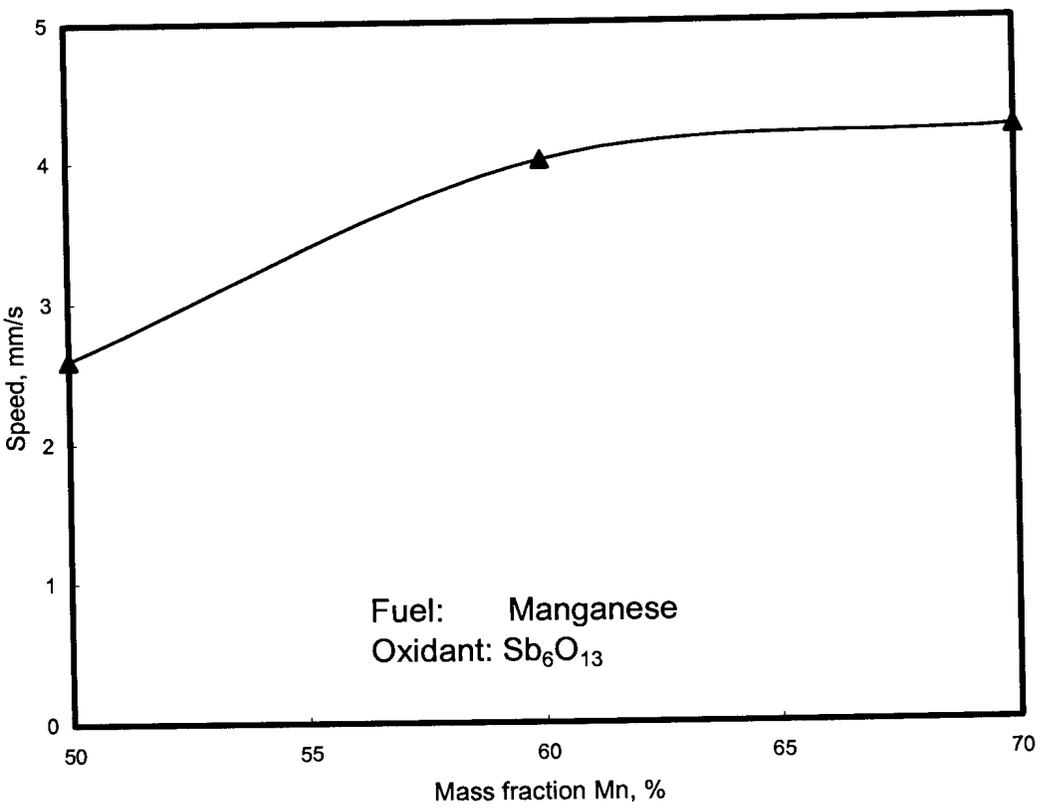

Figure 4.4 Effect of stoichiometry on Sb_6O_{13} – Mn system.

Sb_6O_{13} – Mn system

Figure 4.4 shows that substitution of silicon with a coarse manganese fuel leads to even lower burn rates. Note that only compositions that contain more than 50% Mn ignited and burned in sustained manner.

Bi_2O_3 – Si System

Effect of silicon specific surface area and reagent stoichiometry

Figure 4.5 shows the effect of reagent stoichiometry and silicon particle size on burn rate. The coarse silicon (Type 2) only burned in compositions containing >20% Si. Compositions containing the finer fuels burned over the whole concentration range

tested, i.e. 5-40% silicon (Types 3 and 4). A maximum burn rate was achieved at 20% fuel for Si Type 4. This maximum shifted to a somewhat higher silicon concentration for silicon Type 3. The data for Type 4 showed more scatter than Type 3. This probably indicates that homogeneous mixing was more difficult to achieve with the finer silicon.

Visual observation during the burn tests indicated that the compositions that showed high data scatter, e.g. the mixture containing 20% silicon (Type 4) were also gassier. The latter gave an average burn rate of 126,4 mm/s with a standard deviation of 21,5 mm/s. It is speculated that the variability in the performance of gassy systems is due to variable acceleration or deceleration of the front wave, depending on the direction of the gas transport, either forward or backward, depending on the location of leaks. That gas may be produced by the decomposition at high temperature (1100°C) is proven by the TGA curve for Bi_2O_3 shown in Figure 2, Appendix D.

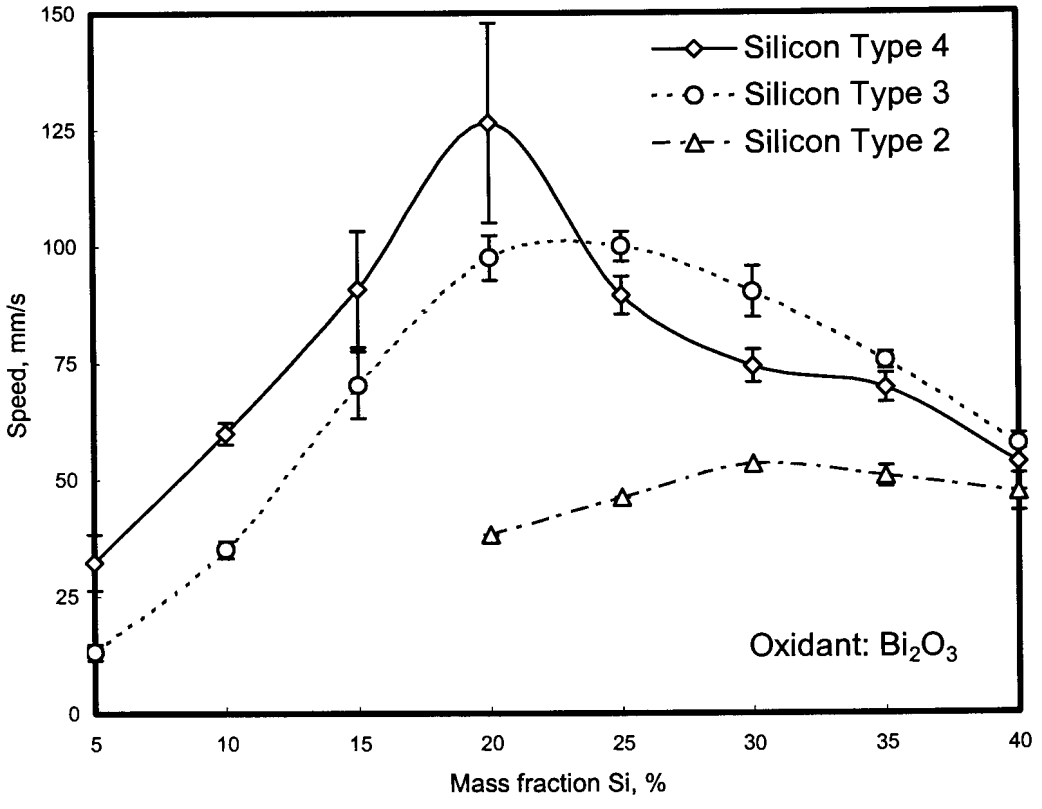

Figure 4.5 Effect of stoichiometry and silicon type on the burning rate of Bi_2O_3 – Si systems.

Effect of additives

The effect of the additives was determined for the composition containing 25% silicon Type 3. It was chosen because it showed little scatter in burn rate. B_2O_3, with its low melting point (450°C), was expected to play the role of a flux. The boron and the $KMnO_4$ respectively present the effects of addition of other fuels and oxidants. The results are shown in Figure 4.5 and indicate that these additives had a minor effect on the burn rate at addition levels up to 7%.

The addition of $KMnO_4$ appears to increase the burn rate when 5% is added. However, at this level the system behaviour becomes very gassy owing to the violent decomposition of $KMnO_4$. Addition of boron led to the production of even more gas.

Boron oxide (B_2O_3) with its low melting point (450°C) was expected to assist the reaction by generating a liquid phase. Instead it played the role of a retarder at all

compositions. This is attributed to the formation of a glassy phase (Levin and McDaniel, 1962).

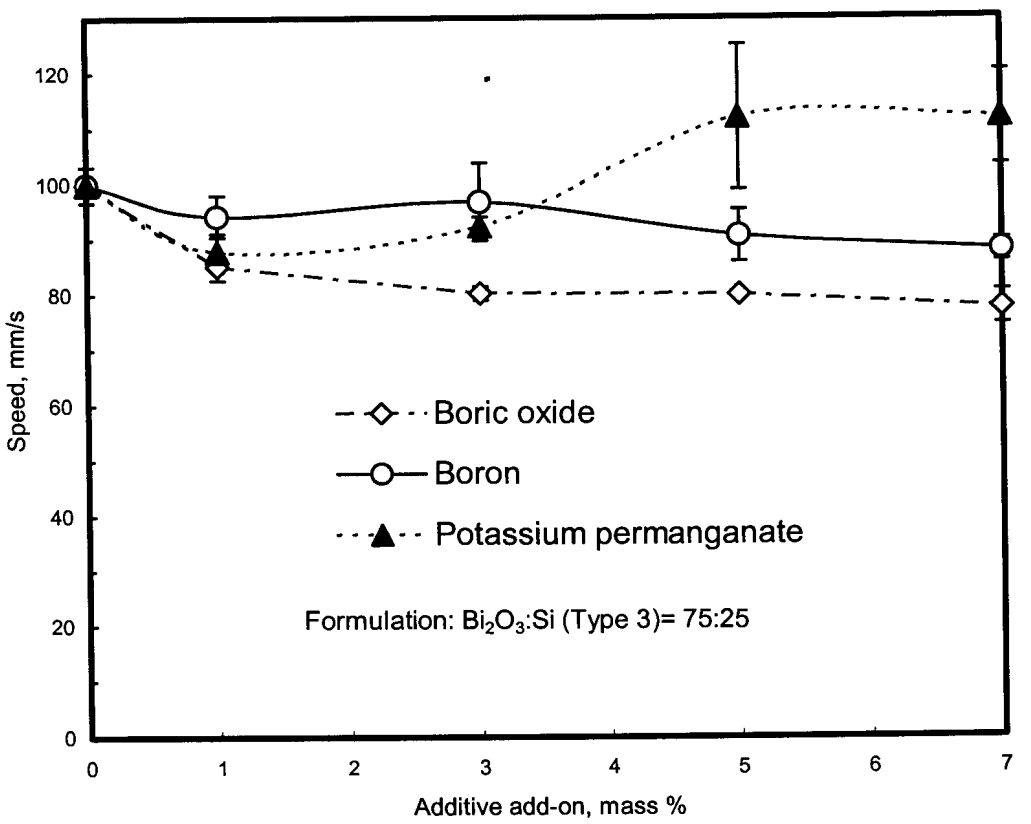

Figure 4.6 Effect of different additives on the burning rate of Bi_2O_3 – 25% Si (Type 3).

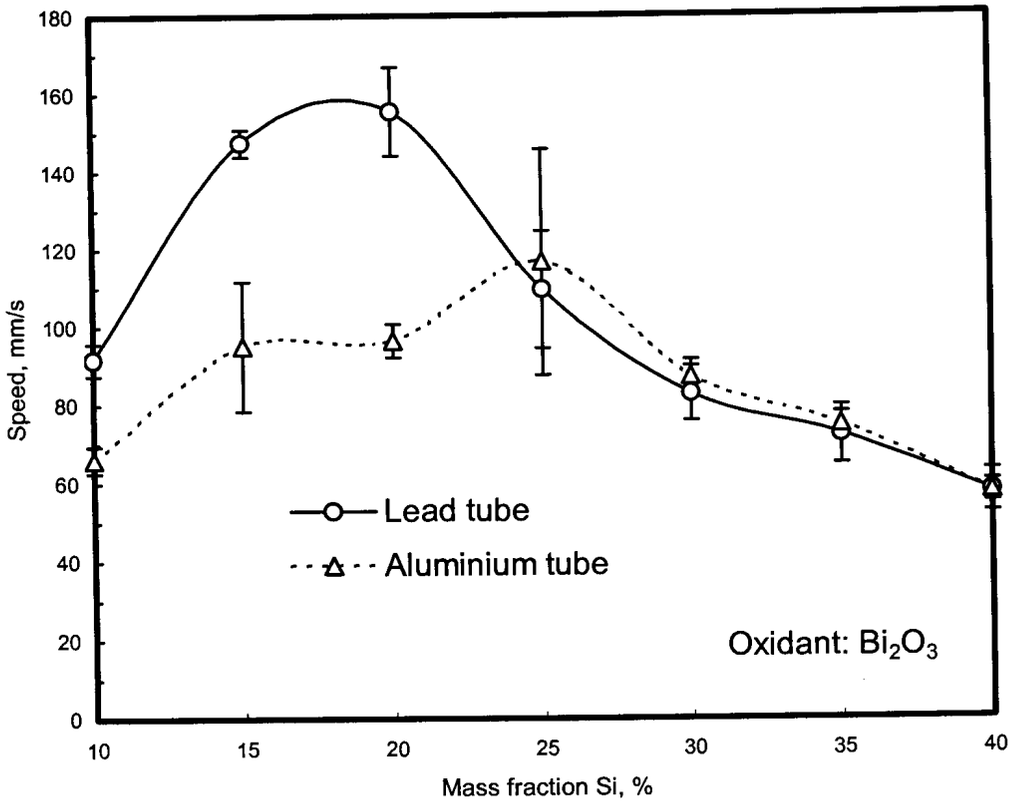

Figure 4.7 Effect of container material on the burn rate of the Bi_2O_3 – Si (Type 4) system.

Effect of tube materials

Figure 4.7 shows the effect of tube wall material on the burn behaviour of the Bi_2O_3 – Si (Type 4) system. At low silicon concentrations the lead tube yields faster burn rates. However, above 25% silicon the burn rates are not affected by the nature of the tube material.

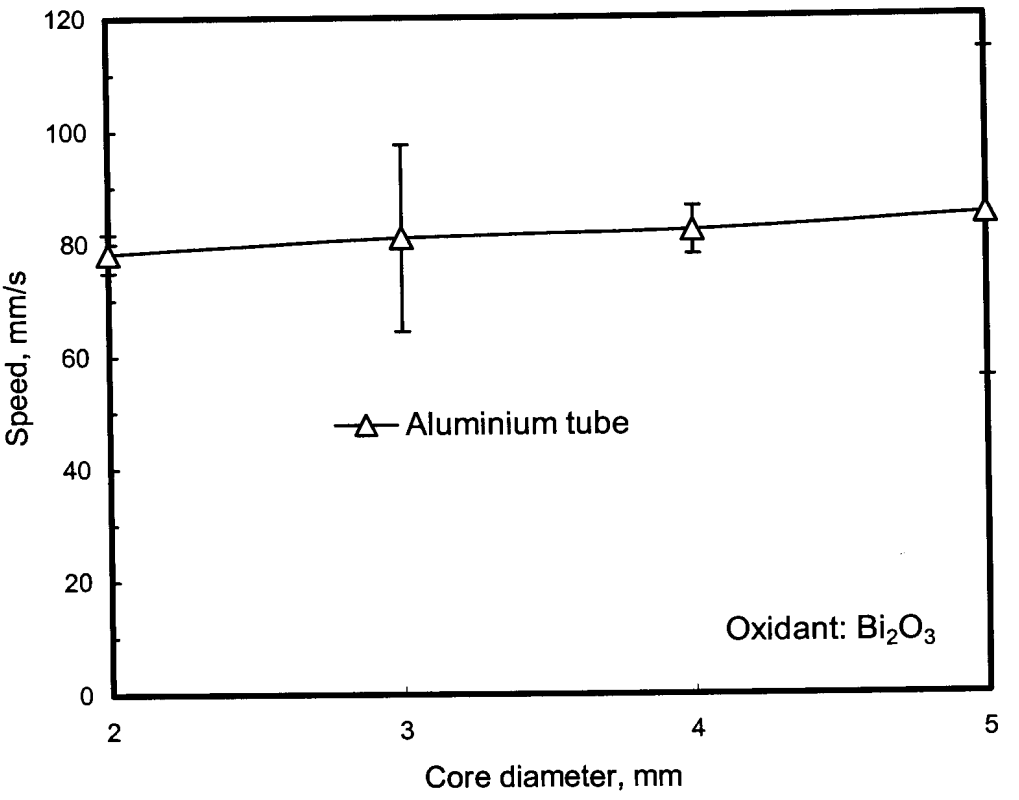

Figure 4.8 Effect of core diameter of tube on the burning rate of Bi_2O_3- 30% Si (Type 3) composition.

Effect of core size

Figure 4.8 shows that the burn rate for a 30% Si (Type 3)- Bi_2O_3 composition in aluminium tubes is not affected by the internal tube diameter when this lies in the range 2 to 5 mm.

Effect of mixing

The higher scatter observed in the burn rates of the Bi_2O_3 – Si systems containing finer silicon suggested that proper mixing might not have been achieved during the preparation of those samples. It was therefore decided to check the effect of using a finer mesh size during the mixing process. Figure 4.9 shows that burn rates are improved when the125 µm is substituted with a 53 µm mesh sieve during mixing. A maximum burn rate of 156 mm/s was obtained for the 20% silicon Type 4 composition (standard deviation 11,4%).

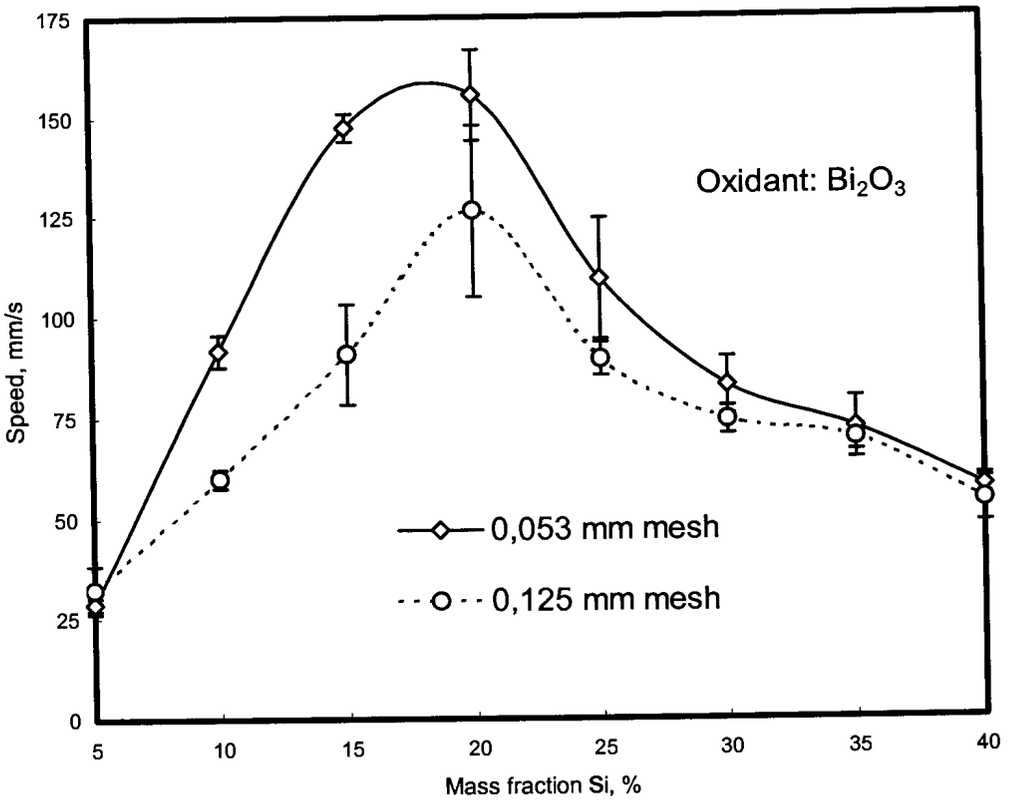

Figure 4.9 Effect of mixing degree on the burning rate of Bi_2O_3- Si (Type 4) system.

4.1.4 Identification of reaction products

Bi_2O_3 -Si system

EDS spectra taken during SEM analysis of the combustion residue from a 30% Si (Type 4) – Bi_2O_3 composition showed large peaks indicating the presence of silica and bismuth (see Plate 3a in Appendix C). XRD analysis of the same sample revealed the presence of metallic Bi (rhombohedral) but also the presence of minor amounts of unburned starting material (Bi_2O_3 and Si). See Figure 6 in Appendix A.

SEM photos showed the presence of a grey mass corresponding to amorphous silica. The bright spots in Plate 3.a, Appendix C, are due to metallic bismuth. Needle-like crystalline deposits were found and identified by EDS as silica. See Plate 4.a and 4.b in Appendix C.

Sb_6O_{13} –Si system

The combustion residue of Sb_6O_{13} – 20% Si (Type 4) from a lead tube were analysed using the SEM – EDS system. The micrographs shown in Plates 5.c and 5.e (Appendix C) reveal the presence of SiO_2 and metallic Sb as the main reaction products. Here too some needle-like crystallites were found at some interfaces and they were also identified to be SiO_2 (Appendix C: Plate 5.a).

XRD patterns revealed the presence of metallic Sb (rhombohedral) and also showed minor peaks due to unreacted Si (Figure 7 in Appendix A). No evidence of crystalline SiO_2 was obtained from the XRD.

5. Conclusion

Antimony hexitatridecoxide (Sb_6O_{13}) and bismuth trioxide were successfully synthesized by controlled thermal decomposition. Sb_6O_{13} was obtained by thermal treatment of colloidal antimony pentoxide (Sb_2O_5) at 315°C for 8 hours. The Bi_2O_3 was synthesised by heating $(BiO)_2CO_3$ at 460°C for 15 hours followed by rapid quenching to room temperature. These compounds were tested as oxidants for silicon in pyrotechnic time delay systems.

Burning rates in the Si (Type 4) – Sb_6O_{13} system were carried out using an initiating starter increment (3 mm) based on a 50% Si (Type 4) – Bi_2O_3 mixture. Experimentally measured rates ranged from ca. 5 to 20 mm/s. The burning rate showed the usual parabolic shape dependence on stoichiometry: A maximum rate was found at 20% Si. The lowest sustainable and reproducible burn rate, in the absence of additives, was 4,8 mm/s (at 10% silicon Type 4). Below this level, the mixtures failed to burn.

The silicon Type 3 presented an unusual situation: Above 20% Si, the propagation of the burning front was faster than for the finer silicon (Type 4). The reasons for this unexpected result are presently unknown. Note however that this fuel did not sustain the propagation for composition containing less than 20% whereas Type 4 did.

Adding inert diluent (fumed silica) to a 10% Si (Type 4) – Sb_6O_{13} mix caused a decreased burn rate at high addition levels. Surprisingly, combustion was sustained up to 10% of diluent, yielding a stable burn rate of 2,3 mm/s. This system is a potential replacement of the conventional barium sulphate-silicon system for long-period delays.

Coarse manganese powder was investigated as a potential substitute for silicon as fuel. Sb_6O_{13}-based compositions sustained combustion in the range 50 to 70% Mn. The burn rates were lower than additive-free silicon-based mixtures.

In the Si-Bi_2O_3 system, compositions containing 5-40% Si did not require a starter element and were ignitable with shock tubing. The mixture containing 20% silicon Type 4 burned fastest. Unfortunately the measured burn rates showed considerable scatter. This is attributed to the gassy combustion of this system. It is concluded that the fast burning Si-Bi_2O_3 system is a potential replacement for the commercial Si-red lead system. Before this system can be implemented the problem of reproducibility needs to be solved.

Fuel particle size did affect the burn rate in the Si-Bi_2O_3 system: Coarse silicon (Type 2) only burned in compositions containing >20% Si. The burn rate did not vary much with the silicon content. Silicon Type 3 compositions showed less scatter in the burn rate. The additives B, B_2O_3 and $KMnO_4$ showed little effect on the burning rate of a composition containing 25% silicon (Type 3) – Bi_2O_3 at addition levels up to 7%.

The effect of the material of construction of the delay element tube was also investigated. Measured burn rates in lead tubes were about 20 - 50% faster than equivalent rates measured using aluminium tubes. This accords with the higher thermal conductive aluminium tubes. They yield lower burn rates owing to the greater lateral loss of energy. Varying the core size of aluminium tubes from 2 to 5 mm did not affect the burn rate of a 30% Si (Type 3) – Bi_2O_3 composition.

Adequate mixing of the ingredients is essential. Its purpose is to break down particle agglomerates and facilitate good mixing, i.e. intimate contact between ingredient particles. The screen mesh size used for brush mixing appears to be an important factor: The burn rate of the 20% Si (Type 4) – Bi_2O_3 composition increased from 126,4 to 155,5 mm/s when a 125 μm screen was replaced by a 53 μm mesh sieve.

There is still a need for more information on the fundamental physico-chemical properties and reaction kinetics for Si-fuel reacting with either Bi_2O_3 or Sb_6O_{13} as oxidant. It is recommended that a DTA study of the reaction kinetics be done.

The use of ceramic tubes should also be investigated as substitutes for the current lead tubes.

References

Aldushin A.P. and Zeinenko K.I. (1992). Combustion of pyrotechnic mixtures with heat transfer from gaseous products. *Comb. Explos. Shock Wave,* **27** (6), 700-703.

Al-Kazraji S.S. and Rees G.J. (1978). The fast pyrotechnic reaction of silicon and red lead -Part 1: Differential thermal analysis studies. *Combust. Flame,* **31**, 105-113.

Al-Kazraji S.S. and Rees G.J. (1979a). Differential thermal analysis studies of the reactions of silicon and lead oxides. *J. Thermal Anal.,* **16**, 35-39.

Al-Kazraji S.S. and Rees G.J. (1979b). The fast pyrotechnic reaction of silicon and red lead - Heats of reaction and rates of burning. *Fuel,* **58**, 139-143.

Barin I. (1989). Thermochemical data of pure substances, Part I & II, VCH, Weinhem.

Barton T.J., Williams N., Charsley E.L., Rumsey J. and Ottaway M.R. (1982). Factors affecting the ignition temperature of pyrotechnics. Proceedings of the 8th International Pyrotechnics Seminar, Chicago, USA, July 12-18, pp 99-111.

Beck M.W. (1984). Intersolid combustion reactions in pyrotechnic systems, *PhD Thesis,* Rhodes University, South Africa.

Beck M.W. and Brown M.E. (1986). Modification of the burning rate of Antimony/Potassium Permanganate pyrotechnic delay compositions. *Combust. Flame,* **66**, 67-75.

Beck M.W. and Brown M.E. (1991). Finite-element simulation of the differential thermal analysis response to ignition of a pyrotechnic composition. *J. Chem. Soc. Faraday Trans.,* **87**(5) 711-715.

Beck M.W. and Flanagan J. (1992). *Delay composition and device.* Patent, US 5 147476.

Beretka J. (1984). Kinetic analysis of solid-state reactions between powdered reactants. *J. Am. Chem. Soc.,* **67**(9), 615-620.

Berger B., Charsley E.L., Rooney J.J. and Warrington S.B. (1995). Thermal analysis studies on the Zirconium/Nickel alloy- Potassium Perchlorate- Nitrocellulose pyrotechnic system. *Thermochim. Acta,* **269/270**, 687-696.

Birchenall C.E. (1986). Oxidation of metals and alloys, in Bever M.B. (Ed.) *Encyclopedia of Materials Science and Engineering,* Vol. 5, Pergamon Press, Oxford.

Boberg T., Carlsson S., Ekman B. and Karlsson B. (1997). *Delay charge and element and detonator containing such a charge,* Patent, US 5 654 520.

Boddington T., Laye P.G., Pude J.R.G. and Tipping J. (1982). Temperature profile analysis of pyrotechnic systems. *Combust. Flame,* **47**, 235-254.

Boddington T., Laye P.G., Tipping J. and Whalley D. (1986). Kinetic analysis of temperature profiles of pyrotechnic systems. *Combust. Flame,* **63**, 359- 368.

Boddington T., Cottrell A., Laye P.G. and Singh M. (1986). Times-to-ignition of pyrotechnics. *Thermochim. Acta,* **106**, 253-261.

Boddington T. and Laye P.G. (1987). Temperature dependence of the burning velocity of gasless pyrotechnics. *Thermochim. Acta* **120**, 203-206.

Boddington T., Cottrell A. and Laye P.G. (1989). Combustion transfer in gasless pyrotechnics. *Combust. Flame,* **79**, 234-241.

Boddington T., Cottrell A. and Laye P.G. (1990). A numerical model of combustion in gasless pyrotechnics. *Combust. Flame,* **76**, 63-69.

Booth F. (1953). The theory of self-propagating exothermic reactions in solid systems. *Trans. Farad. Soc.*, **49**, 272-281.

Brammer A.J., Charsley E.L., Griffiths T.T., Rooney J.J. and Warrington S.B. (1996). A study of the pyrotechnic performance of the Silicon- Bismuth oxide system. Proc. 22th Int. Pyrotechn. Sem., Fort Collins Colorado USA, 447-460

Brauer K.O. (1974). *Handbook of Pyrotechnics,* Chemical Publishing Company, NY.

Brown M.E. (1989). Thermal analysis of energetic materials. *Thermochim. Acta,* **148**, 521-531.

Brown M.E., Taylor S.J. and Tribelhorn M.J. (1998). Fuel-oxidant particle contact in binary pyrotechnic reactions. *Propellant, Explosives, Pyrotechnic*, **23**, 320-327.

Brown M.E. (2001). Some thermal studies on pyrotechnic compositions. *J. Thermal. Anal. Cal.*, **65**, 323-334.

Brydson J.A. (1975). Plastics materials. 3^{d} Ed., Newnes – Butterworths, London.

Carr D.S. (1990). Lead compounds, in *Ullmann's Encyclopedia of Industrial Chemistry,* 5th Ed., Vol. A15, Elvers B. (Ed), VCH Publishers, Weinheim, pp. 249- 257.

Cheng C-K., Huang C-R. and Wu Y.Y. (1984). Studies on the delay mix of Zr/ Fe_2O_3. Proceedings of The 12th Symposium on Explosives and Pyrotechnics, San- Diego, California, USA, March 13-15, Vol. 5, pp 33-38.

Charsley E.L., Ford M.C., Tolhurst D.E., Barid-Parker S., Boddington T. and Laye P.G. (1978). Differential thermal analysis and temperature profile analysis of pyrotechnic delay systems: Mixtures of Tungsten and Potassium Dichromate. *Thermochim. Acta,* **25**, 131-141.

Charsley E.L., Boddington T., Gentle J.R. and Laye P.G. (1978). Differential thermal analysis and temperature profile analysis of pyrotechnic delay systems: Slow burning mixtures of Boron and Potassium Dichromate. *Thermochim. Acta*, **22**, 175-186

Charsley E.L., Chen C., Boddington T., Laye P.G. and Pude J.R.G. (1980). Differential thermal analysis and temperature profile analysis of pyrotechnic delay systems: Ternary mixtures of Silicon, Boron and Potassium Dichromate. *Thermochim. Acta,* **35**, 141-152.

Charsley E.L., Cox C.T., Ottaway M.R., Barton T.J. and Jenkins J.M., (1982). Investigation of the ignition temperature of pyrotechnic systems using a purpose designed differential thermal analysis apparatus. *Thermochim. Acta*, **52**, 321-332

Conkling J.A. (1996). Pyrotechnics. In Kroschwitz, J.I. (Ed.), *Kirk-Othmer's Encyclopedia of Chemical Technology,* 4th Ed., Vol. 20, John- Wiley and Sons, New York, pp. 680- 697.

Crider J F (1982). Self-propagating high temperature synthesis - A soviet method for producing ceramic material, 519-526.

Davies N., Griffiths T.T., Charsley E.L. and Rumsey J.A. (1985). Studies on gasless delay compositions containing Boron and Bismuth trioxide. Int. Jahrestag. – Fraunhofer-Inst. Treib- Explosivst. CA 103:198070j (1985).

De Vito S.C. (1995). Lead compounds (Industrial toxicology). In Kroschwitz J.I. (Ed.), *Kirk-Othmer's Encyclopedia of Chemical Technology,* 4th Ed., Vol. 15, John Wiley and Sons, New York, pp. 155-157.

Howlett S.L. and May F.G.J. (1974). Ignition and reaction of Boron fueled pyrotechnic delay compositions: Part1. Boron-Potassium Dichromate and Boron-Silicon-Potassium Dichromate systems. *Themochim. Acta*, **9**, 213-216.

JANAF Thermochemical Tables (1971). United States Department of Commerce and National Bureau of Standards, Washington.

Jander W. (1927). Reactions in the solid state at high temperatures. *Z. Anorg. Allg. Chem.*, **163**, 1-30 & 31-52.

Kaslin R. (1947). Chemie und industrie **57**, 144.

Keski J.R. (1972). Bismuth oxide ceramics, *Ceramic Bulletin*, **51**(6), 527-531.

Khaikin B.I. and Merzhanov A.G. (1966). Theory of thermal propagation of a chemical reaction front. *Comb. Exp. Shock Waves*, **2**(3), 36-46.

Krone U. and Lancaster R. (1992). Pyrotechnics, in Gerhartz W.B. (Ed), *Ullmann's Encyclopedia of Industrial Chemistry,* 5th Ed., Vol. A22, VCH Publishers, Weinheim, pp. 437-452.

Kruger J., Winkler P., Luderitz E. and Luck M. (1985). Bismuth, Bismuth alloys and Bismuth compounds. In Elvers, B. (Ed.), *Ullmann's Encyclopedia of Industrial Chemistry,* 5th revised Ed., A4, VCH Publishers, Weinheim, pp. 171-189.

Koga N. and Tanaka H. (2002). A physico-geometric approach to the kinetics of solid-state reactions as exemplified by the thermal dehydration and decomposition of inorganic solids. *Thermochim. Acta*, **388**, 41-61.

Koga N. and Criado J.M. (1998). Kinetic analysis of solid-state reactions with a particle size distribution. *J. Am. Ceram. Soc.*, **81**(11), 2901-2909.

Kosanke K.L., Kosanke B.J. and Dujay R.C. (2000). Pyrotechnic particle morphology-low melting point oxidizers. *Journal of Pyrotechnics*, Issue 12, Winter, 5-15.

Kosanke K.L. and Kosanke B.J. (1997). Pyrotechnic ignition and propagation: A review. *Journal of Pyrotechnics*, Issue 6, Winter, 17-29.

Laye P.G. (1997). Tying up loose ends. *Thermochim. Acta,* **300**, 237-245.

Laye P.G. and Charsley E.L. (1987). Thermal analysis of pyrotechnics. *Thermochim. Acta*, **120**, 325-349

Lee I., Reed R.R., Brady V.L. and Finnegan S.A. (1997). Energy release in the reaction of metal powders with fluorine containing polymers, *J. Thermal Anal.,* **49**, 1699-1705.

Lee J.-S. and Hsu C.-K. (2001). The DSC studies on the phase transition, decomposition and melting of Potassium Perchlorate with additives. *Thermochim. Acta*, **367-368**, 367-370.

Levin E.M. and McDaniel C.L. (1962). The system Bi_2O_3-B_2O_3. *J. Am. Ceram. Soc.*, Vol.**45**(8), 355-360.

Lide D.R. (Ed.) (1992). *CRC Handbook for Chemistry and Physics,* CRC Press, Boca Raton,Florida.

Liley P.E., Read R.C. and Buck E. (1984). *Perry's Chemical Engineers' Handbook,* 6th Ed., McGraw-Hill Book Company, New York.

McLain J.H. (1980). *Pyrotechnics from the viewpoint of solid state chemistry*, Franklin Institute Press, Philadelphia, Pennsylvania.

Mellor J.W. (1925). The Silicon, in *a comprehensive treatise on inorganic and theoretical chemistry,* VolumeVI, Longmans, Green and co., London.

Mellor J.W. (1933). The antimonious acids and the antimonites, in a *Comprehensive treatise on inorganic and theoretical chemistry,* Volume IX, Longmans, Green and co., London.

Moghaddam A.Z. and Rees G.J. (1981). The fast pyrotechnic reaction of Silicon with Lead oxides: Differential scanning calorimetry and hot-stage microscopy studies, *Fuel,* **60**, 629-632.

Munir Z.A. (1988). Synthesis of high temperature materials by self-propagating combustion methods. *Ceramic Bulletin*, **67**(2), 342-349.

Naeser G. and Scholz W. (1958). Kolloid Zeitschrift, **156**, 1-8.

Norgrove A.H.C., Jones A.F. and King-Hele J.A. (1991). Effects of solid to gas conversion in detonator delay elements. *Combust. Science and Technology,* **76**, 133-157.

Oliveira A.A.M. and Kaviany M. (1999). Role of inter- and intraparticle diffusion in nonuniform particle size gasless compacted-powder combustion synthesis-I: Formulation. *Int. J. Heat Mass Transfer,* **42**, 1059-1073

Parrott J.E. and Stuckes A.D. (1975). *Thermal Conductivity of Technological Materials,* Pion Limited, Bristol.

Perry R.H. and Chilton C.H. (1973). *Chemical Engineer's Handbook.* 5th Ed. McGraw-Hill, Inc., New York.

Pourbaix M. (1966). Silicon, in *Atlas of Electrochemical Equilibria in Aqueous Solutions,* Franklin J.A. (Translator). National Association of Corrosion Engineers and Cebelcor.

Rogers J.W., Erickson K.L. and Belton D.N., Springer R.W., Taylor T.N. and Beery J.G. (1988). Low temperature diffusion of oxygen in titanium and titanium oxide films. Applied Surface Sci. **35**, 137-152.

Rugunanan R.A. (1991a). Intersolid pyrotechnic reactions of Silicon. *PhD Thesis,* Rhodes University, South Africa.

Ricco I.M.M (2004). Alternative oxidants and processing procedures for pyrotechnic time delays. *MEng. Thesis*, University of Pretoria, South Africa.

Rugunanan R.A. and Brown M.E. (1991b). Reactions of powdered silicon with some pyrotechnic oxidants, *J. Thermal Anal.,* **37**, 1193-1211.

Rugunanan R.A. and Brown M.E. (1994a). Combustion of binary and ternary Silicon/oxidant pyrotechnic systems, Part I: Binary systems with Fe_2O_3 and SnO_2 as oxidants. *Combust. Science and Technology,* **95**, 61-83.

Rugunanan R.A. and Brown M.E. (1994b). Combustion of binary and ternary Silicon/oxidant pyrotechnic systems, Part II: Binary systems with Sb_2O_3 and KNO_3 as oxidants. *Combust. Science and Technology,* **95**, 85-99.

Rugunanan R.A. and Brown M.E. (1994c). Combustion of binary and ternary Silicon/oxidant pyrotechnic systems, Part III: Ternary systems. *Combust. Science and Technology,* **95**, 101-115.

Runyan W. (1996). Silicon and Silicon alloys, in Kroschwitz, J.I. (Ed.). *Kirk-Othmer's Encyclopedia of Chemical Technology,* 4th Ed., Vol. 21, John- Wiley and Sons, New York, pp. 1084-1104.

Schmalzried H. (1976). Solid-state reaction, in Hannay N.B. (Ed.), *Treatise on Solid-State Chemistry*, Vol.4, 233-279, Plenum Press, New York.

Schwab G.M. and Gerlach J. Z. (1967). Physik Chem. Neue Folge, **56**, 121.

Schwartz A. M. and Elving P.J. (1983). Surface Chemistry: Utilization in analysis, in

Treatise On Analytical Chemistry, Vol.3 section D, pp 84-148, John Wiley & Sons, New York.

Smit K.J., De Yong L.V. and Gray R. (1996). Observation of infrared emission spectra from Silicon combustion products. *Chem. Phys. Lett.* **254**, 197-202

Snegirev A.Y. and Talalov V.A. (1991). Determination of kinetic parameters for a pyrotechnic mixture, *Inorganic Materials,* **27**, 462-467.

Taylor R. (1986). Thermal conductivity of ceramics *in* Bever M. (Ed.), *Encyclopedia of Materials Science and Engineering,* Volume 7, Pergamon Press, Oxford.

Taylor S.J. (1994). Computer modeling of pyrotechnic combustion. *PhD Thesis,* Rhodes University, South Africa.

Tribelhorn M.J., Blenkinsop M.G. and Brown M.E. (1995a). Combustion of some Iron-fuelled binary pyrotechnic systems.*Thermochim. Acta,* **256**, 291-307.

Tribelhorn M.J., Venables D.S. and Brown M.E. (1995b). Combustion of some Zinc-fuelled binary pyrotechnic systems. *Thermochim. Acta,* **256**, 309-324.

Triblehom M.J., Venables D.S. and Brown M.E. (1995c). A thermoanalytical study of some Zinc- fuelled binary pyrotechnic systems. *Thermochim. Acta,* **269/270**, 649-663.

Tulis A.J. (1980). Flowability techniques in the processing of powdered explosives, propellants and pyrotechnics. *J. Hazard. Materials,* **4**, 3-10.

Varma A., Rogachev A.S., Mukasyan A.S. and Hwang S. (1998). Combustion synthesis of advanced materials: Principles and applications, *Adv. Chem. Eng.,* **24**, 79-226.

Varma A. (2000). Form from fire. *Scientific American,* **283**(2) 44-47.

Wang L.L., Munir Z.A. and Maximov M. (1993). Review thermite reactions: Their utilisation in the synthesis and processing of materials. *J. Mat. Sci.,* **28**, 3693-3708.

Wilson M.A. and Hancox R.J. (2001). Pyrotechnic delays and thermal sources. *Journal of Pyrotechnics*, Issue 13, Summer, 9-30.

Wolf H. U. (1985). Barium and Barium compounds in Wolfgang G (Ed.) *Ullmann's Encyclopedia of Industrial Chemistry,* 5th Ed., Vol. A3, VCH Publishers, Weinheim, pp. 325-341.

Yoganarasimhan S. R. (1988). Effects of gas-phase mass transport in the pyrotechnic system red Lead-Silicon-Potassium Perchlorate. *J. Thermal Anal.,* **34**, 937-947.

Yoganarasimhan S.R. and Josyulu O.S.(1987). Reactivity of the ternary pyrotechnic system red Lead-Silicon-Ferric oxide. *Defence Sci. J.*, **37**(1), 73-83.

Zeulehner W., Neuer B. and Rau G. (1993). Silicon. In Elvers, B. (Ed.), *Ullmann's Encyclopedia of Industrial Chemistry,* 5th revised Ed., A23, VCH Publishers, Weinheim, pp. 721-748.

Appendix A

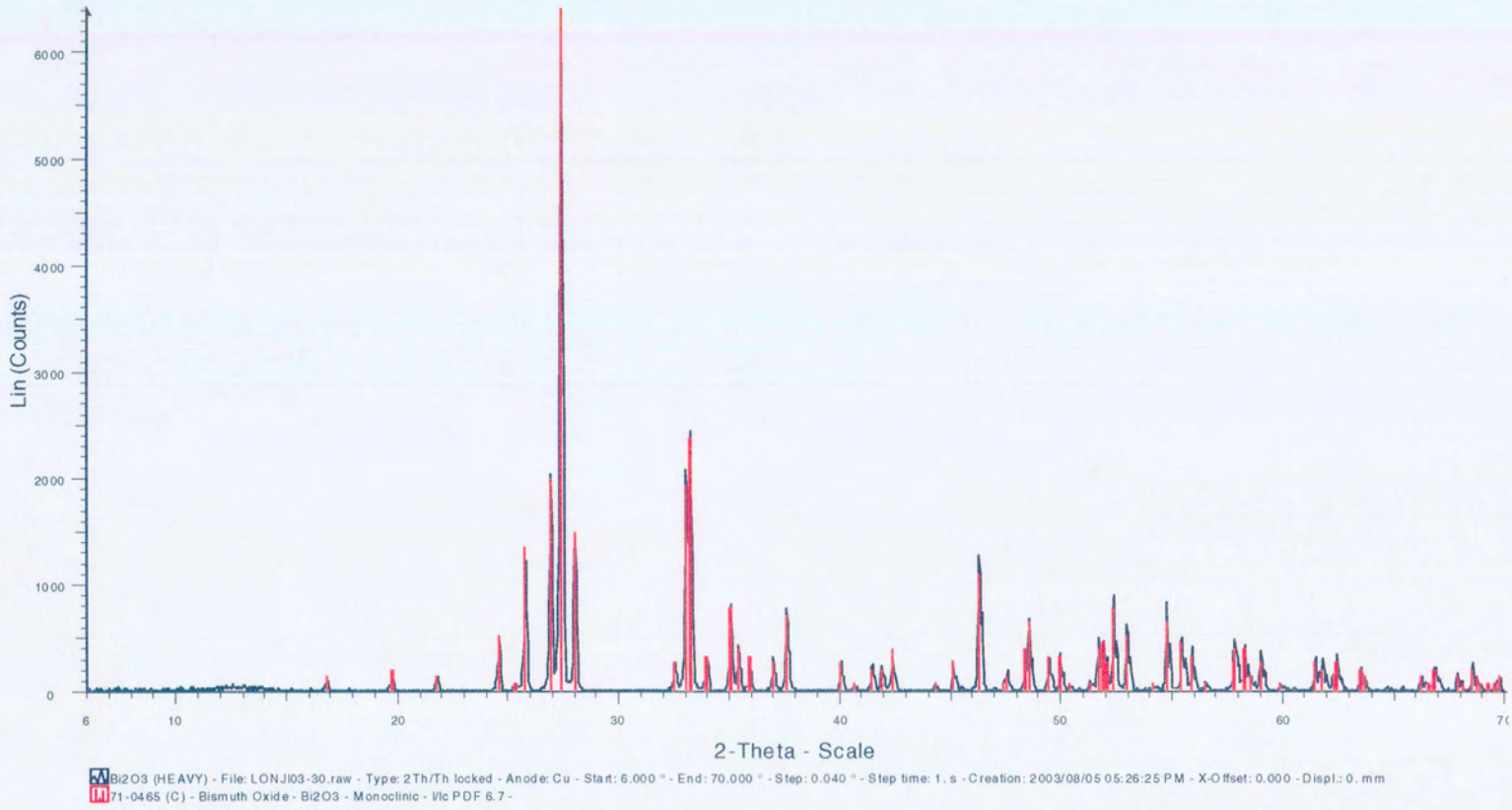

Figure 1 XRD pattern of Bi_2O_3 produced by thermal decomposition of $Bi_2O_2CO_3$ at 460°C during 15 hours.

Appendix A

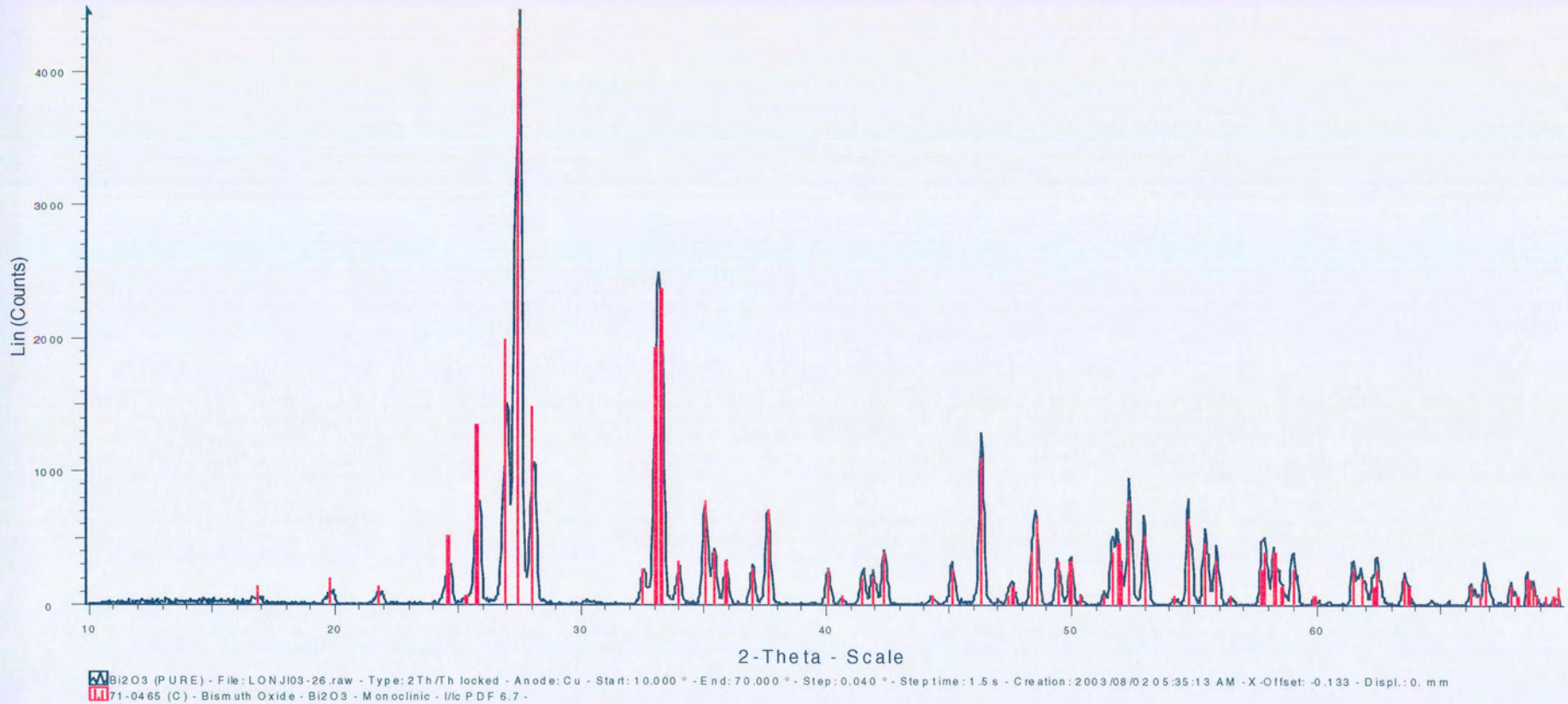

Figure 2 XRD pattern of pure Bi_2O_3

Appendix A

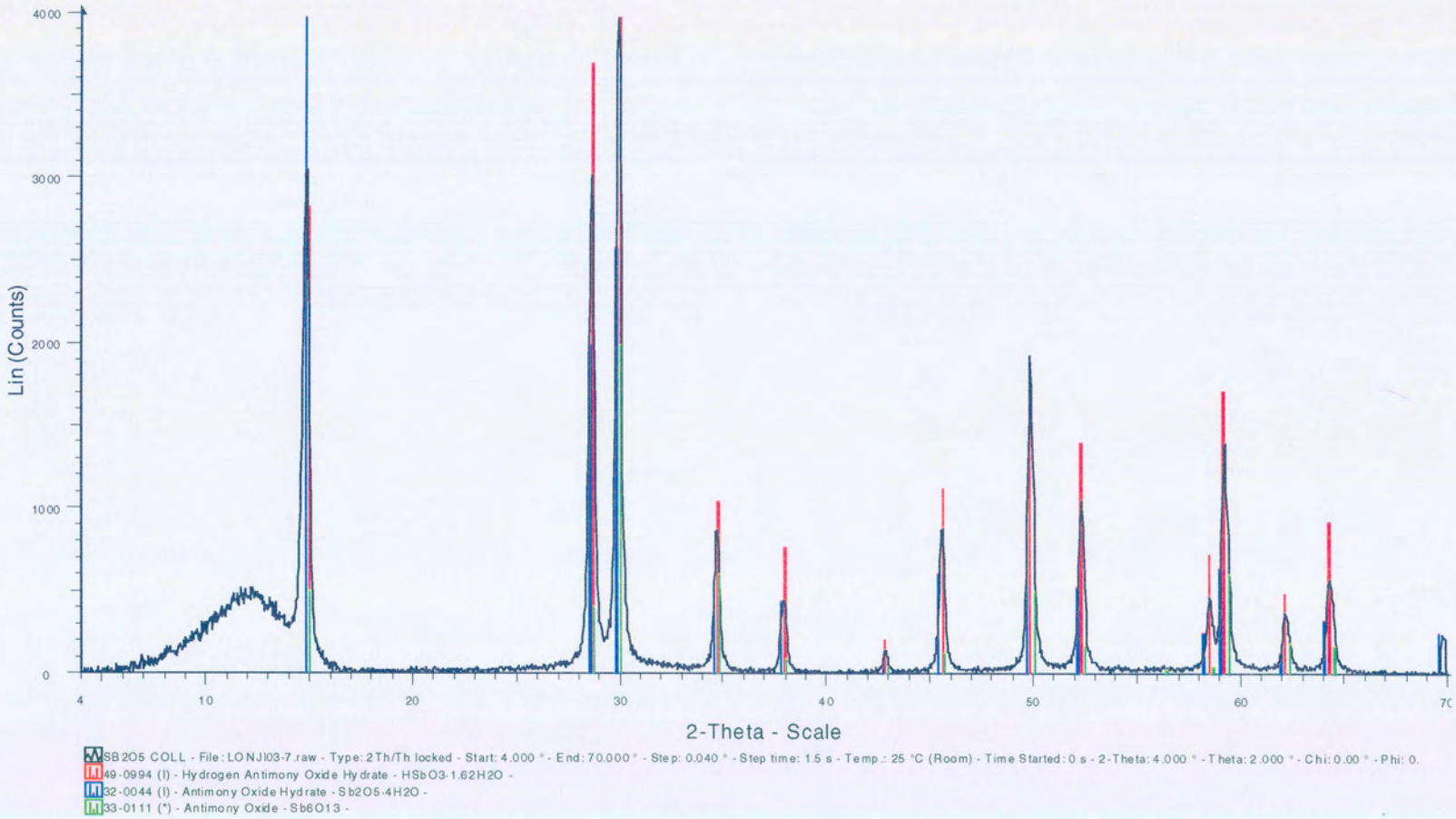

Figure 3 XRD Pattern of the Colloidal Sb_2O_5.

Appendix A

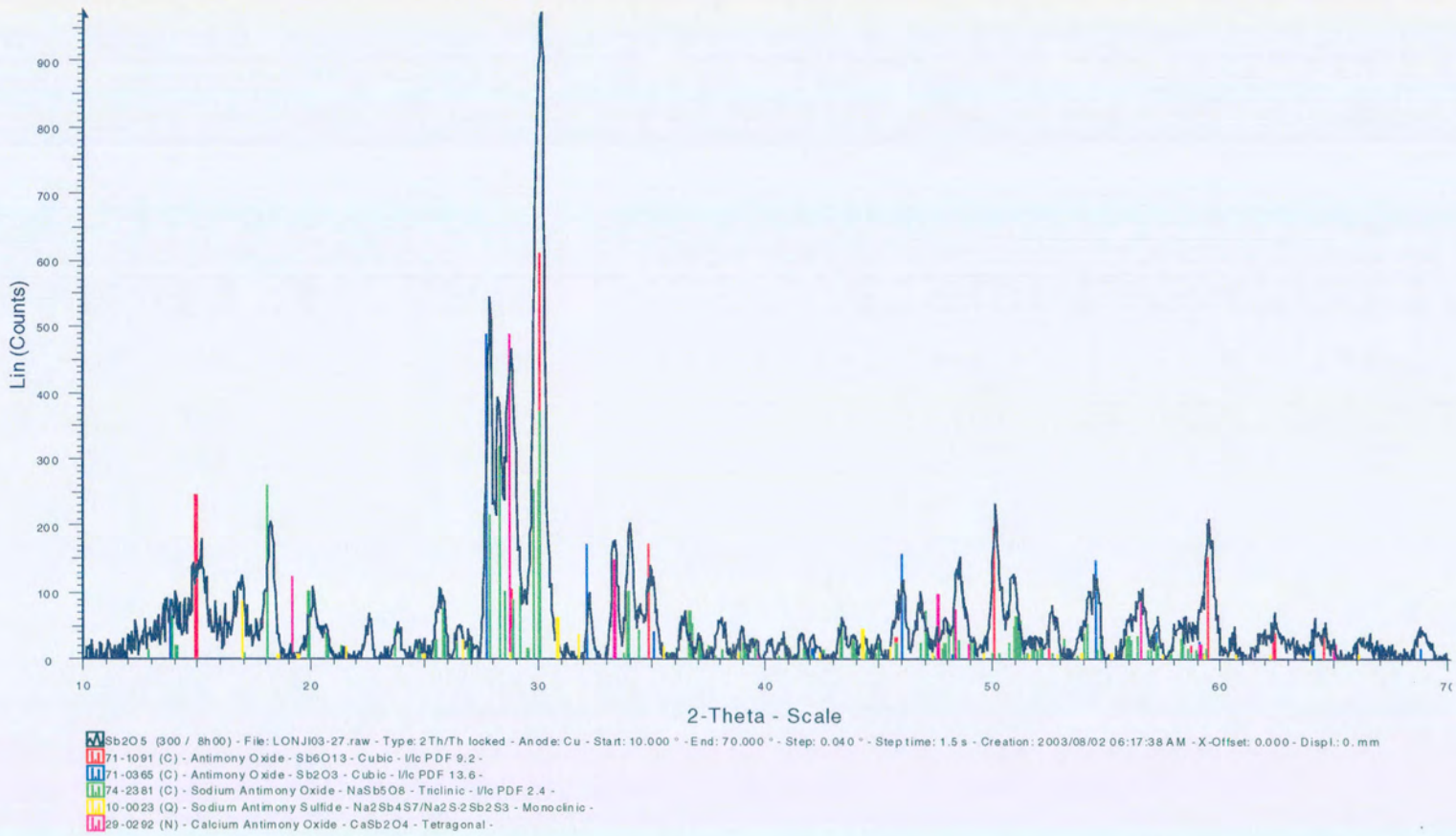

Figure 4 XRD pattern of a product resulting from the thermal decomposition of Sb_2O_5 in an uncovered crucible

Appendix A

.

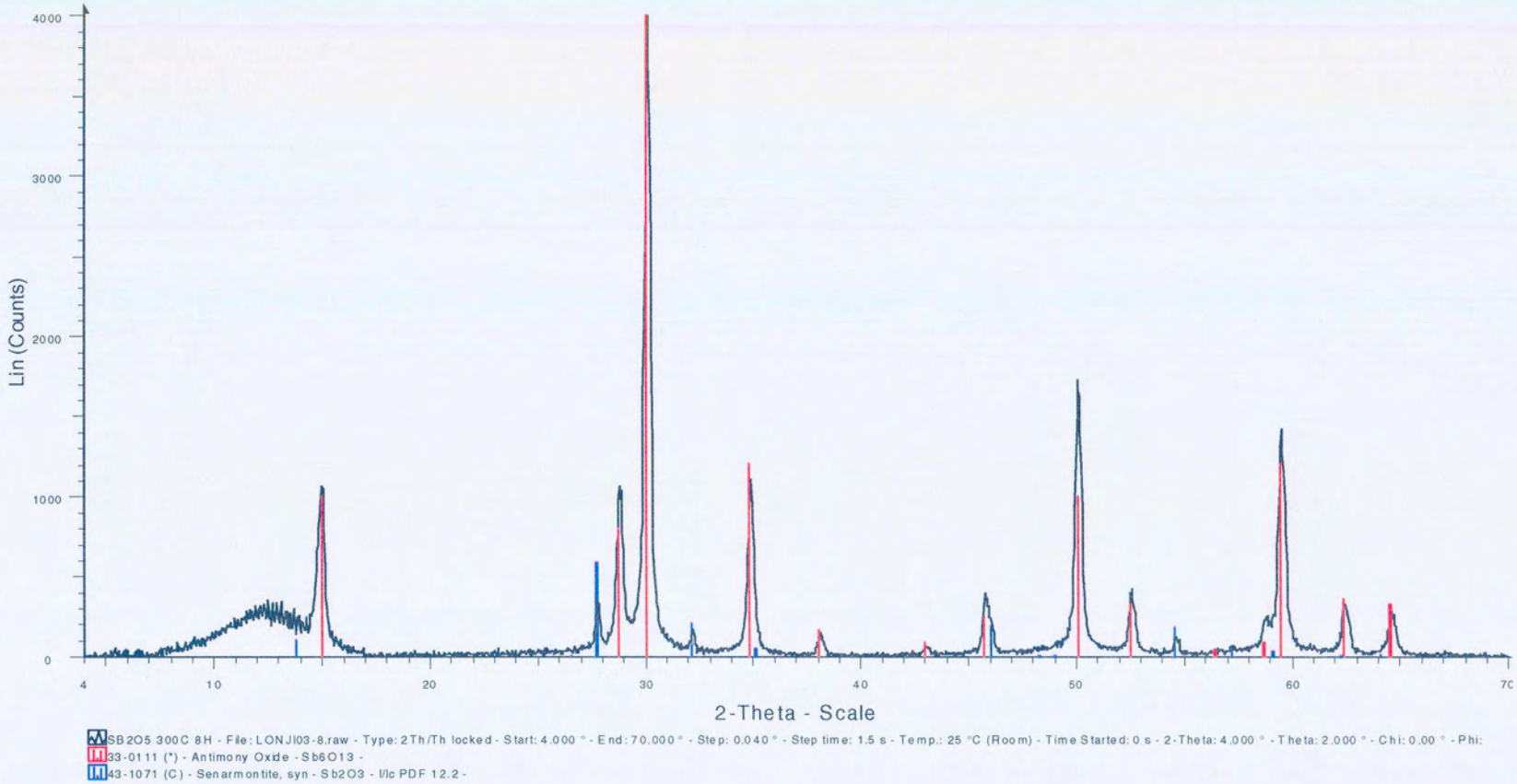

Figure 5 XRD pattern of Sb_6O_{13} from the thermal decomposition of Sb_2O_5 in a covered crucible.

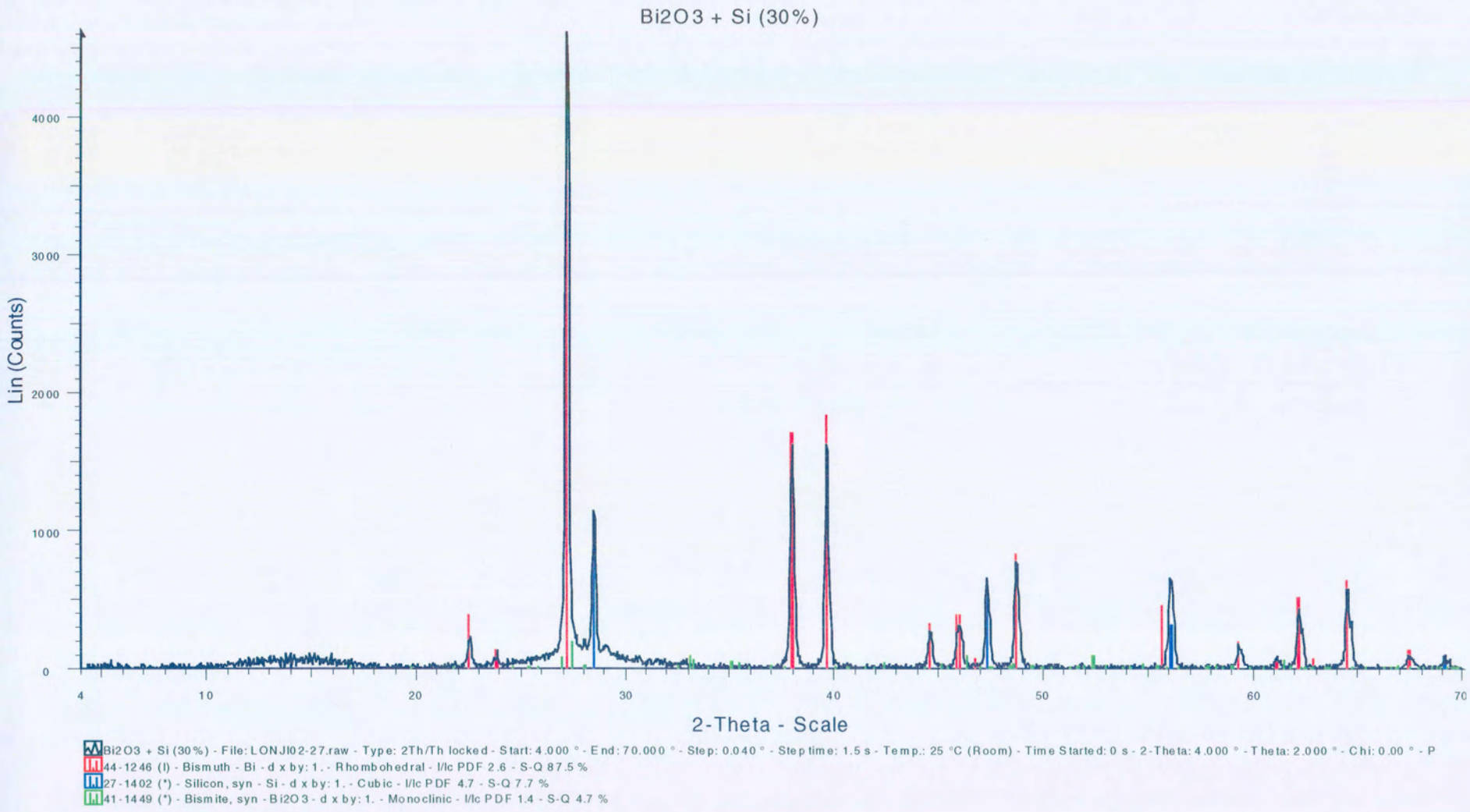

Figure 6 XRD pattern of a combustion product from the system (Bi_2O_3-30%Si –type 4)

Appendix A

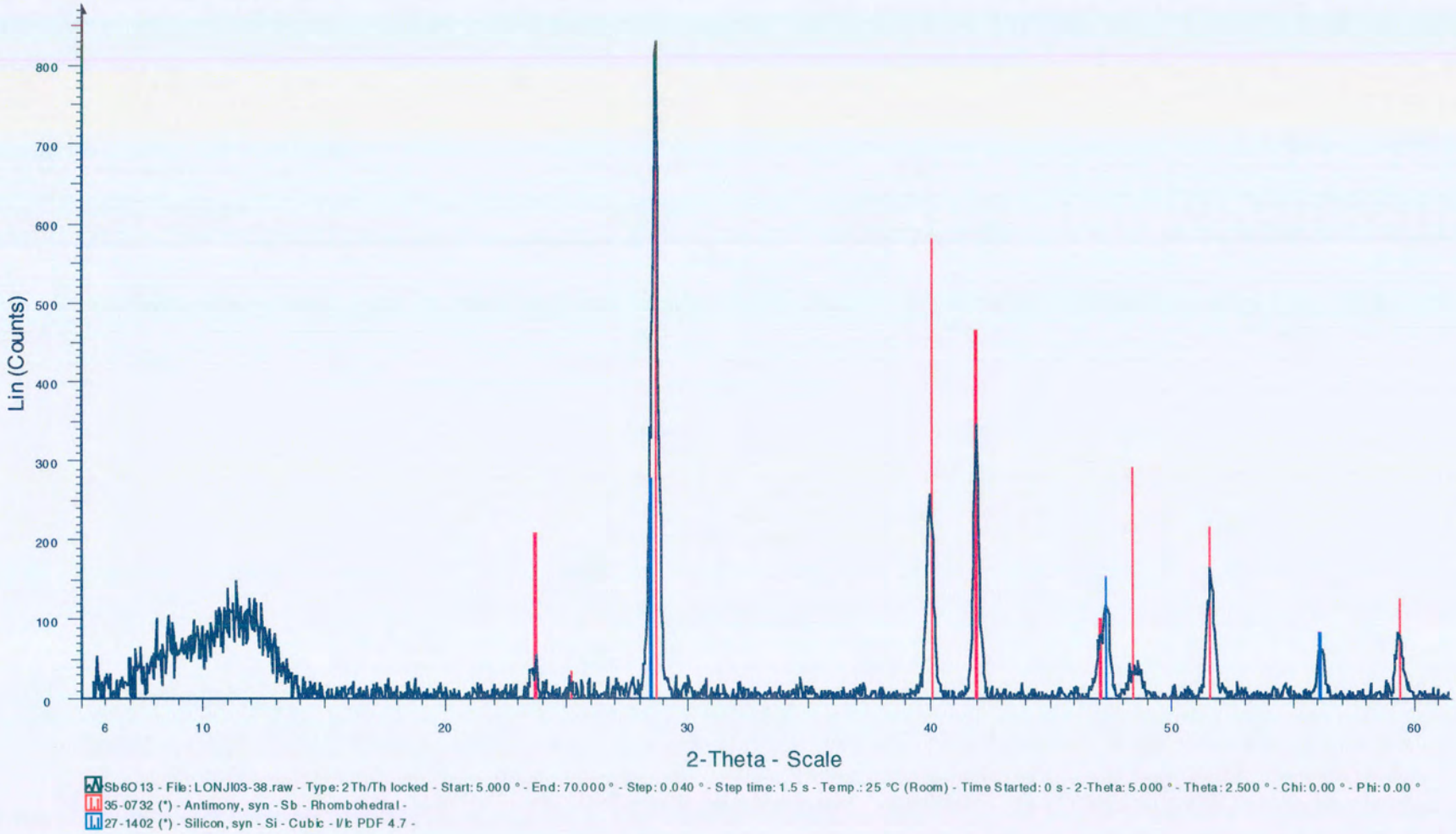

Figure 7 XRD pattern of a combustion product from the system (Sb_6O_{13}-20%Si –type 4)

Appendix B

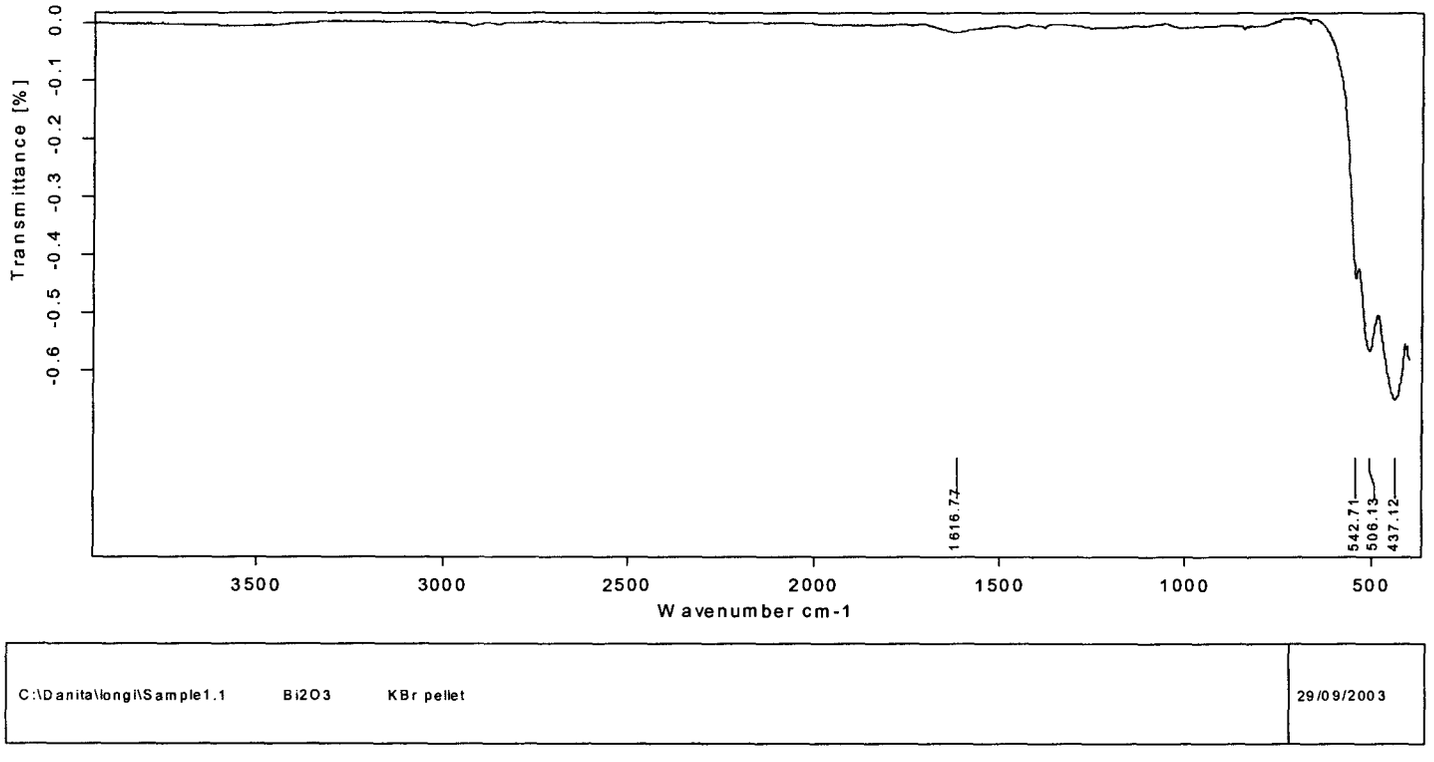

Figure 1 FT-IR Diagram of Pure Bi_2O_3.

Appendix B

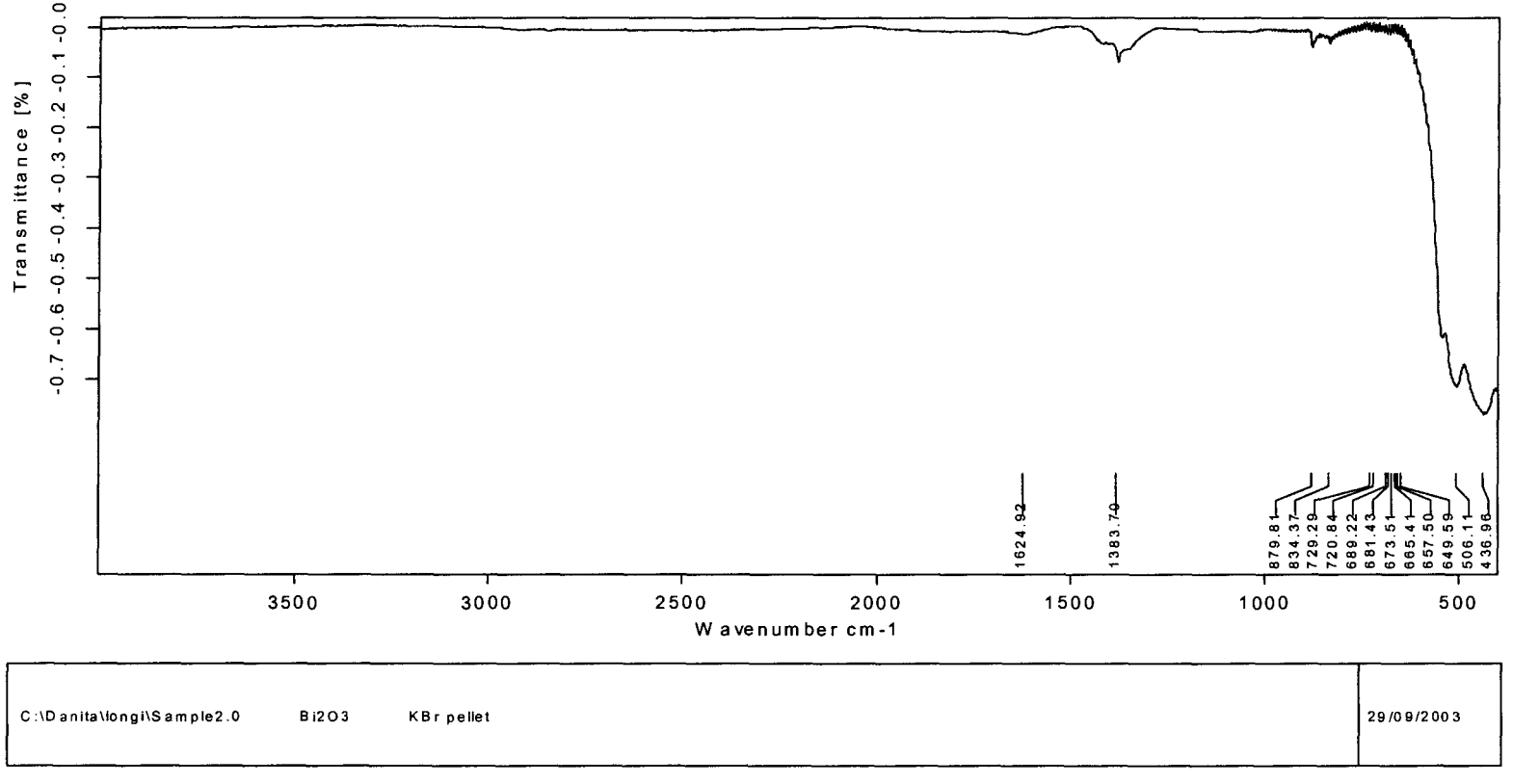

Figure 2 FT-IR diagram of Bi_2O_3 produced from thermal decomposition of $Bi_2O_2CO_3$ at 460℃ during 15 hours.

Appendix C

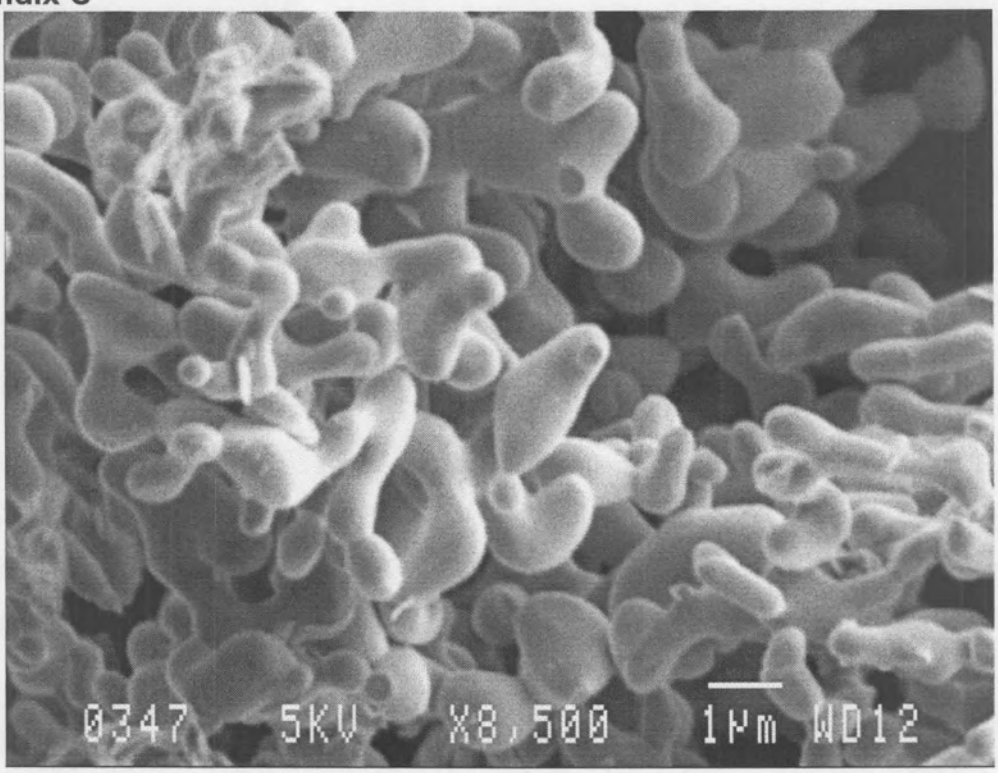

Plate 1 SEM micrograph for Bi_2O_3

Appendix C

2.a

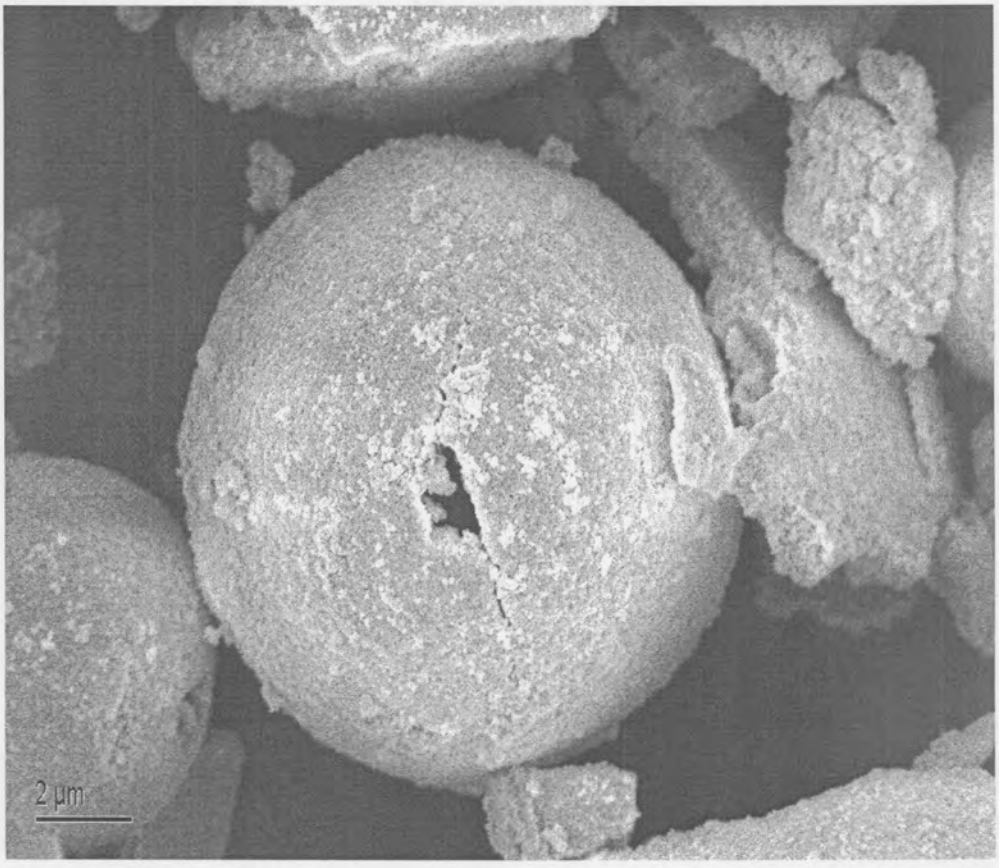

Plate 2.a SEM micrograph for Sb_6O_{13}.

Appendix C

2.b

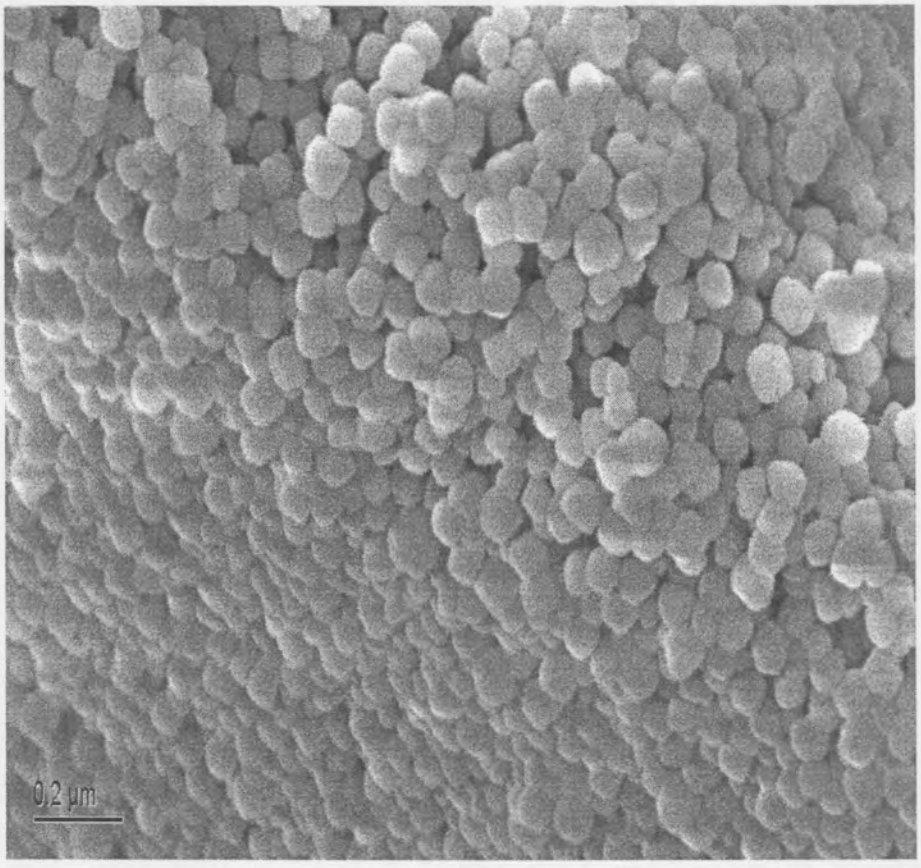

Plate 2.b SEM micrograph for a sub-layer Sb_6O_{13}.

Appendix C: 3.a

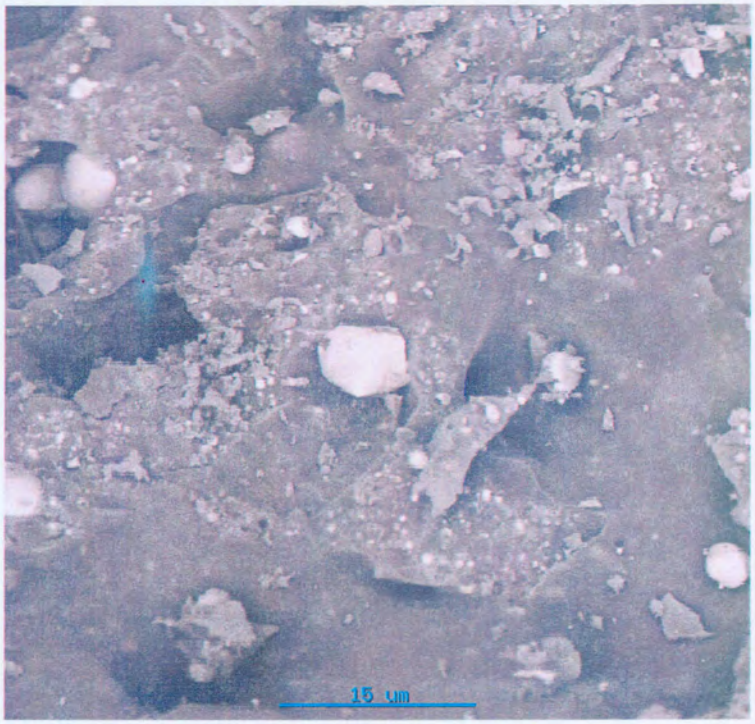

Plate *3.a SEM micrograph of a residue from the combustion of Bi2O3 – 30% Si (type 4) in open air.*

3.b

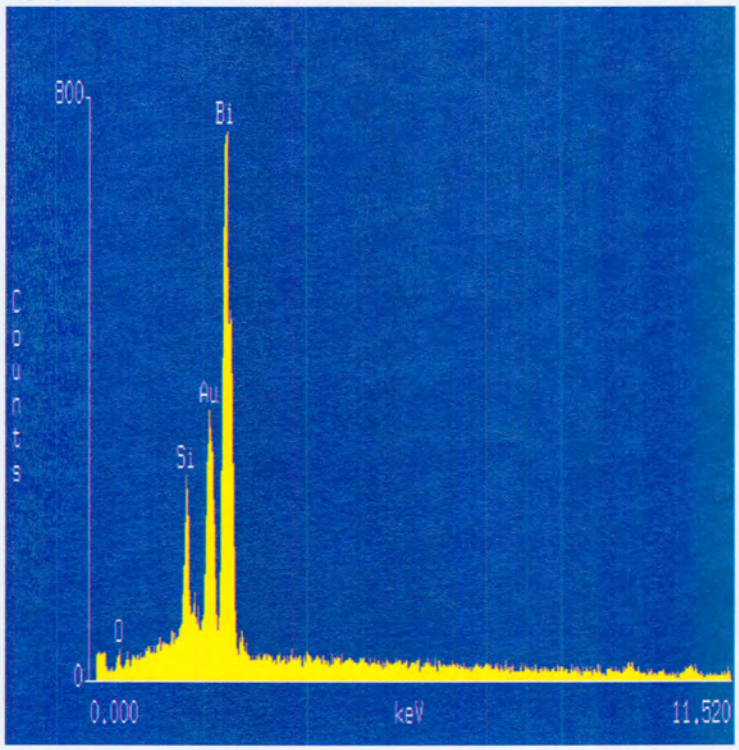

Figure 3.b EDS spectra obtained from a specific point on the glassy mass taken on the micrograph 3a.

Appendix C

4.a

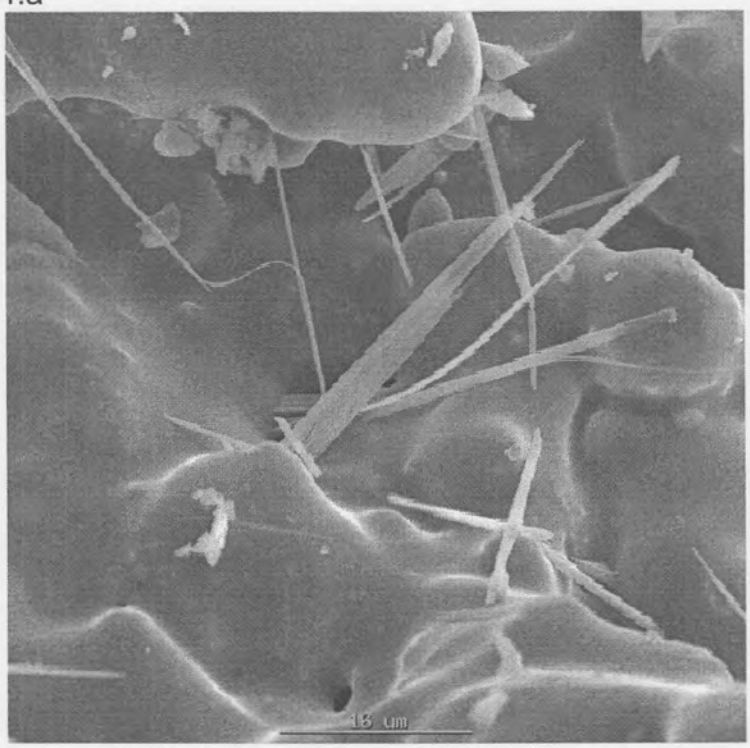

4.b

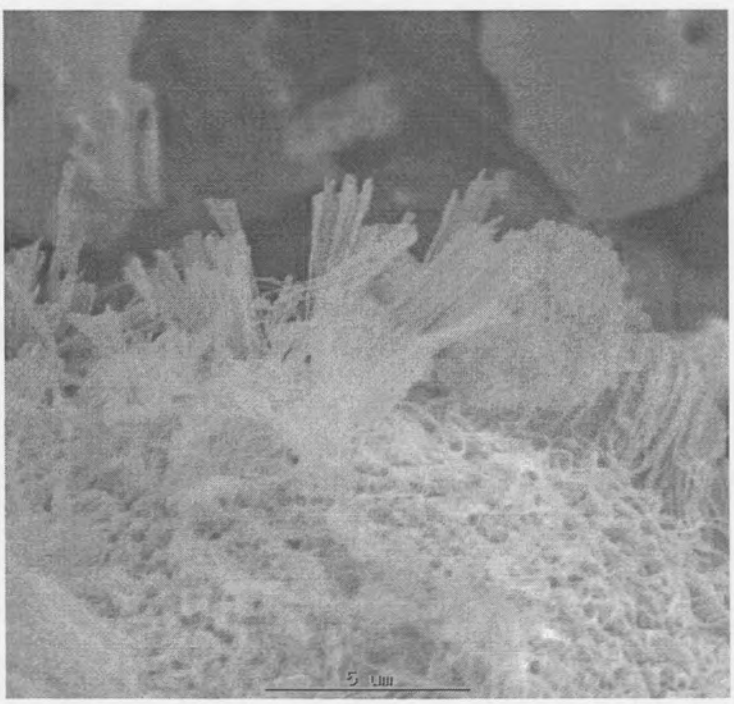

Plates 4.a and 4.b SEM micrograph: Residue from the combustion of Bi2O3 – 30% Si (type 4), in confined lead tube.

Appendix C

4.c

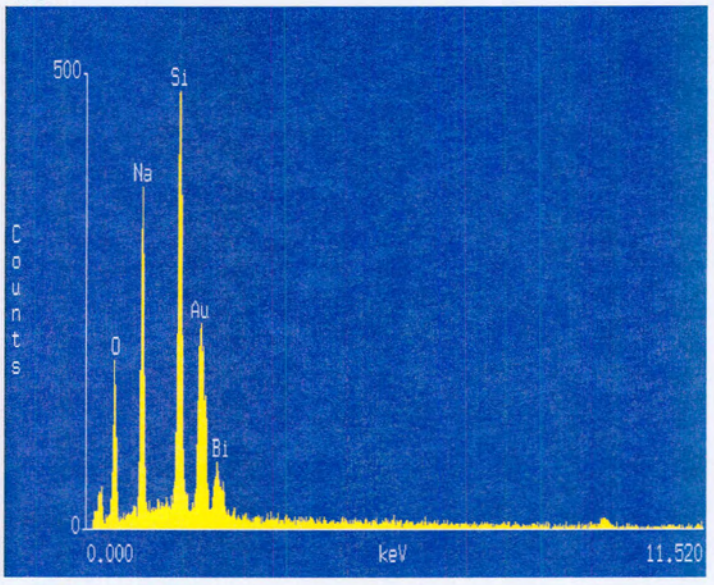

Figure 4.c EDS spectra from a needle considered on the micrographs 4.a or 4.b.

Appendix C

5.a

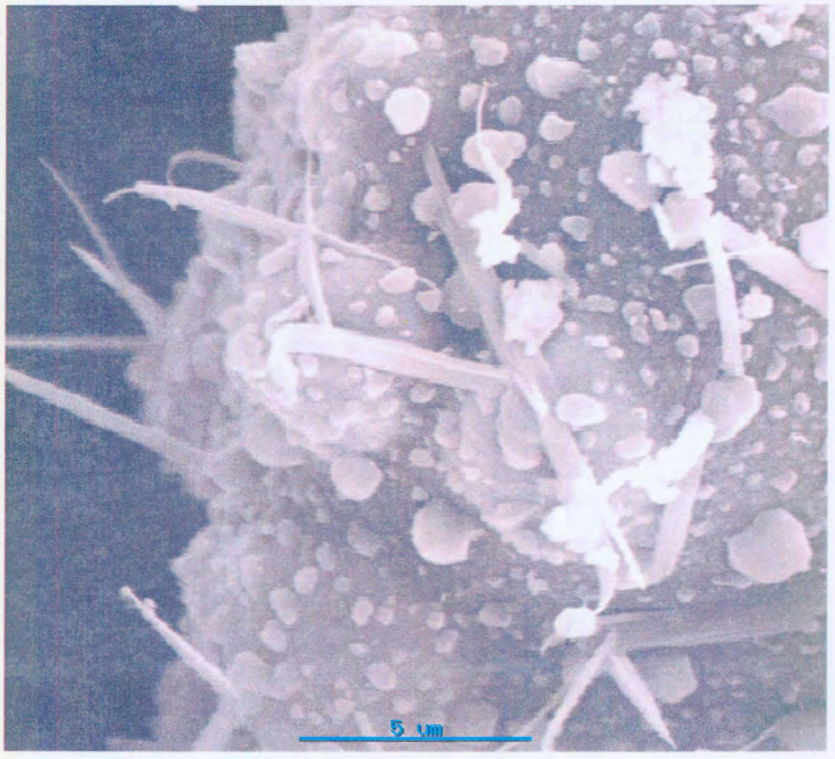

Plate 5.a Micrographs for the residue from the combustion of Sb_6O_{13} - 20%Si (type 4) in lead tube.

5.b

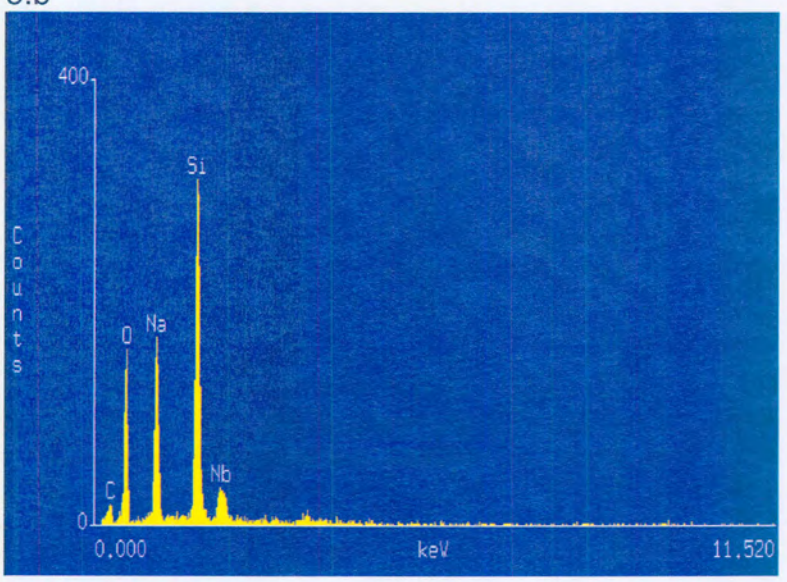

Figure 5.b EDS spectra for a specific needle selected on the micrograph 5.a.

Appendix C 5.c

Plate 5. c Micrographs for the residue from the combustion of Sb_6O_{13} - 20%Si (type 4) in lead tube.

5.d

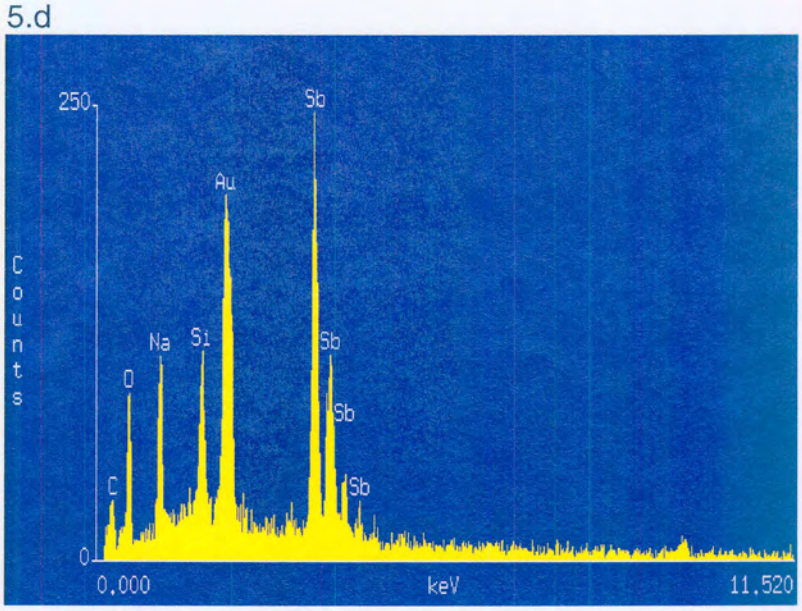

Figure 5.d EDS spectra done on the body of the hemispherical particle selected on the micrograph 5.c

Appendix C 5.e

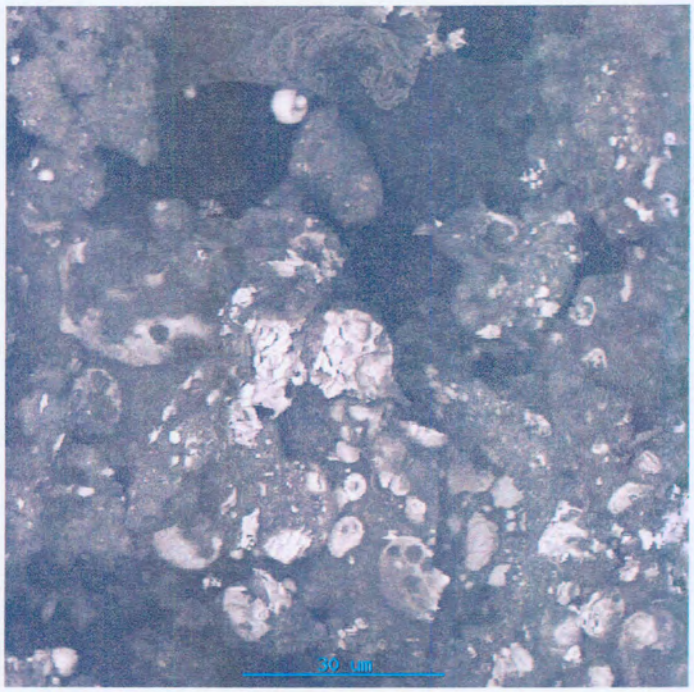

Plate 5.e Micrographs for the residue from the combustion of Sb_6O_{13} - 20%Si (type 4) in lead tube.

5.f

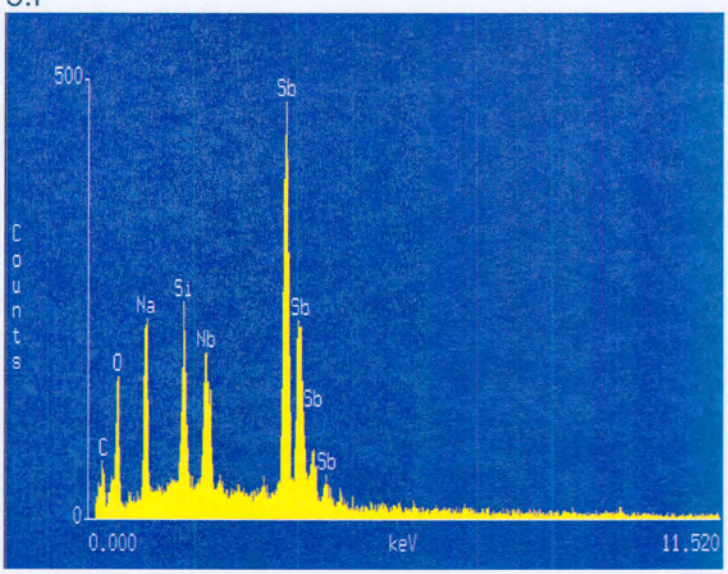

Figure 5.f EDS spectra done on the surface of a specific bright particle selected on the micrograph 5.e.

Appendix D

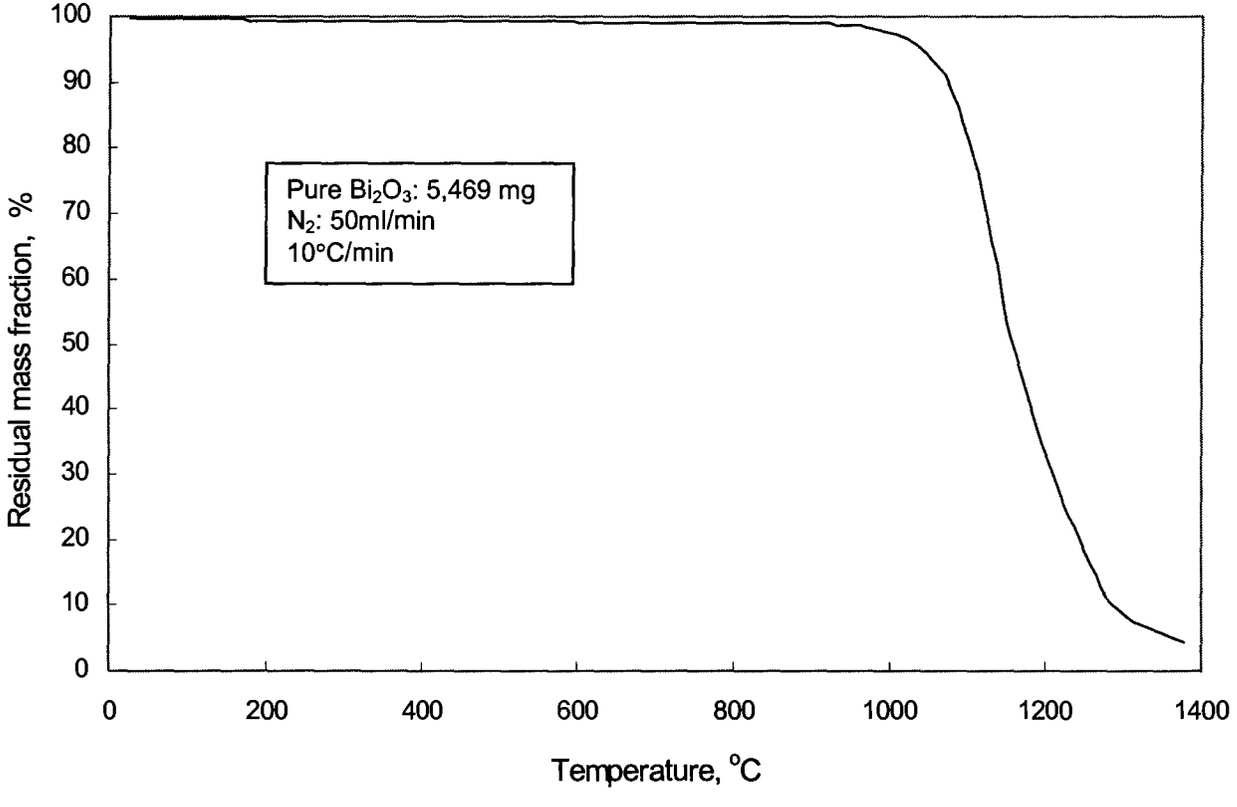

Figure 1 TGA curve of Pure Bi_2O_3.

Appendix *D*

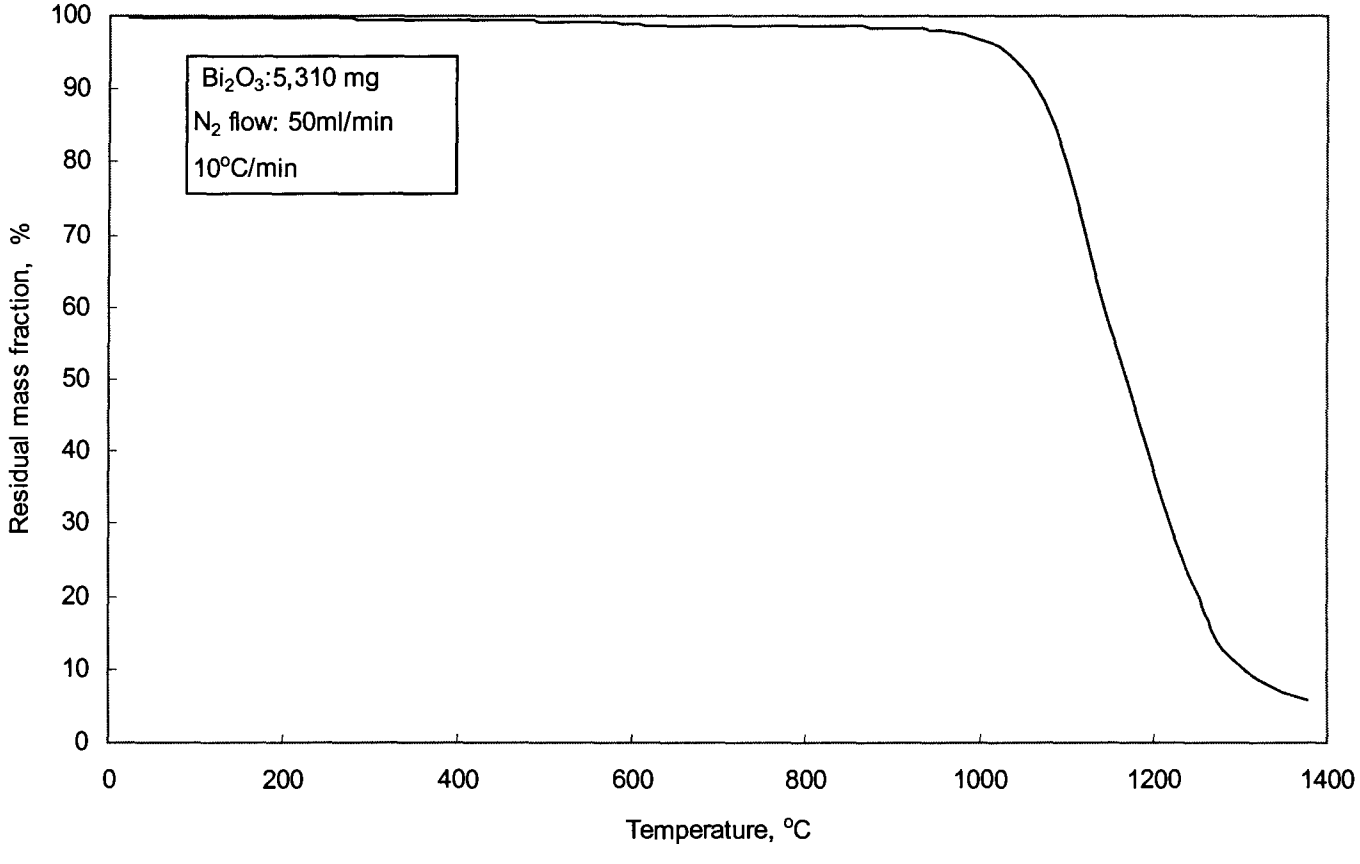

Figure 2 TGA curve of Bi_2O_3 produced from thermal decomposition of $Bi_2O_2CO_3$ at 460℃ during 15 hours.

Appendix D

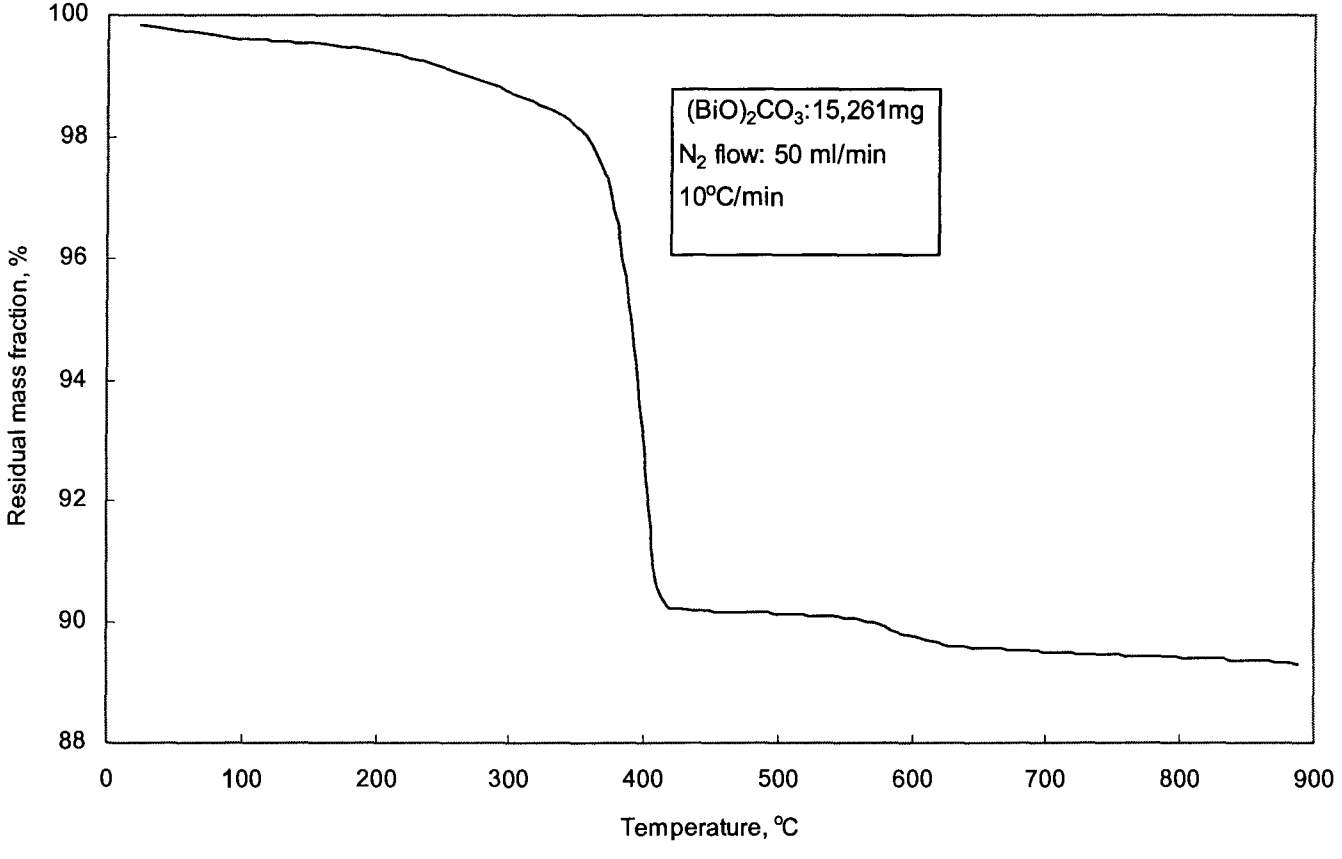

Figure 3 TGA curve of $Bi_2O_2CO_3$.

Appendix D

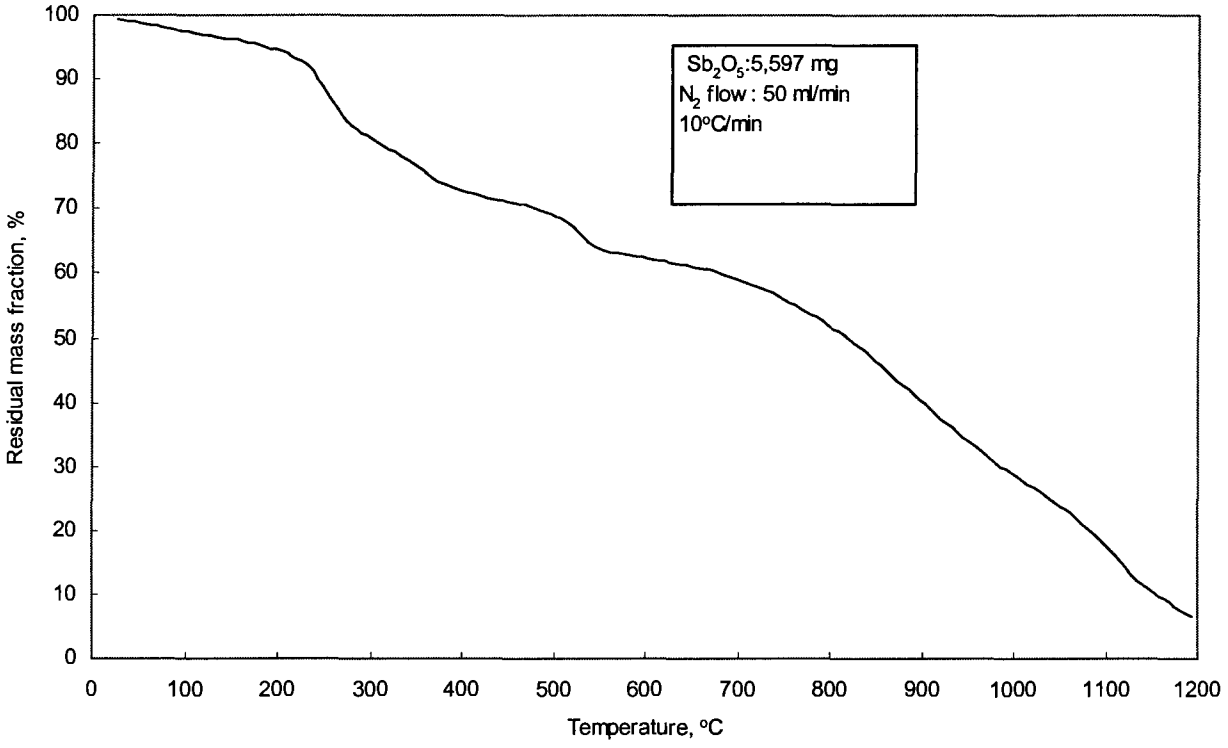

Figure 4 TGA curve of the colloidal Sb_2O_5.

Appendix D

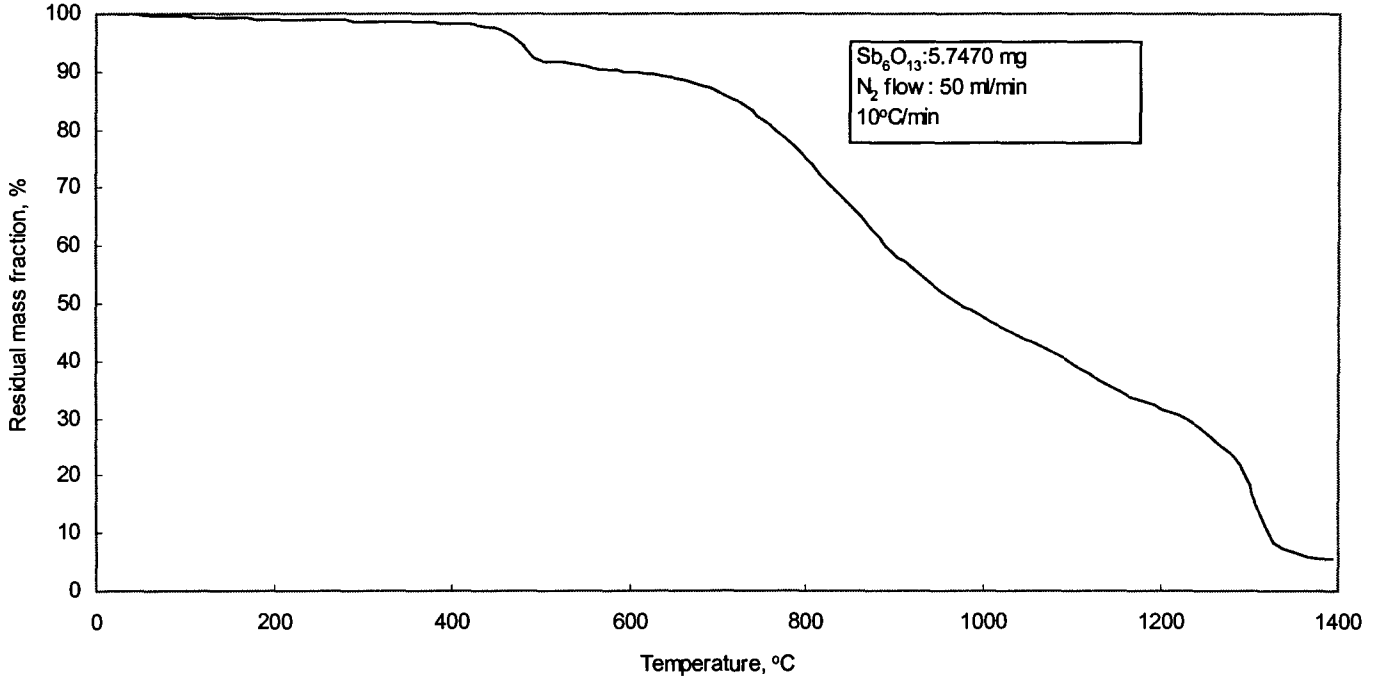

Figure 5 TGA curve of Sb_6O_{13} produced from thermal decomposition of Sb2O5 at 315°C during 8 hours.